INFORMATION TO USERS

This manuscript has been reproduced from the microfilm master. UMI films the text directly from the original or copy submitted. Thus, some thesis and dissertation copies are in typewriter face, while others may be from any type of computer printer.

The quality of this reproduction is dependent upon the quality of the copy submitted. Broken or indistinct print, colored or poor quality illustrations and photographs, print bleedthrough, substandard margins, and improper alignment can adversely affect reproduction.

In the unlikely event that the author did not send UMI a complete manuscript and there are missing pages, these will be noted. Also, if unauthorized copyright material had to be removed, a note will indicate the deletion.

Oversize materials (e.g., maps, drawings, charts) are reproduced by sectioning the original, beginning at the upper left-hand corner and continuing from left to right in equal sections with small overlaps.

ProQuest Information and Learning
300 North Zeeb Road, Ann Arbor, MI 48106-1346 USA
800-521-0600

Synthesis, Photophysics and Photochemistry of Substituted 2,7-Di-(*t*-butyl)-*trans*-10b,10c-dimethyl-10b,10c-dihydropyrenes

by

Molina Audrey Lorraine Sheepwash
B.Sc., University of Guelph, 1998

A Dissertation Submitted in Partial Fulfillment of the
Requirements for the Degree of

DOCTOR OF PHILOSOPHY

in the Department of Chemistry

We accept this dissertation as conforming
to the required standard

Dr. Cornelia Bohne, Co-supervisor (Department of Chemistry)

Dr. Reginald H. Mitchell, Co-supervisor (Department of Chemistry)

Dr. Peter C. Wan, Department Member (Department of Chemistry)

Dr. Arthur Watton, Outside Member (Department of Physics and Astronomy)

Dr. Frances L. Cozens, External Examiner (Department of Chemistry, Dalhousie University)

Supervisors: Dr. C. Bohne
Dr. R.H. Mitchell

ABSTRACT

The photochromism of several simple substituted and [e]-annelated 10b,10c-dimethyl-10b,10c-dihydropyrene derivatives was studied using steady state and time resolved fluorescence techniques as well as chemical actinometry and laser flash photolysis (LFP). The purpose of this study was to determine the mechanism of the photoisomerization between the closed, coloured dimethyldihydropyrene isomer and the open, colourless metacyclophanediene isomer. A detailed understanding of the switching mechanism of such compounds will allow for the rational design of multichromophoric switches in the future.

Fluorescence from the dimethyldihydropyrene isomers was weak ($\phi < 0.03$). The simple substituted systems exhibited sharp emissions comprised of a single transition while the [e]-annelated derivatives emission were broader and resolved into two bands at low temperature (77 K). The fluorescence lifetimes for the dimethyldihydropyrene isomers were between 2.4 and 5.6 ns. The emission for the metacyclophanediene isomers was found to be very structured with lifetimes between 12 and 17 ns for most derivatives.

The photoisomerization was found to proceed through the singlet excited state and bond breakage / formation occurred on the nanosecond timescale as determined by LFP. The triplet excited state, although formed, was not involved in the switching mechanism. The ring opening isomerization quantum yields were found to be low for the simple substituted systems (≤ 0.012) but were improved upon [e]-annelation (0.042 – 0.095). The ring closing isomerization quantum yields for the annelated systems were found to be much higher than the ring opening efficiencies (0.28 – 0.42) and were insensitive to substitution or the nature of the fused arene moiety. Future synthesis and studies should be based on the [e]-annelated architectures.

Examiners:

Dr. Cornelia Bohne, Co-supervisor (Department of Chemistry)

Dr. Reginald H. Mitchell, Co-supervisor (Department of Chemistry)

Dr. Peter C. Wan, Department Member (Department of Chemistry)

Dr. Arthur Watton, Outside Member (Department of Physics and Astronomy)

Dr. Frances L. Cozens, External Examiner (Department of Chemistry, Dalhousie University)

TABLE OF CONTENTS

LIST OF TABLES

LIST OF FIGURES

LIST OF SCHEMES

List of Numbered Compounds

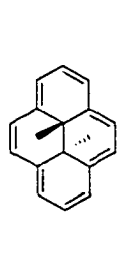

1

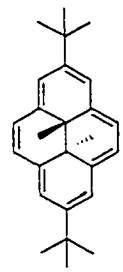

2

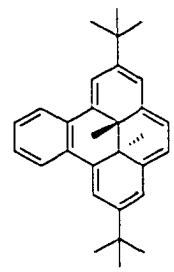

3

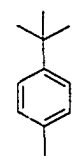

4

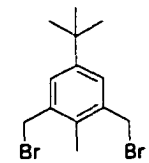

5

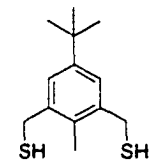

6

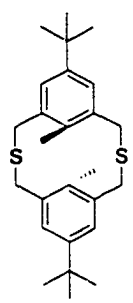

7

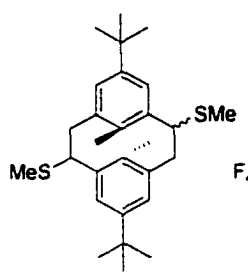

8

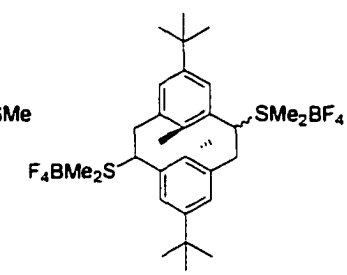

9

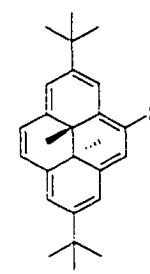

10

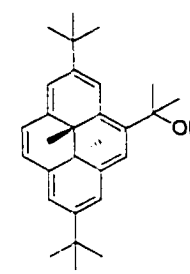

11

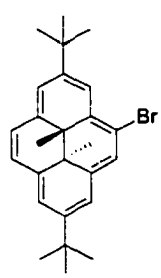

12

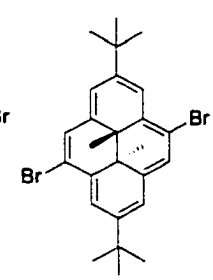

13

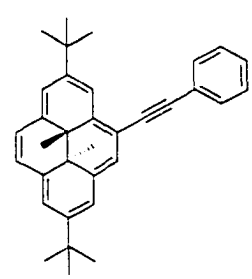

14

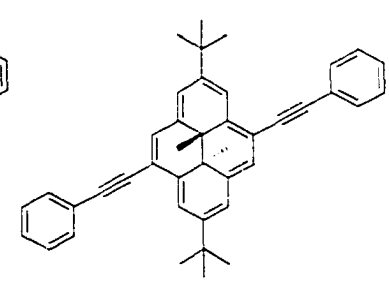

15

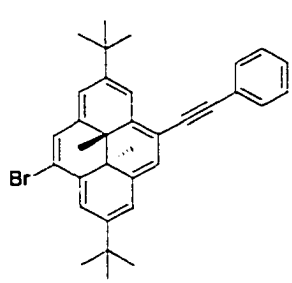

16

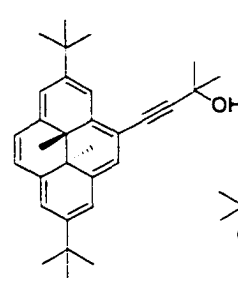

17

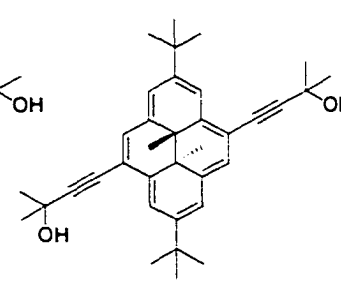

18

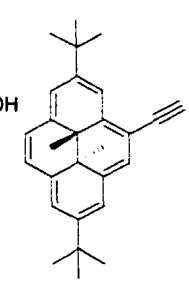

19

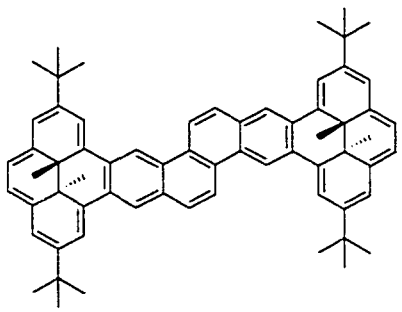

20

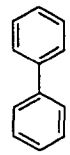

21

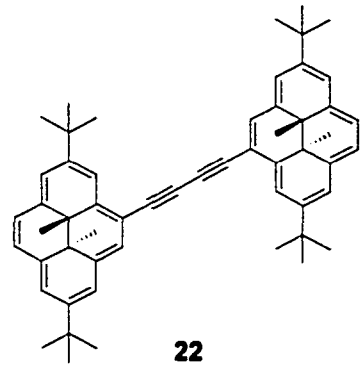

22

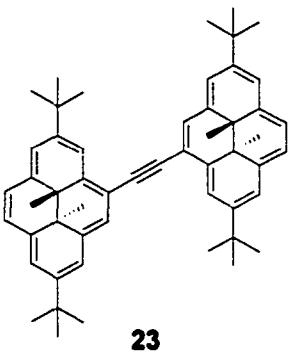

23

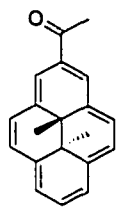

24

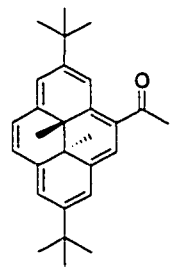

25

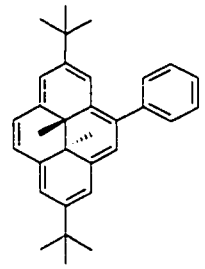

26

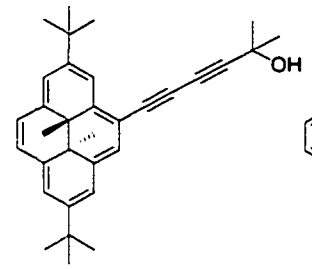

27

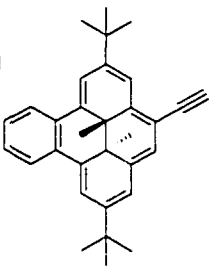

28

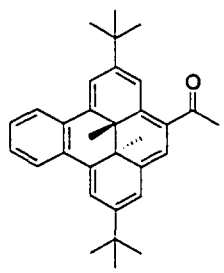

29

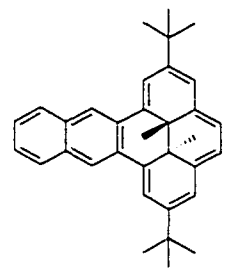

30

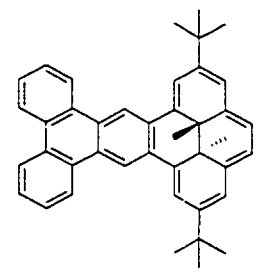

31

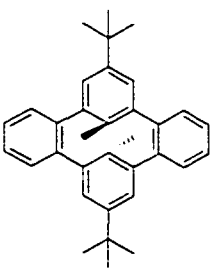

32

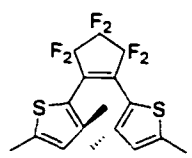

33

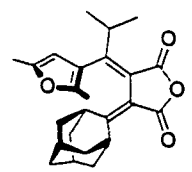

34

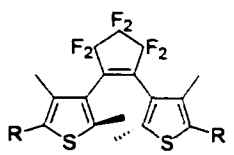

35: R = H
36: R = C_6H_6
37: R = *p*-C_6H_5OMe
38: R = *p*-$C_6H_5N(Me)_2$
39: R = C_5H_7

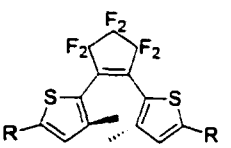

40: R = C_6H_6
41: R = *p*-C_6H_5OMe
42: R = *p*-$C_6H_5N(Me)_2$

LIST OF ABBREVIATIONS

A	absorbance
ACN	acetonitrile
ΔA	change in absorbance
ΔA_{max}	maximum transient absorption (LFP kinetics)
ΔA_{res}	residual absorption after decay of transient (LFP)
ΔA_T	triplet excited state absorption (LFP)
β-car	β-carotene
BPh	benzophenone
n-BuLi	n-butyllithium
c	concentration (absorption)
c	speed of light (2.998×10^8 m·s^{-1})
CHX	cyclohexane
CI	chemical ionization
COSY	correlated spectroscopy
CPD	cyclophanediene (open isomer)
CPD→DMDHP	ring closing isomerization
d	doublet (NMR)
DAD	diode array detector (HPLC)
DMDHP→CPD	ring opening isomerization
DMDHP	*trans*-10b,10c-dimethyl-10b,10c-dihydropyrene
ε	molar absorptivity coefficient ($M^{-1}cm^{-1}$)
E	energy
E_{S1}	singlet excited state energy
E_T	triplet excited state energy
F	fluorescence
FLD	fluorescence detector (HPLC)
ϕ_x	quantum yield

η_x	refractive index
h	hours
h	Planck's constant (6.626×10^{-34} J·s)
HETCOR	heteronuclear correlation spectrocopy
HOMO	highest occupied molecular orbital
HPLC	high performance liquid chromatography
HRMS	high resolution mass spectroscopy
I	intensity
I_o	initial intensity
IC	internal conversion
IR	infrared spectroscopy
ISC	intersystem crossing
$k_{CPD \rightarrow DMDHP}$	CPD→DHP isomerization rate constant
$k_{DMDHP \rightarrow CPD}$	DHP→CPD isomerization rate constant
k_f^o	fluorescence rate constant
k_o	intrinsic decay rate constant
k_{obs}	observed rate constant
k_q	quenching rate constant
k_x	rate constant
λ	wavelength (nm)
l	pathlength (cm)
LFP	laser flash photolysis
LUMO	lowest unoccupied molecular orbital
M	multiplet
min	minutes
MS	mass spectroscopy
ν	frequency (s^{-1})
N_A	Avagadro's number (6.022×10^{23} mol^{-1})
NMR	nuclear magnetic resonance
NOESY	nuclear Overhauser enhancement spectroscopy
P	phosphorescence

ppm	parts per million
Q	quencher
s	second, singlet (NMR)
s	standard
S_x	singlet excited state
SOC	spin orbit coupling
SPC	single photon counting
τ_o	intrinsic lifetime (k_o^{-1})
τ_s	fluorescence lifetime ($(k_f^o)^{-1}$)
t	triplet (NMR)
t_x	time (min)
T_x	triplet excited state
u	unknown
UV	ultra-violet
V_x	volume
Vis	visible (light)
VR	vibrational relaxation

ACKNOWLEDGEMENTS

The author would like to express her thanks to Dr. David McGillivray for mass spectrometric analysis and Christine Greenwood for recording the NMR spectra. Thanks to Drs. Timothy R. Ward and R. Scott Murphy for training and assistance. Thanks also to Yunxia Wang and Subhajit Bandyopadhyay for supplying several compounds for study. The author would like to express her sincere gratitude to Drs. Cornelia Bohne and Reginald H. Mitchell for their support and supervision over the past four years.

For Martin

CHAPTER 1: INTRODUCTION

1.1 Photophysics[1]

Photophysics is concerned with molecules that have been excited and return to their ground electronic states without undergoing a chemical change. In other words, photophysics deals only with changes in the quantum states of the molecule. No new chemical species is formed from the absorption of energy, excitation of the electrons to a higher energy state and subsequent de-excitation. This is different from photochemistry (see below), which is concerned with the formation of new chemical species upon absorption of a photon.

1.1.1 Electronic States

The electrons of a molecule can be excited through the absorption (A) of a photon of light by a chromophore. Once excited, there are several photophysical deactivation processes that the molecule can undergo to eliminate this excitation energy. These deactivation pathways can be split into two groupings: nonradiative transitions, which occur without emission, and radiative processes involving the emission of light. Radiative and nonradiative processes can be further broken down into specific types based on the spin multiplicity of the initial and final states involved with the transition.

Electrons possess a spin angular momentum, each with a spin quantum number of $\pm$ ½. The electrons can be thought of as precessing around their axis as they orbit the nucleus, thus generating angular momentum. Spin multiplicity refers to alignment of the electron's magnetic angular momentum with respect to some applied magnetic field (Figure 1.1). The vectors can be thought of as being 'spin up' or 'spin down' and are conventionally illustrated by the use of arrows (i.e. $\uparrow$ or $\downarrow$) or the symbols α and β. The total spin angular momentum is denoted as S and can be calculated by summing the vectors for an electronic state in an applied magnetic field. The spin multiplicity is then calculated from the total spin angular momentum and is given by 2S+1. As can be seen from Figure 1.1, there are four possible orientations for the electrons to align with an applied magnetic field. Three of these orientations lead to additive vectors giving a total spin angular momentum of 1 ($(\pm½) + (\pm½)$). The other combination of vectors result in a

net angular momentum of zero ((+½) + (-½)). This leads to a spin multiplicity for the parallel spins of 3 (2(1)+1) and a spin multiplicity for the antiparallel spins of 1 (2(0)+1) giving the terms triplet and singlet.

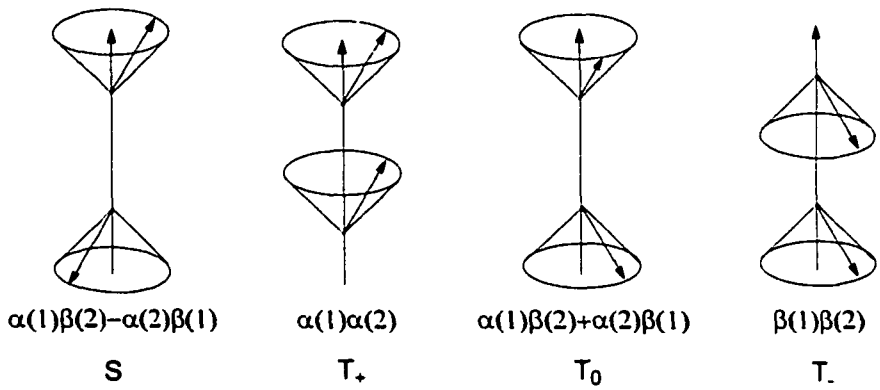

Figure 1.1. Vector representation of singlet and triplet electronic states.

Radiative processes involving the emission of light upon de-excitation from excited electronic states to lower energy electronic states of the same spin multiplicity are termed fluorescence (F). Fluorescence is most commonly seen as the $S_1 \rightarrow S_0$ transition. Emission of light due to a transition from an excited electronic state to a lower energy electronic state of differing multiplicity (e.g. $T_1 \rightarrow S_0$) is known as phosphorescence (P).

The nonradiative process involving two states of the same multiplicity is known as internal conversion (IC). Intersystem crossing (ISC) involves a transition between two electronic states of different spin multiplicity and requires a spin flip as a result (change in angular momentum vector direction). Nonradiative transitions are between isoenergetic levels. This can result in a large degree of vibrational energy that may be lost, through collisions, to the surrounding solvent molecules.

Nonradiative transitions can also occur within a given electronic state, between different vibrational energy states. The loss of energy resulting from the transition between higher energy and lower energy vibrational states is known as vibrational relaxation (VR).

Nonradiative and radiative transitions can be conveniently illustrated by use of a Jablonski diagram (Figure 1.2). As a general rule, radiative transitions are those shown by straight arrows while wavy arrows indicate nonradiative processes.

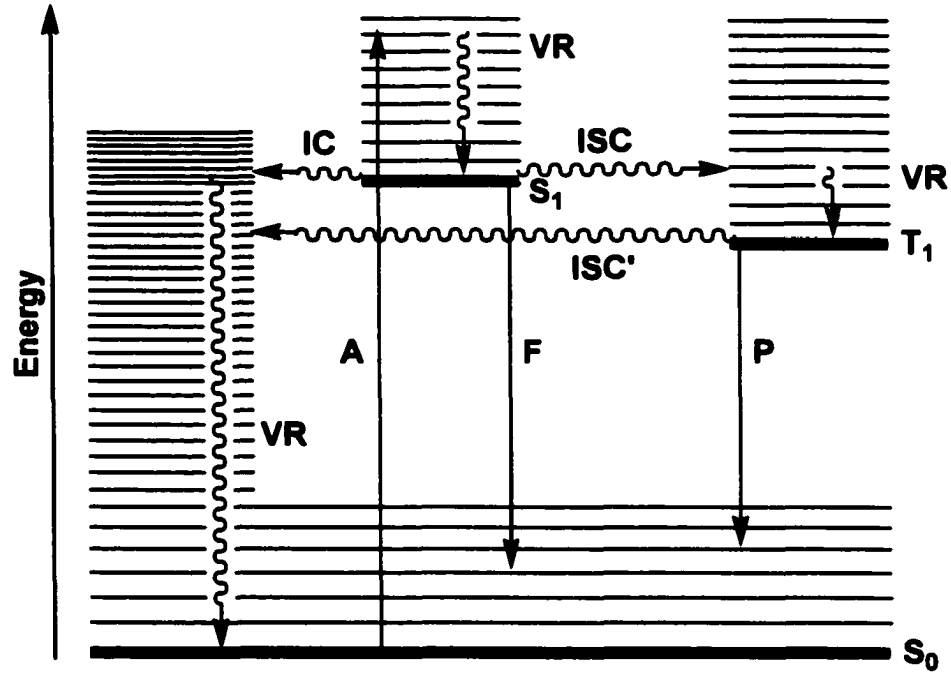

Figure 1.2. A Jablonski diagram illustrating radiative (absorption (A), fluorescence (F) and phosphorescence (P)), and nonradiative (internal conversion (IC) and intersystem crossing (ISC)) pathways between the ground electronic singlet state (S_0) and the excited electronic singlet (S_1) and triplet (T_1) states. Vibrational relaxation (VR), between different vibrational states within an electronic state, is also shown.

1.1.2 Absorption

Absorption involves the interaction of a chromophore with a discrete quantum of light (photon). A chromophore is the part of the molecule that is primarily responsible for its photochemical and photophysical activity. The chromophore absorbs light of a specific energy (Equation (1.1)), which corresponds to at least the difference in energy between the initial and final electronic states of the molecule. The absorption of energy causes the ground state electrons to be excited to a higher energy electronic state. These electronic transitions are also accompanied by various vibrational transitions.

$$E = h\nu = \frac{hc}{\lambda} \qquad \textbf{Equation (1.1)}$$

where E is the energy of the transition, h is Planck's constant (6.626×10^{-34} J·s), ν is the frequency of light, c is the speed of light (2.998×10^{8} m·s^{-1}) and λ is the wavelength of the light.

Assuming a transition is allowed, the most intense absorption bands occur when the orbital overlap between the vibrational states of the ground electronic state and the vibrational states of the excited electronic state are the greatest (Figure 1.3). Absorption to other vibrational states may occur but will be less intense due to decreased overlap. In solution phase, vibrational fine structure is generally seen more clearly in non-polar solvents than polar solvents, as there is less interaction between the solvent and the chromophore. If the equilibrium internuclear distance (r_{eq}) is the same for the electronically excited state as it is for the ground state, then one would expect the (0,0) transition to be the most intense band (Figure 1.3a). Generally, this is not the case as the excited electronic state will have some antibonding character that results in the weakening of the bond of the chromophore. This leads to a longer equilibrium internuclear bond distance in the excited electronic state than in the ground electronic state and results in the most intense band being a vibrational transition other than the (0,0) transition (Figure 1.3b).

The intensity of an absorption band is measured by comparing the intensity of an incident light beam (I_o) with the intensity of light beam after it has passed through the solution containing the chromophore (I). This value is known as the absorbance of the compound and is denoted by A. The absorbance of a compound is directly related to its concentration (c), the pathlength the light must travel through the sample (l), and the molar absorptivity coefficient (ε). This relationship is known as the Beer-Lambert Law and is shown in its various forms in Equation (1.2).

$$A = \varepsilon c l = -\log\left(\frac{I}{I_o}\right) = \log\left(\frac{I_o}{I}\right) \qquad \textbf{Equation (1.2)}$$

The molar absorptivity coefficient is essentially a measure of the efficiency of a given transition. Allowed transitions usually have molar absorptivity coefficients in the

range of 10^3-10^5 $M^{-1}cm^{-1}$, while 'forbidden' transitions generally have an ε of less than 10^2 $M^{-1}cm^{-1}$.

Although certain transitions are 'forbidden' they are still observed. This is because the selection rules are based on the assumption that the nuclear, electronic, and vibrational components can be separated and dealt with individually, exclusive of one another (Born-Oppenheimer approximation). In reality, this is not always true. Due to spin-orbit and vibronic coupling effects, the selection rules can break down and 'forbidden' transitions may be seen, although they are less likely to occur than allowed transitions.

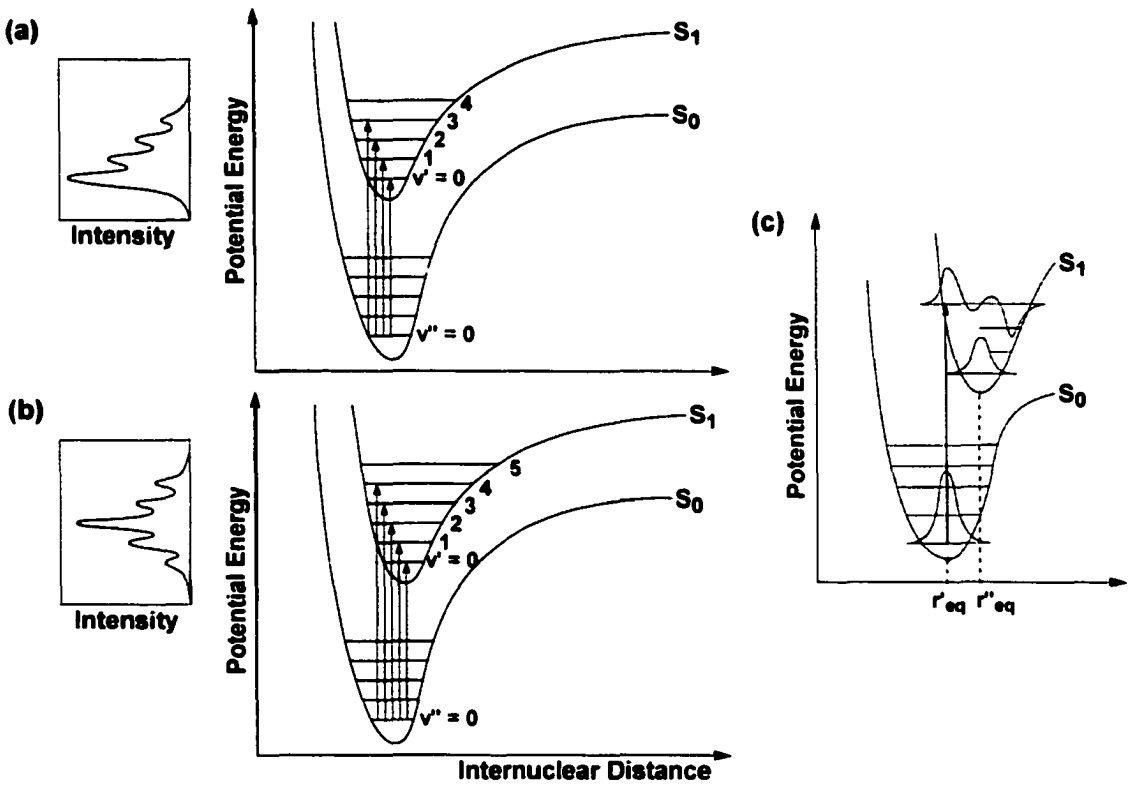

Figure 1.3. Potential energy curves for the ground and first excited electronic states showing the effect of geometry on the absorption spectrum when (a) the geometry of the two electronic states is constant, and (b) the excited electronic state has a larger internuclear distance than the ground electronic state. Also shown is a schematic representation of the overlap of the orbital wavefunctions associated with the vibrational levels of the ground and excited electronic states (c) (Gilbert, A.; Baggott, J., Essentials of Molecular Photochemistry © CRC Press, 1991/CANCOPY).

1.1.3 Fluorescence

Fluorescence involves the de-excitation of a molecule from a higher energy electronic state to a lower energy electronic state of the same spin multiplicity with the excess energy being given off in the form of a photon of light. Fluorescence can be thought of in a similar manner to absorbance, although in reverse. That is, assuming a transition is permitted, maximum fluorescence emission will occur when the greatest orbital overlap exists between the vibrational states of the excited electronic state and the vibrational states of the ground (or lower energy) electronic state. Emission may also be seen to other vibrational states where the orbital overlap is less but the emission intensity will be smaller. As with absorption, if there is no change in geometry associated with excitation then one would expect the maximum fluorescence intensity to be the (0,0) band. Generally, this is not the case, as the excited electronic state tends to have a longer internuclear equilibrium distance than the ground electronic state. This leads to a band other than the (0,0) transition being the band of maximum intensity.

In solution, collisions with solvent molecules or vibrational relaxation usually result in the excited electronic state losing any vibrational energy it may have acquired during absorption. This results in all emission occurring from the lowest energy vibrational state of the excited electronic state, which leads to a red shift of the emission spectrum with respect to the absorption spectrum. If there is no change in the geometry of the molecule upon excitation, then the (0,0) band of the absorption spectrum and the (0,0) band of the fluorescence spectrum should have the greatest intensity and overlap. On the other hand, a significant difference between the geometry of the ground electronic state and the geometry of the excited state can lead to fluorescence spectra that does not overlap with the absorption spectrum. This is because the largest vibrational overlap will occur between the lowest vibrational level ($v'' = 0$) in the excited electronic state and higher vibrational levels ($v' > 0$) in the ground electronic state (Figure 1.3c). The shift or difference between the absorption maximum and the fluorescence maximum that results is known as a Stokes shift.

Molecules that have a greater degree of rigidity will exhibit more vibrational fine structure than those that can sample a variety of conformations. When a molecule can

exist in several conformations then the spectrum that is obtained is an average of the emission from the different conformations and tends to be unstructured.

Fluorescence is measured at a ninety-degree angle to the excitation beam to avoid interference from scattered excitation light. In order to obtain a fluorescence emission spectrum, the compound of interest must be excited where it absorbs. The emission range is then scanned as the excitation wavelength is kept constant. The result is an emission spectrum that shows the range that emission is seen for a given excitation wavelength.

By setting the detection wavelength where emission is known to occur and scanning the excitation wavelength range one can also measure a fluorescence excitation spectrum. An excitation spectrum shows the range of excitation wavelengths that give rise to a particular emission. An excitation spectrum can be used to determine if more than one species is responsible for a given fluorescence. This is accomplished by taking several excitation spectra with different emission wavelengths. If the spectra overlap exactly, then the emission is due to a single species.

1.1.3.1 Lifetimes

Upon excitation, a concentration of excited molecules is formed which then decay back to their ground electronic states. Assuming only emission is occurring, this process can be explained by first order kinetics (Equation (1.3)).

$$[R^*] = [R^*]_o e^{-k_r^o t} \qquad \textbf{Equation (1.3)}$$

where *[R*]* is the concentration of the excited state, the subscript *o* refers to the concentration of the excited state at time t=0, and k_r^o is the radiative rate constant.

The lifetime of a process is the time it takes for the excited species to decay to 1/e of its initial concentration. The natural lifetime (τ_r^o) for a given radiative process, in the absence of other deactivation pathways, is given as follows:

$$\tau_r^o = \frac{1}{k_r^o} \qquad \textbf{Equation (1.4)}$$

In systems where non-radiative processes such as internal conversion and intersystem crossing directly compete with fluorescence, the lifetime that is measured is not equivalent to the lifetime given in Equation (1.4). In this case, the measured lifetime includes contributions from all processes that give rise to the decay of the excited state. The expression for the decay of [R*] (Equation (1.3)) remains the same but k_r^o is now replaced with k_f, where k_f is the sum of all deactivation processes responsible for the decay of the excited state (i.e. $k_f = k_f^o + k_{isc} + k_{ic}$). This gives an equation for the fluorescence lifetime as follows:

$$\tau_f = \frac{1}{k_f} = \frac{1}{k_f^o + k_{isc} + k_{ic}} \qquad \textbf{Equation (1.5)}$$

where τ_f is the radiative lifetime, k_f^o is the radiative rate constant, which is equivalent to k_r^o in the absence of other deactivation pathways, k_{isc} is the intersystem crossing rate constant and k_{ic} is the rate constant for internal conversion.

1.1.3.2 Fluorescence Quantum Yields

Quantum yields allow for a measure of the efficiency of a given photo-induced event. In the case of fluorescence, the efficiency of emission is measured by comparing how many molecules in a given volume emit over a specified time compared to the total number of photons absorbed by the solution over the same period of time (Equation (1.6)).

$$\phi_f = \frac{number\ of\ molecules\ fluorescing\ /\ unit\ time\ /\ unit\ volume}{number\ of\ photons\ absorbed\ /\ unit\ time\ /\ unit\ volume} \qquad \textbf{Equation (1.6)}$$

Although the equation above is an easy way to visualize what the fluorescence quantum yield is, it does not give a clear understanding of how such a value could be experimentally determined. The ratio in Equation (1.6) can also be considered as a ratio of the intensity of the light emitted (I_f) to the intensity of the light absorbed (I_a). Due to

difficulties in measuring the intensity of the light absorbed by a solution, it is easier to express the relationship as a ratio of the change in concentration of the photons as in Equation (1.7).

$$\phi_f = \frac{I_f}{I_a} = \frac{\frac{d}{dt}[h\nu']}{-\frac{d}{dt}[h\nu]} \qquad \textbf{Equation (1.7)}$$

Rate expressions can be determined by looking at the various processes the molecule can undergo. It can be seen from Scheme 1.1 that the change in photon concentration from the fluorescence process (*d/dt[hν']*) can be substituted by the rate for fluorescence. A similar substitution can be done for the change in concentration of absorbed photons (*-d/dt[hν]*) with the rate for absorption.

		Rate
$R + h\nu \rightarrow R^*$	Absorption	$k_a[R][h\nu]$
$R^* \rightarrow R + h\nu'$	Fluorescence	$k_f^\circ[R^*]$
$R^* \rightarrow R$	Other deactivation processes	$\Sigma' k_i[R^*]$

Scheme 1.1 Rate expressions for excitation and de-excitation processes.

Substitution of these rates into Equation (1.7) gives the following:

$$\phi_f = \frac{k_f^\circ[R^*]}{k_a[R][h\nu]} \qquad \textbf{Equation (1.8)}$$

where k_f° is the fluorescence rate constant, *[R*]* is the concentration of excited molecules, k_a is the absorption rate constant, *[R]* is the concentration of ground state molecules and *[hν]* is the concentration of photons absorbed.

The rate of change of [R*] can be equated to the sum of the rates of fluorescence and other deactivation processes less the rate of absorption. Under steady-state

conditions, [R*] remains constant and thus, the change in [R*] is zero. Rearrangement leads to an expression for [R*] as seen in Equation (1.9).

$$[R^*] = \frac{k_a[R][h\nu]}{k_f^o + \Sigma' k_i} \qquad \textbf{Equation (1.9)}$$

where $\Sigma' k_i$ is the sum of the rate constants for all deactivation pathways other than fluorescence.

Substitution of the expression for [R*] into Equation (1.8) leads to a relationship for the fluorescence quantum yield as related to rate constants (or lifetimes).

$$\phi_f = \frac{k_f^o}{k_f^o + \Sigma' k_i} = \frac{k_f^o}{\Sigma k_i} = \frac{\tau_f}{\tau_f^o} \qquad \textbf{Equation (1.10)}$$

where Σk_i ($k_f^\circ + \Sigma' k_i$) is the sum of the rate constants for all deactivation pathways, τ_f ($1/\Sigma k_i$) is the corresponding lifetime for the sum of all deactivation pathways, and τ_f° ($1/k_f^\circ$) is the radiative lifetime.

1.1.3.3 Quenching

Quenching provides a nonradiative deactivation pathway by which a molecule may lose its excited state energy and return to its ground electronic state. A quencher can be any molecule that is capable of accepting another molecule's excited state energy when it is introduced into solution. In the case of fluorescence, this leads to a loss of fluorescence intensity and in turn, decreases the fluorescence quantum yield. Ideally, the quencher should not absorb in the same region as the compound being studied. Absorption of the excitation energy by the quencher interferes with the excitation of the molecules being investigated and decreases the fluorescence intensity as an artifact and not because of quenching.

In order to determine an expression for the quenching rate constant one must determine what other processes can contribute to the overall scheme. Scheme 1.1 shows

the rates for absorption, fluorescence and other deactivation pathways. In the case of quenching, a fourth rate must be included (Scheme 1.2).

		Rate
$R^* + Q \rightarrow R + Q$	Quenching	$k_q[R^*][Q]$

Scheme 1.2 Rate expression for a quenching process.

The rate of change of [R*] must now include the rate for quenching (Equation (1.11)).

$$-\frac{d}{dt}[R^*] = k_q[R^*][Q] + k_f^o[R^*] + \Sigma' k_i[R^*] - k_a[R][h\nu] \qquad \textbf{Equation (1.11)}$$

where k_q is the quenching rate constant and *[Q]* is the concentration of quencher.

As previously mentioned, under steady-state conditions, the rate of change of [R*] is zero. This gives a modified equation for the concentration of excited molecules.

$$[R^*] = \frac{k_a[R][h\nu]}{k_q[Q] + k_f^o + \Sigma' k_i} \qquad \textbf{Equation (1.12)}$$

Substitution of Equation (1.12) into Equation (1.8) gives an expression for the fluorescence quantum yield that takes the effect of quenching into account.

$$\phi_f = \frac{k_f^o}{k_q[Q] + k_f^o + \Sigma' k_i} = \frac{k_f^o}{k_q[Q] + \Sigma k_i} = \frac{k_f^o}{k_q[Q] + k_f} \qquad \textbf{Equation (1.13)}$$

where k_f (Σk_i) is the rate constant for the sum of all the deactivation pathways.

In the absence of quencher, the above equation simplifies to the expression previously determined for the fluorescence quantum yield in Equation (1.10). Taking the

ratio of Equation (1.10) to Equation (1.13) one obtains a relationship for the quenching rate constant.

$$\frac{\phi_f^o}{\phi_f} = \frac{k_f^o}{k_f} \cdot \frac{k_f + k_q[Q]}{k_f^o} = 1 + \frac{k_q[Q]}{k_f} \qquad \textbf{Equation (1.14)}$$

The above expression can be related to fluorescence intensity by substitution with the first part of Equation (1.7). The resulting equation is known as the Stern-Volmer equation.

$$\frac{I_f^o}{I_f} = 1 + \frac{k_q[Q]}{k_f} = 1 + k_q\tau_f[Q] = 1 + K_{SV}[Q] \qquad \textbf{Equation (1.15)}$$

where K_{SV} ($k_q\tau_f$) is the Stern-Volmer constant.

Graphing the ratios of fluorescence intensities with quencher (I_f) and without quencher (I_f°), against various quencher concentrations ([Q]) gives K_{SV} as the slope. If the lifetime has already been determined then the quenching rate constant can be calculated. This method can also be used as an indirect method for determining the lifetime of a compound if the quenching rate constant is known or can be calculated independently.

1.1.4 Intersystem Crossing[2]

Intersystem crossing involves the transition between isoenergetic vibrational levels of electronic states with different spin multiplicities. This transition is forbidden according to the Born-Oppenheimer approximation because it requires an inversion of spin. Changing the spin of an electron requires a change in its angular momentum. This change must be accompanied by another change in angular momentum such that the overall angular momentum of the system is conserved. Spin-orbit coupling (SOC) allows this transition to take place. Spin-orbit coupling conserves momentum by coupling the spin flip with an orbital jump. Thus, the change in spin angular momentum is compensated for by the change in orbital angular momentum. Although spin-orbit

coupling provides only a weak perturbation to the system (0.3-0.001 kcal/mol), it is sufficient to allow forbidden transitions to occur but with a lower probability than allowed transitions.

Spin orbit coupling is proportional to the fourth power of the atomic number (i.e. SOC α Z^4). Therefore, as the atomic number increases, the contribution from spin orbit coupling increases accordingly. This is known as the heavy atom effect and serves to increase the probability of intersystem crossing occurring by inducing spin-orbit coupling.

Intersystem crossing is enhanced when the difference in energy between the excited singlet state and excited triplet state (ΔE_{ST}) is small. The rate constant for intersystem crossing can be approximated by the inverse of the energy difference between the excited singlet and triplet electronic states plus some contribution due to spin orbit coupling (k_{isc} α $1/\Delta E_{ST}$ + $SOC_{probability}$). A transition is favoured when it occurs between electronic states with different configurations (El-Sayed Rule). Allowed transitions include $n,\pi^* \rightarrow \pi,\pi^*$ and $n,\pi^* \rightarrow n^2$ while forbidden transitions include $n,\pi^* \rightarrow n,\pi^*$ and $\pi,\pi^* \rightarrow \pi,\pi^*$.

1.2 Photochemistry[1]

As mentioned above, photochemistry is concerned with the formation of new chemical species upon light induced excitation. This area covers a broad range of reactions in organic chemistry such as electron transfer, hydrogen abstraction, α-cleavage reactions and pericyclic reactions to name but a few. Although there are many photochemical mechanisms by which these new chemical species may be formed, the following text will deal primarily with pericyclic reactions as these directly relate to the project being discussed.

1.2.1 Pericyclic Reactions[3]

Pericyclic reactions can be described as concerted reactions that proceed via a cyclic transition state. These types of reactions may proceed thermally or photochemically depending on the orbital symmetry constraints (see below) and have been found to be highly stereospecific. There are three main categories of pericyclic

reactions: cycloaddition reactions, where two pi systems combine to form a cyclic compound; electrocyclic reactions, where a conjugated polyene is transformed into a cyclic compound; sigmatropic rearrangements, where a sigma bond migrates to a new position within a pi system through a reorganization of the electrons. The reverse reactions for each of the categories listed above are also pericyclic reactions.

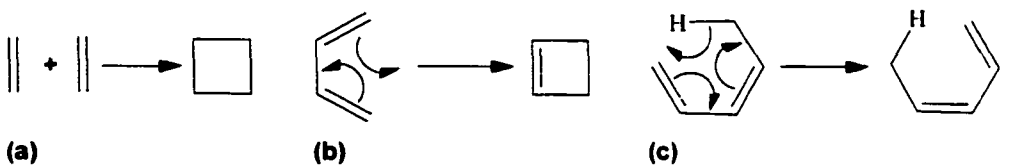

Scheme 1.3. Examples of pericyclic reactions: (a) cycloaddition; (b) electrocyclization; (c) sigmatropic rearrangement.

Pericyclic reactions have a nomenclature used to designate these types of reactions. The nomenclature for this group of reactions refers to the number of electrons involved in the reaction as well as the type of orbital that is involved. For example, the reaction shown in Scheme 1.3a, would be denoted as a $[2\pi_s+2\pi_s]$ or simply a [2+2] cycloaddition. The 2 refers to the number of electrons on each fragment that are involved in the new bond formation. The π indicates that a pi-orbital is involved in forming the new bond. Another modification to the nomenclature is the inclusion of a subscript referring to whether the reaction proceeds suprafacially (*s*) or antarafacially (*a*). The significance of suprafacial versus antarafacial reactions will be discussed below.

1.2.1.1 Woodward-Hoffman Rules

According to the Woodward-Hoffmann rules a ground state pericyclic reaction is allowed by symmetry when the total number of (4n+2) suprafacial and (4n) antarafacial components is odd.[1] To understand what this means in a practical sense it is necessary to look at the nomenclature derived for such reactions (see above). The thermal cyclodimerization of ethene is denoted by $[2\pi_s + 2\pi_s]$. It can be seen from the subscripts that there are no antarafacial components in this case. However, there are two (4n+2) suprafacial components where n=0 (i.e. there are two 2's preceding the π). The number of suprafacial and antarafacial components added together gives an even number (2 + 0 =

2) indicating that the thermal process is forbidden. In the case of a $[2\pi_s + 2\pi_a]$ cyclodimerization of ethene, the process is allowed because there is one suprafacial (4n+2) component and no 4n antarafacial components (there is one (4n+2) antarafacial component that is not considered).

A simplified version of how these rules relate to each type of pericyclic reaction is illustrated in Table 1.1 below. These selection rules are based on the 4n+2 Hückel rule of aromaticity and assume a quasi-planar aromatic transition state for pericyclic reactions.

Table 1.1. Simplified Woodward-Hoffmann rules for pericyclic reactions.

	Electrocyclic[a]		**Sigmatropic**[b]		**Cycloaddition**[b]	
	Δ	**hν**	**Δ**	**hν**	**Δ**	**hν**
4n	con	dis	supra-antara	supra-supra	supra-antara	supra-supra
4n+2	dis	con	supra-supra	supra-antara	supra-supra	supra-antara

[a] con refers to conrotatory and dis refers to disrotatory motion (see below).
[b] antara refers to antarafacial and supra refers to suprafacial (see below).

Suprafacial and antarafacial refer to the face of the molecule on which the reaction is occurring. In the case of cycloadditions, suprafacial indicates that the orbitals involved in the bond formation are reacting on the same side (face to face). Conversely, antarafacial implies that one set of orbitals is reacting face to face while the other has to change its geometry in order to react. In other words, they are reacting on opposite sides. The concept of suprafacial and antarafacial attack are illustrated in Figure 1.4.

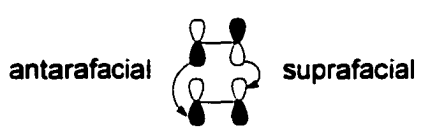

Figure 1.4. A suprafacial-antarafacial reaction illustrating the difference between suprafacial and antarafacial reaction modes. It should be noted that the one molecule attacks from above and not from behind the other molecule.

It should be noted that although some reactions are allowed antarafacially, this only applies to systems where *n* is sufficiently large to permit the reaction geometry necessary to be achieved. When n is too small the molecule cannot distort itself enough

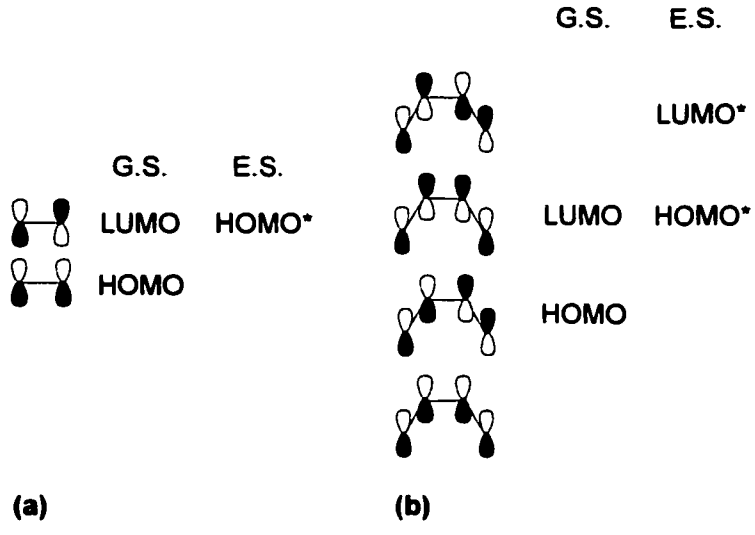

Figure 1.5. Frontier molecular orbitals of (a) ethene, and (b) 1,3-butadiene. The HOMO and LUMO FMOs are labeled for clarity.

Any reaction of this type can be considered as the reaction between the HOMO of one compound and the LUMO of the other compound. Under thermal conditions, the ground state HOMO and LUMO for each compound are involved in the reaction. In the excited state, one of the compounds reacts from its ground state HOMO or LUMO and the other molecule involves its excited state HOMO or LUMO (denoted HOMO* or LUMO* for clarity).

The reaction of two molecules of ethene (Figure 1.6a) shows that the thermal reaction does not have the correct orbital overlap for the ground state HOMO and LUMOs. The photochemical reaction, however, does have the correct orbital overlap between the ground state LUMO and excited state HOMO*. This shows that a suprafacial [2+2] cycloaddition occurs photochemically and not thermally. The converse is true when the reaction is antarafacial in nature.

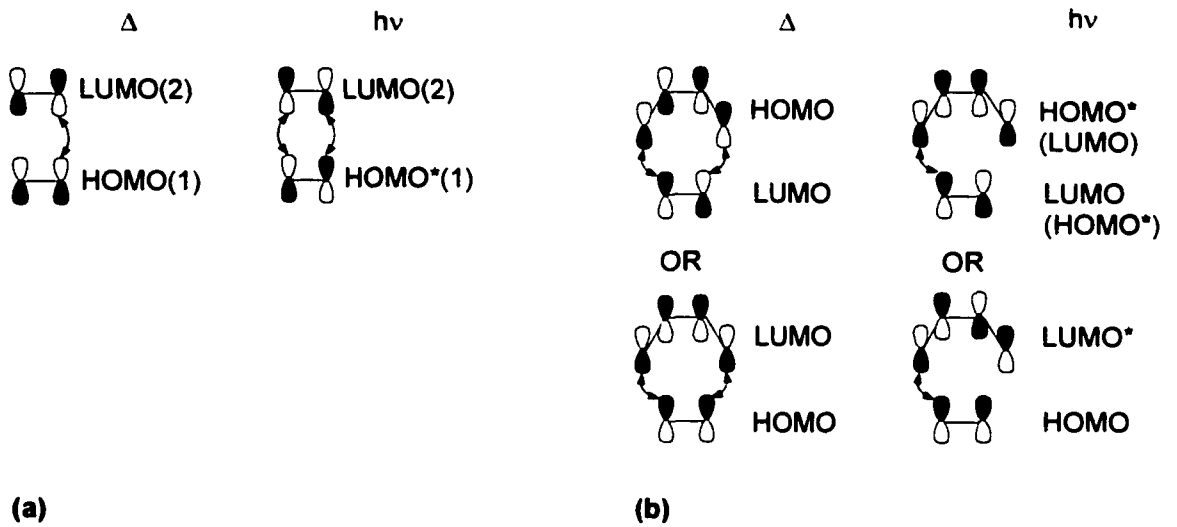

Figure 1.6. Frontier molecular orbital picture for the thermal (Δ) and photochemical (hν) reaction pathways for (a) ethene and ethene (bracketed numbers indicate which molecule the orbital is from), and (b) ethene and 1,3-butadiene.

The [4+2] reaction of ethene and butadiene (Figure 1.6b) illustrates that suprafacial cycloadditions involving 4n+2 electrons are thermally allowed by orbital symmetry but are photochemically forbidden. It is clear from the orbital picture that an antarafacial photochemical reaction would be allowed while the thermal reaction would be forbidden.

1.2.1.3 Sigmatropic Rearrangements

Sigmatropic rearrangements involve the migration of a sigma bond within a pi system. Examples of such reactions include hydride shifts, the Cope reaction, and the Claisen rearrangement. The nomenclature for these reactions is similar to other pericyclic reactions. The naming consists of two numbers in a square bracket separated by a comma. The first number is the starting position of the bond that will be migrating (usually 1) and the second number is the final position for the migrating bond. For example, [1,3] refers to a sigma bond that has migrated from atom 1 to atom 3. Modifications to this nomenclature occur when more than one bond migrates. An example of this is the Cope rearrangement where two simultaneous [1,3] sigmatropic shifts occur. In such a case the nomenclature shows the final position for both bonds, i.e. [3,3].

Sigmatropic shifts or rearrangements can be thought of analogously to cycloadditions. In order to understand why certain reactions are allowed or forbidden, it is again necessary to examine the FMOs of the molecule. For these types of reactions, the atoms on the bond that is broken and the rest of the system are considered separately. In the case of propene, the carbon-hydrogen bond is considered as one entity (Figure 1.7a, red oval) and the remainder of the molecule is treated as ethene (Figure 1.7a, blue circle). The same principles are then applied as with the cycloadditions. The LUMO of one part of the molecule and the HOMO of the other portion of the molecule are examined and it is determined whether the reaction is permitted by orbital symmetry.

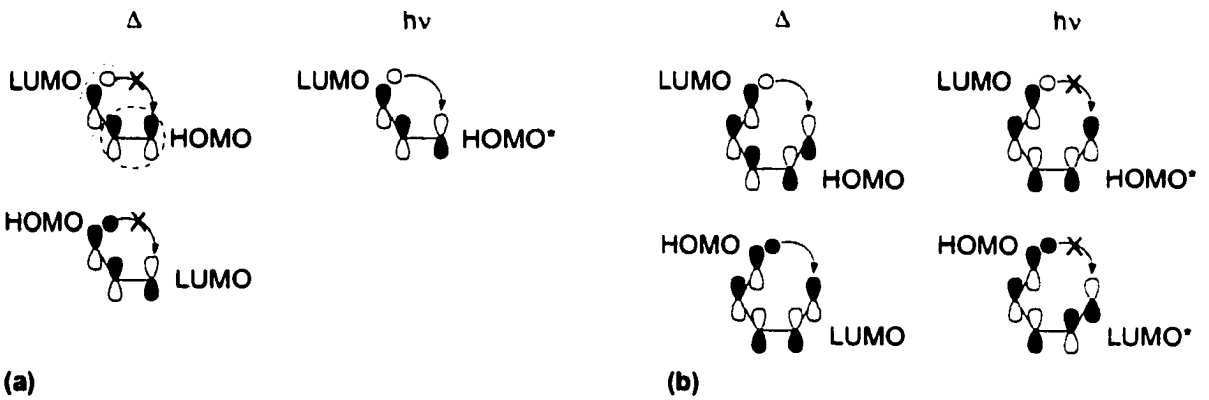

Figure 1.7. Frontier molecular orbitals for the thermal (Δ) and photochemical (hν) reaction pathways for (a) [1,3], and (b) [1,5] sigmatropic shifts. The red oval and blue circle indicate the two parts of the molecules that are considered when determining the FMOs involved.

For a [1,3] sigmatropic shift, it can be shown (Figure 1.7a) that the thermal suprafacial reaction is forbidden but the suprafacial photochemical reaction is allowed. The opposite is found for a [1,5] sigmatropic shift (Figure 1.7b) where the suprafacial reaction is allowed thermally. This confirms the Woodward-Hoffman rule that states a suprafacial reaction involving 4n electrons occurs photochemically while a reaction involving 4n+2 electrons occurs thermally.

As previously mentioned, antarafacial reactions can occur for systems where n is sufficiently large. It can be seen from Figure 1.7a though, that an antarafacial thermal reaction would not be able to occur regardless of the orbital overlap because the molecule cannot reach the required geometry. The two bonds are not long enough to allow the

hydrogen to react at the bottom lobe of the pi-orbital on the third carbon. Where the number of electrons involved is larger (≥6), the length of the carbon chain allows the molecule to adopt a configuration where the first carbon can be positioned under the last carbon in the chain and an antarafacial reaction can take place.

1.2.1.4 Electrocyclization Reactions

The Woodward-Hoffmann rules indicate that an electrocyclization reaction involving 4n electrons proceeds thermally with conrotatory motion. The same type of reaction can also proceed photochemically but with disrotatory motion. The terms conrotatory and disrotatory simply refer to the direction in which the bond must rotate to obtain orbital overlap between the pi-orbitals forming the new sigma bond. In the case of conrotatory motion, the bonds are rotated in the same direction (i.e. both clockwise) and disrotatory indicates the bonds are rotating in opposite directions (i.e. one clockwise, the other counterclockwise).

Unlike the cycloadditions and sigmatropic rearrangements, electrocyclization reactions only involve the HOMO of the molecule under investigation. This is because the reaction is intramolecular in nature. Examination of the orbitals on the atoms that are to form the new sigma bond will determine which way the bonds must rotate. This rotation leads to a very specific stereochemistry depending on the reaction mode employed. Scheme 1.4 shows how the stereochemistry of a tetra-substituted 1,3-butadiene molecule is affected when the reaction is done under thermal and photochemical conditions.

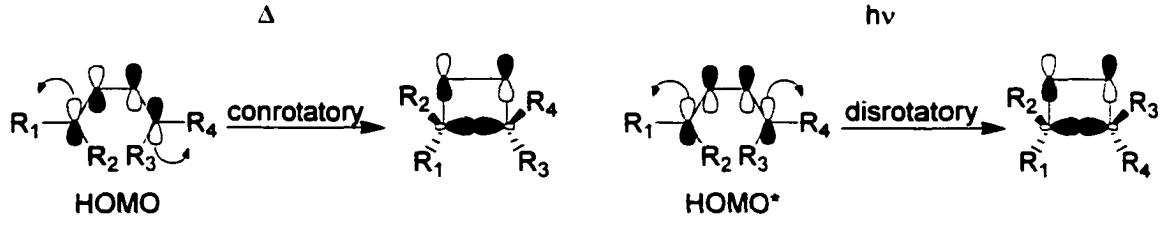

Scheme 1.4. Frontier molecular orbital diagram for the thermal (Δ) and photochemical (hν) electrocyclic reactions for a substituted 1,3-butadiene.

Under thermal conditions, the orbitals on the terminal carbons must both rotate counterclockwise (or both clockwise, conrotatory) to obtain orbital overlap. If the orbitals were to rotate in the opposite directions then the orbitals lobes would have different phases and the bond could not form. When the molecule is excited, the ground state LUMO becomes the HOMO* and results in both bonds needing to rotate in opposite directions, or in a disrotatory manner, to obtain orbital overlap. If functional groups are present on the terminal carbons, then one can confirm the mechanism of the reaction. When the reaction proceeds thermally R_1 and R_3 would be on the same face of the ring. A photochemical reaction would lead to R_1 and R_3 being on opposite faces of the ring.

1.2.2 Nonconcerted Cyclization Reactions[2]

Few photochemical reactions are concerted. More commonly they involve some intermediate such as a radical species. For the most part, cycloadditions, sigmatropic rearrangements and electrocyclizations involving π,π^* singlet excited states proceed in a concerted fashion. However, the same types of reactions involving triplet states or n,π^* singlet states do not necessarily follow a similar reaction path and may not be predicted by the Woodward-Hoffmann rules.

To understand diradical-based reactions, it is necessary to look at the general rules governing the reactions of triplet and singlet biradicals. Firstly, singlet and triplet biradicals only yield products with singlet and triplet multiplicities respectively. If intersystem crossing between singlet and triplet biradicals is efficient then that process can compete with other reaction pathways. The most stable triplet biradicals are formed when the spins are as far apart as possible. Internal conversion between a singlet biradical and a triplet biradical is dependent on the proximity of the radical centers to one another. The closer the radical pairs are held to each other, the larger the energy difference between the singlet and triplet biradical becomes and as a result, the probability of intersystem crossing is decreased.[4]

Singlet excited states with π,π^* configuration are expected to undergo pericyclic photoreactions (i.e. proceed via a concerted mechanism). The π,π^* singlet excited states of acyclic polyenes often possess a tendency to twist about the double bonds, leading to a zwitterionic intermediate or cis/trans isomerization. Triplet excited states of π,π^*

configuration are not expected to undergo pericyclic reactions because they generally produce a diradical, exciplex or zwitterionic product that initiates other reactions such as hydrogen/electron abstraction, addition to double bonds, radicaloid rearrangements or homolytic fragmentations.

Most photochemical cyclization reactions are not concerted and involve some intermediate such as a diradical, zwitterion or exciplex. Those reactions involving a singlet excited state of n,π^* configuration or triplet excited states of π,π^* configuration can lead to any or all of the above intermediates. Diradicals, zwitterions and exciplexes may also reversibly convert between one another and the initial species. Scheme 1.5 illustrates the differences between the three intermediates. It should be noted that although pericyclic reactions appear to be concerted, this does not rule out the possibility of an intermediate that is too short-lived to be directly observed.

$$A^* + B \rightarrow \begin{cases} (\ddot{A}\cdots B)^{\bullet} & \textit{Exciplex} \\ (\dot{A}\text{-}\dot{B})^{\bullet} & \textit{Diradical} \\ (A^- + B^+)^{\bullet} & \textit{Zwitterion} \end{cases}$$

Scheme 1.5. Pictorial representation of the differences between an exciplex, diradical and zwitterion.

1.2.3 Actinometry[5]

Actinometry provides a means by which one can measure the efficiency or quantum yield of a given photochemical process. In order to determine the efficiency of a reaction, it is necessary to quantitatively measure the number of photons absorbed by a sample over a period of time. Measuring the number of incident photons is a difficult process. It would be preferable to be able to measure single photons as they irradiate the sample but most detection devices that are capable of measuring such events are not efficient enough. It would be possible to use such devices if their detection efficiency was constant over time. Examples of detection devices that fit this description are photomultipliers, photodiodes and thermopiles. These detectors convert the number of photons they detect into a current or temperature change that is proportional to the energy of the incident photons, which in turn, is proportional to the number of incident photons.

Problems with this type of set up are that all the radiation must irradiate the sample and different detectors have different sensitivities so measurements made on different instruments would not be comparable. A standard is also required with these systems to calibrate the instrument response.

An alternative to directly measuring the number of photons is chemical actinometry. This involves using a compound that undergoes a photochemical process where the efficiency is known. By knowing the efficiency of the reaction and determining the amount of product formed, it is possible to determine the number of photons that irradiate the sample for a given time, also known as the photon flux. The advantages of this technique are that it is highly reproducible, and insensitive to fluctuations of the light source.

Perhaps the most common chemical actinometer is the potassium ferrioxalate actinometer. Parker and Hatchard[6,7] first proposed the method in the 1950's. The chemistry behind this actinometer is as follows:

(1) $2[Fe(C_2O_4)_3]^{3-} + H^+ \rightarrow [Fe(C_2O_4)]^+ + [Fe(C_2O_4)_2]^- + 3(C_2O_4)^{2-} + H^+$

(2) $[Fe(C_2O_4)]^+ + h\nu \rightarrow Fe^{2+} + (C_2O_4)^{\cdot-}$

(3) $[Fe(C_2O_4)]^+ + (C_2O_4)^{\cdot-} \rightarrow Fe^{2+} + (C_2O_4)^{2-} + 2CO_2$

(4) $Fe^{2+} + 3phen \rightarrow [Fe(phen)_3]^{2+}$

Scheme 1.6. Steps involved in the photolysis of the potassium ferrioxalate actinometer.

The first step involves a disproportionation of the iron oxalate in the presence of sulfuric acid. A photon is then absorbed by the iron (III) oxalate cation fragment, which causes free iron (II) to be liberated in solution. The oxalate radical anion produced in the second step can then react with another iron (III) oxalate cation to give a second equivalent of iron (II). After irradiation is complete, phenanthroline is added to complex the free iron (II) in solution. The iron (II) phenanthroline complex has a distinct absorption band at 510 nm (11100 $M^{-1}cm^{-1}$). The concentration of the complex can then be determined from the absorption and in turn, the concentration of free Fe^{2+} created by photolysis can be

calculated. The quantum yields of the potassium ferrioxalate actinometer have been measured between 250 and 500 nm.

The intensity of light irradiating a sample can be calculated from knowledge of the concentration of product from the photochemical process ($[Act]_{h\nu}$, mol/L), the volume of solution being irradiated (V_o, L), the irradiation time (t_o, min) and the efficiency of the process (ϕ_o, quantum yield). Equation (1.16) gives the relationship as follows:

$$Intensity = \frac{[Act]_{h\nu} V_o}{\phi_o t_o} = \frac{\Delta A_o V_o}{\varepsilon_o l_o \phi_o t_o} \qquad \textbf{Equation (1.16)}$$

where ΔA_o is the change in absorbance associated with the photochemical process of the chemical actinometer at a given wavelength, ε_o is the molar absorptivity coefficient for the actinometer at the monitoring wavelength and l_o is the pathlength of the cell.

Once the photon flux (Equation (1.16)) has been determined, it is relatively straightforward to determine the efficiency of another photochemical process. Equation (1.6) can be modified to apply to any photochemical process.

$$\phi_r = \frac{moles\ of\ product\ formed\ /\ unit\ time\ /\ unit\ volume}{number\ of\ photons\ \ absorbed\ /\ unit\ time\ /\ unit\ volume} \qquad \textbf{Equation (1.17)}$$

where the number of photons absorbed per unit time per unit volume is simply the photon flux from Equation (1.16). The moles of product formed per unit time per unit volume are easily measured by observing the change in absorption during the photochemical process. Equation (1.18) shows the relationship.

$$moles = \frac{[P]_{h\nu} V}{t} = \frac{\Delta A\, V}{\varepsilon\, l\, t} \qquad \textbf{Equation (1.18)}$$

where $[P]_{h\nu}$ is the concentration of product formed photochemically, V is the volume of unknown solution irradiated, t is the irradiation time of the unknown, ΔA is the change in

absorbance for the process being studied, ε is the molar absorptivity coefficient of the unknown at the monitoring wavelength and l is the pathlength of the cell.

Substitution of Equations (1.16) and (1.18) into Equation (1.17) gives the equation for the efficiency of a photochemical process as measured by chemical actinometry.

$$\phi_x = \frac{\phi_o \varepsilon_o l_o t_o \Delta A V}{\varepsilon l t \Delta A_o V_o} \qquad \textbf{Equation (1.19)}$$

1.2.4 LFP[8]

Flash photolysis allows for the direct determination of the lifetimes of excited states and intermediates. In flash photolysis, a solution is irradiated with a short burst of light from a flash lamp or laser. The pulse must necessarily be shorter than the lifetime that is being measured or the decay of the excited state and the excitation of the molecules will occur at the same time. This will lead to a profile that includes both processes. If the pulse profile of the lamp was sufficiently reproducible then the lamp profile could be subtracted out to give the decay. Unfortunately, the pulse profile is usually not reproducible from pulse to pulse.

Laser flash photolysis allows for much shorter pulses and as such, permits the detection of shorter-lived transients (nanosecond and sub-nanosecond) than conventional flash photolysis techniques (microsecond to microsecond). This technique is not only useful for obtaining kinetics of excited states and other photochemical transients but it also allows for the measurement of transient absorption spectra.

The light pulse generates a high concentration of molecules in the excited state. The kinetics of these excited molecules are then monitored by examining the change in the absorption of the excited molecules with time. This is possible because the absorbance is proportional to the concentration of excited molecules. The absorbance of a transient is measured relative to the absorbance of the species initially present in solution, i.e. as the change in absorbance (ΔA).

The decay of a single species can be fitted using the equation for a pseudo first order kinetics decay to obtain the rate constant (Equation (1.3)) of the process. Transient

absorption spectra are obtained by setting time windows (Figure 1.8a) within the kinetics traces at which the absorption will be measured for each wavelength. This gives a spectrum, at a specific time within the decay, for the transient species (Figure 1.8b).

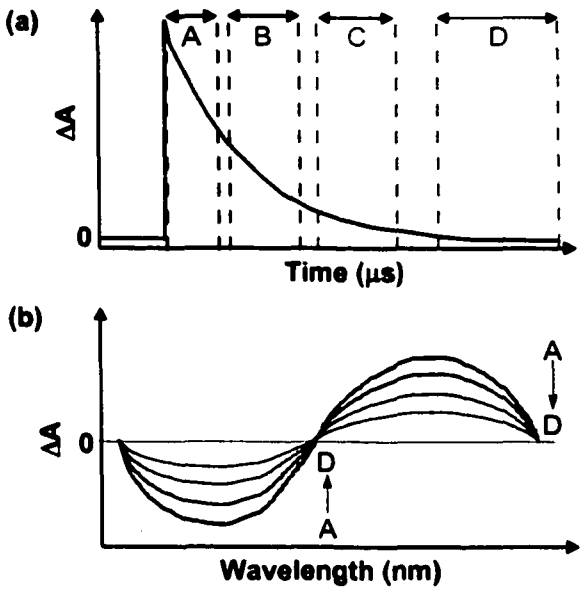

Figure 1.8. Example of (a) transient kinetics decay trace used to obtain the (b) transient absorption spectrum at various time delays (A → D) within the transient decay.

As mentioned for the transient kinetics, the transient absorption spectrum is often recorded as a difference spectrum. In such a case, a negative absorption (Figure 1.8b) corresponds to the bleaching or disappearance of the species that was initially present in solution. Conversely, a positive absorption in the transient absorption spectrum corresponds to the absorption of the new species created upon excitation (transient). It is important to note that positive signals are only seen when the molar absorptivity coefficient of the transient is larger than that of the species initially present in solution (i.e. $\varepsilon_{transient} > \varepsilon_{initial\ species}$).

1.2.4.1 Quenching

Quenching studies are useful for determining the identity of transients (e.g. multiplicity). As previously mentioned, quenchers can provide an excited molecule with an alternate nonradiative deactivation pathway to follow. In the quenching process the rate constant for the decay of a given excited state is faster than it would otherwise be.

This leads to a decrease in the excited state lifetime with increasing quencher concentration.

The change in the lifetime in the presence of quencher can be accounted for by a slight modification to Equation (1.15). The ratio of the lifetimes in the absence and presence of quencher (τ_o/τ_{obs}) is equal to the ratio of intensities given in Equation (1.15). Substitution of the lifetime ratio followed by division of both sides of the equation by τ_o gives the relationship between lifetime and quencher concentration (Equation (1.20)).[1,9]

$$\frac{1}{\tau_{obs}} = \frac{1}{\tau_o} + k_q[Q] \quad \textbf{OR} \quad k_{obs} = k_o + k_q[Q] \qquad \textbf{Equation (1.20)}$$

where τ_{obs} is the observed lifetime, k_{obs} $(1/\tau_{obs})$ is the observed rate constant in the presence of quencher and τ_o is the lifetime in the absence of quencher (substituted for τ_f).

If the quenching process occurs due to energy transfer, the electronic state of the quencher that is accepting the energy must be of lower energy than the excited state of the donor molecule for quenching to occur. The quencher and the excited molecules electronic states must also be of the same multiplicity and configuration in order for energy transfer to occur.

1.3 History of Photochromism and Photoswitches[10]

Fritsche initially observed photochromic behaviour in 1867 when he noticed that tetracene produced a colourless compound when exposed to light and air.[10a] This compound was found to regenerate tetracene upon heating. In 1876, ter Meer saw a similar phenomenon with potassium salts of dinitroethane.[10b] Phipson also observed a gatepost whose paint was black in sunlight but appeared white at night.[10c] In 1899, Marckwald coined the term *phototropy* to explain the colour change he saw in his studies of benzo-1-naphthiridine and tetrachloronaphthalen-1(4H)-one.[10d]

During the period of 1900-1920, there was a significant amount of research performed in this area by groups such as Wislicenus[10e] and Biltz.[10f,g,h] After a decade where little was accomplished, the 1940s saw a resurgence of interest in the field. In 1950, Hirshberg coined a more appropriate term for the phenomenon being studied,

namely, photochromism (phos=light; chroma=colour).[10i] Hirshberg was also the first to point out the potential applications of photochromic compounds in areas such as photochemical memory devices.

1.3.1 Photochromism

As mentioned above, the term photochromism was eventually given to the property being studied in the mid-twentieth century. Today photochromism is defined as the "reversible transformation of a single chemical species being induced in one or both directions by electromagnetic radiation between two states having different distinguishable absorption spectra".[10] Several classes of organic molecules have been shown to exhibit photochromic behaviour. Some of these include cis/trans isomerizations, photocyclizations, electrocyclizations as well as keto-enol tautomerizations. A great deal of research in this area is concerned with the application of photochromic compounds as molecular switches or photoswitches.

The most common photochromic compounds convert between a colourless (or pale yellow) and coloured form, with the colourless form generally being the more stable of the two molecules. This is known as positive photochromism while the reverse, where the coloured form is the more stable of the two compounds, is known as negative or inverse photochromism. Photochromic compounds can be further divided, depending on their thermal stability. Photogenerated molecules that are thermally stable are classified as P-type (photochemically reversible type) and those that are thermally reversible are known as T-type (thermally reversible type).[11]

1.3.2 Photoswitches[10]

A photoswitch should meet the requirements for a photochromic compound as well as be fatigue resistant and bistable (P-type photochromism). Several 'photoswitches' have been published in the literature in recent years, although very few exhibit all the qualities listed above. Most conversions are not yet thermally irreversible while others exhibit significant photodegradation after few switching cycles. Some of the most promising results have come out of the subset of photoswitches that are based on

electrocyclization reactions. These include classes of compounds such as fulgides and diarylethenes (see below).

1.3.2.1 Fulgides[12,13]

Fulgides are one of the oldest groups of known photochromic molecules based on a 6π-electrocyclization. They can be described as derivatives of dialkylidenesuccinic anhydrides (Scheme 1.7). Upon UV irradiation, the open (E, colourless / yellow) form can undergo one of two main processes. These include isomerization to the coloured closed form or E-Z isomerization. Visible irradiation results only in conversion of the closed form into the open E isomer. In order to exhibit photochromism fulgides require at least one aryl group on one of the methylene carbons.

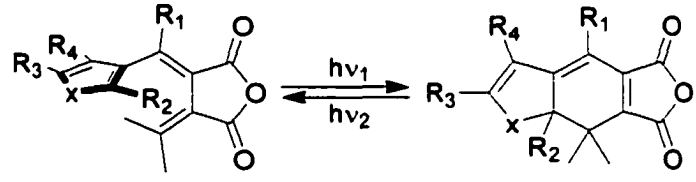

Scheme 1.7. Example of a fulgide structure and the isomerization between the open and closed isomers.

Several structural modifications to the fulgide backbone have been introduced to eliminate unwanted side reactions such as oxidative aromatization,[14] hydrogen transfer,[14-18] E-Z isomerization[15-20] and the thermal disrotatory opening.[14-18,20,21] These modifications include the introduction of a methyl group on the ring forming carbon of the aryl group,[16] introduction of heteroaromatic aryl groups (i.e. furan, thiophene) instead of phenyl[17,20] as well as the introduction of an isopropylidene substituent as the other methylene group.[16]

Photochromism for the fulgides has been seen in the solid-state as well as in solution, polymers and glasses.[22-24] Laser flash photolysis experiments have shown the interconversion between the colourless and coloured forms occurs within 10 ps in polymer films.[25-28]

Currently, research in this area is focused on the applications of these types of systems in areas such as optical memories[29-31] and the switching of various properties. These properties include fluorescence,[32,33] non-linear optics, supramolecular host-guest interactions, chiral and chiroptical switching,[34] liquid crystalline switching[35] and biological activity.[36,37]

1.3.2.2 Diarylethenes[38,39]

Diarylethenes are another promising group of photochromic compounds. The open (colourless / yellow) form is the synthetically produced isomer that converts to the more highly coloured closed form. Scheme 1.8 shows the typical structure of diarylethenes as well as the interconversion between the open and closed forms.

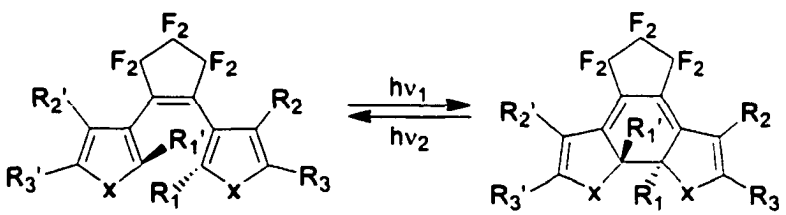

Scheme 1.8. Example of a diarylethene structure showing the interconversion between the open and closed isomers.

Several derivatives have been found to exhibit P-type photochromism (see above).[40] All open isomers have been found to be thermally stable. The coloured isomer's thermal stability was found to be dependent on the aryl group.[41,42] It was found that aryl groups with low aromatic stabilization energy (i.e. furan, thiophene, thiazole) lead to thermal stability while compounds containing aryl groups with higher aromatic stabilization energies (i.e. phenyl, pyrrole and indole) were thermally unstable.

These diarylethenes have also been shown to be remarkably resistant to photofatigue.[40,42-45] Derivatives with substitution at the 4-position of the aryl group (R_2, R_2', Scheme 1.8) can be switched repeatedly for more than 1000 cycles (in absence of oxygen). Response times (switching rate constants) have been determined by picosecond

and femtosecond laser flash photolysis (see above) to be on the order of 10 ps (10^{11} s^{-1}) in both solution and solid phase.[46-51]

Advantages of these types of switches are that they have a short synthetic route and they not only exhibit photochromism but also experience changes in other properties as a result of the switching.[52-68] These other properties include changes in their geometrical and electronic structures as well as changes in their refractive indices and chiral properties. Extension of these types of compounds into areas such as host-guest interactions,[59-62] photoelectrochemical switching,[64,65] liquid crystalline switches,[63] and photooptical switching (refractive index change)[66,67] are currently being studied.

1.4 History of Dimethyldihydropyrenes

Dimethyldihydropyrenes are 14π-electron annulenes with methyl groups on the carbons forming the transannular bond (Scheme 1.9). According to the Hückel 4n+2 rule of aromaticity, dimethyldihydropyrenes (DMDHPs) are aromatic. Indeed, it has been found that dimethyldihydropyrenes exhibit a ring current as evidenced by the chemical shifts for the internal methyl protons (-4 ppm), which are significantly shielded.[69] The protons on the periphery also experience the ring current but in this case it is a deshielding effect that gives them a chemical shift of about 8 ppm.

Dimethyldihydropyrenes have been found to be useful as aromaticity probes.[70-74] This is possible because the internal methyls are held at the center of the molecule and experience such a strong shielding effect due to the aromatic ring current. It has been found that the chemical shift of these methyl groups, as measured by proton NMR, is very sensitive to the nature of fused arene groups. This gives a handle for determining the relative aromaticity of various arene groups by comparison of the change in chemical shift upon fusion. Simple aryl substitution does not significantly affect the chemical shift of the internal methyl groups as it does not disrupt the DMDHP ring current.

Dimethyldihydropyrenes have also been found to undergo a valence isomerization to the 'open' metacyclophanediene (CPD) isomer (**1**, Scheme 1.9a).[75-77] The closed DMDHP absorbs strongly in the visible with bands in the 600-700 nm region. The CPD isomer, however, absorbs in the ultraviolet region and shows no appreciable absorption above 350 nm. The shift in absorption is due to the loss of conjugation in CPD as a result

of the phenyl rings no longer being planar with respect to one another (**1'**, Scheme 1.9a). Dimethyldihydropyrenes can be described as photochromic molecules as they undergo an isomerization between two forms, each with distinct absorption spectra.

This class of molecules currently falls under the category of T-type photochromism as the open CPD isomer is seen to thermally return to the more stable DMDHP isomer. In some cases, the metacyclophanediene isomer is the more stable of the two isomers.[78] In such a case the DMDHP is seen to thermally revert to the more stable CPD isomer. The energy difference between the two isomers can be modulated to some extent by substituents. Introduction of electron withdrawing groups in the 2-position of compound **1** has been shown to increase the thermal rate constant while electron donating groups such as methyl and t-butyl (**2**, Scheme 1.9b) have shown only a marginal decrease.[69,76] Simple substitution of compound **2** does not seem to have much of an effect, however, fusion of aromatic groups onto the [e]-face can significantly alter the thermal rate constant. The difference in enthalpy between the DMDHP isomer and the CPD isomer of **2** is ca. 3 kcal/mol.[77] This energy difference is seen to decrease to 1.1 kcal/mol for the benzo-[e] analog of **2** (**3**, Scheme 1.9c). The activation energy is seen to

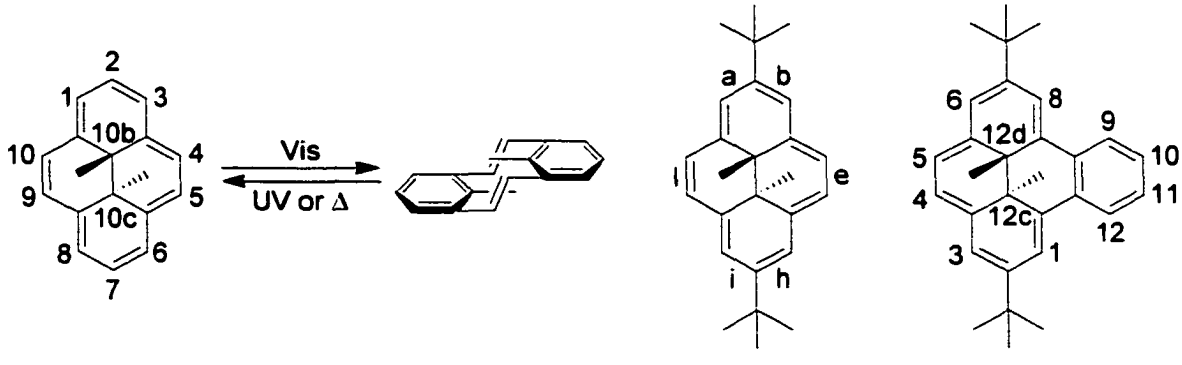

Scheme 1.9. (a) Isomerization between the closed dimethyldihydropyrene (DMDHP, **1**) and the open metacyclophanediene (CPD, **1'**), (b) 2,7-bis-t-butyl-dimethyldihydropyrene (2,7-di-*t*-butyl-DMDHP, **2**) and (c) benzo-[e]-DMDHP (**3**). The numbering of the carbons is illustrated on compounds **1** and **3** while the lettering of the faces is shown on compound **2**.

increase from 23 kcal/mol to 25 kcal/mol on going from **2** to **3**. This leads to a three-fold decrease in the thermal rate constant for **3**.[69]

The isomerization between DMDHP and CPD is classified as a 6π-electrocyclization. According to the Woodward-Hoffmann rules (see above), if this reaction is concerted, the conrotatory isomerization is allowed photochemically in both directions but the thermal return is forbidden. The thermal reaction is allowed if it proceeds in a disrotatory fashion, leading to the *cis*-dimethyldihydropyrene (Scheme 1.10). The fact that the thermal return occurs to give the *trans*-DMDHP implies that either the thermal return is not concerted or the Woodward-Hoffmann rules are not applicable. It has been suggested based on theoretical calculations that the thermal isomerization proceeds in a concerted fashion and represents a truly symmetry 'forbidden' reaction.[77,79] The forward thermal reaction is not seen.

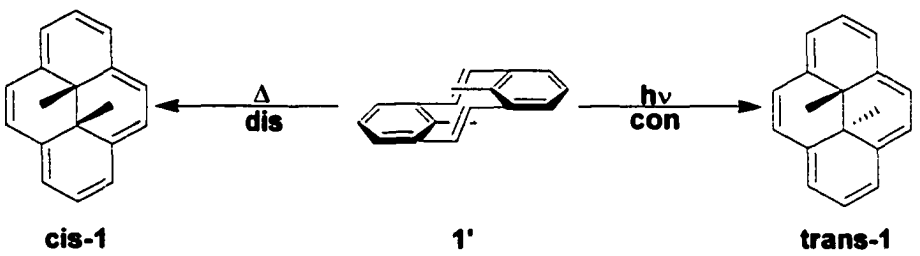

Scheme 1.10. Possible Woodward-Hoffmann allowed processes involving the conrotatory photochemical ring closure of *trans*-CPD to *trans*-DMDHP and the disrotatory thermal ring closure of *trans*-CPD to *cis*-DMDHP.

Currently synthesis is focused on t-butyl-DMDHP derivatives (**2**, Scheme 1.9b) because the system is more accessible than DMDHP.[80] Significant research has gone into the synthesis of several substituted dimethyldihydropyrenes, including multichromophoric architectures.[69,81] Much of the recent work in this area has concentrated on the use of fused aromatic groups as spacers between two DMDHPs utilizing compound **3** as a building block.[81]

Although the synthetic aspects of these systems have been well explored, the photophysical and photochemical processes have not been studied in detail. Some preliminary studies into the ring opening quantum yields have been performed.[76,82] It was suggested in the literature that the quantum yield for the ring opening reaction was

low although substitution with electron withdrawing groups (nitro, formyl, benzoyl) at the 2-position were shown to significantly increase the quantum yield relative to **1**. The ring closing quantum yield was quoted as being unity.[76] It has been argued that the photochemical reaction proceeds through the singlet excited state since oxygen was found to have no effect on the isomerization quantum yields.[76]

1.5. Research Objectives

The main goal of this research was to determine the isomerization mechanism through a comprehensive study of the photophysics and photochemistry of the dimethyldihydropyrene system. To this end, the effect of various substituents on the isomerization was studied. Determination of the transients involved in the switching will make it possible to design more efficient switches in the future.

Another of the objectives of this project was to synthesize compounds containing two dimethyldihydropyrene units separated by a conjugated spacer group. In this case an acetylene spacer was chosen as it eliminates any steric hindrance as seen with spacer groups previously employed such as benzene (interactions of hydrogens, *vide infra*). These types of compounds would also be prototypes for two switches connected by a *molecular wire* or *conjugated rod*.[83]

CHAPTER 2: SYNTHESIS

2.1 Introduction

The synthesis of 2,7-di-*t*-butyl-dimethyldihydropyrene (**2**) is well established and is shown in Scheme 2.1.[80] The synthesis starts from *p*-*t*-butyltoluene (**4**), which is bromomethylated at the 2- and 6- positions using trioxane, $ZnBr_2$ and HBr. Half of the bromide compound (**5**) is then converted to its corresponding thiol (**6**). Thiol-**6** is then condensed with the other half of bromide-**5** to give a mixture of syn and anti thiacyclophanes (**7**). A Stevens rearrangement of the latter leads to the ring contracted [2.2]cylcophanes (**8**). Methylation of the bridge –SMe using Borch reagent gives the

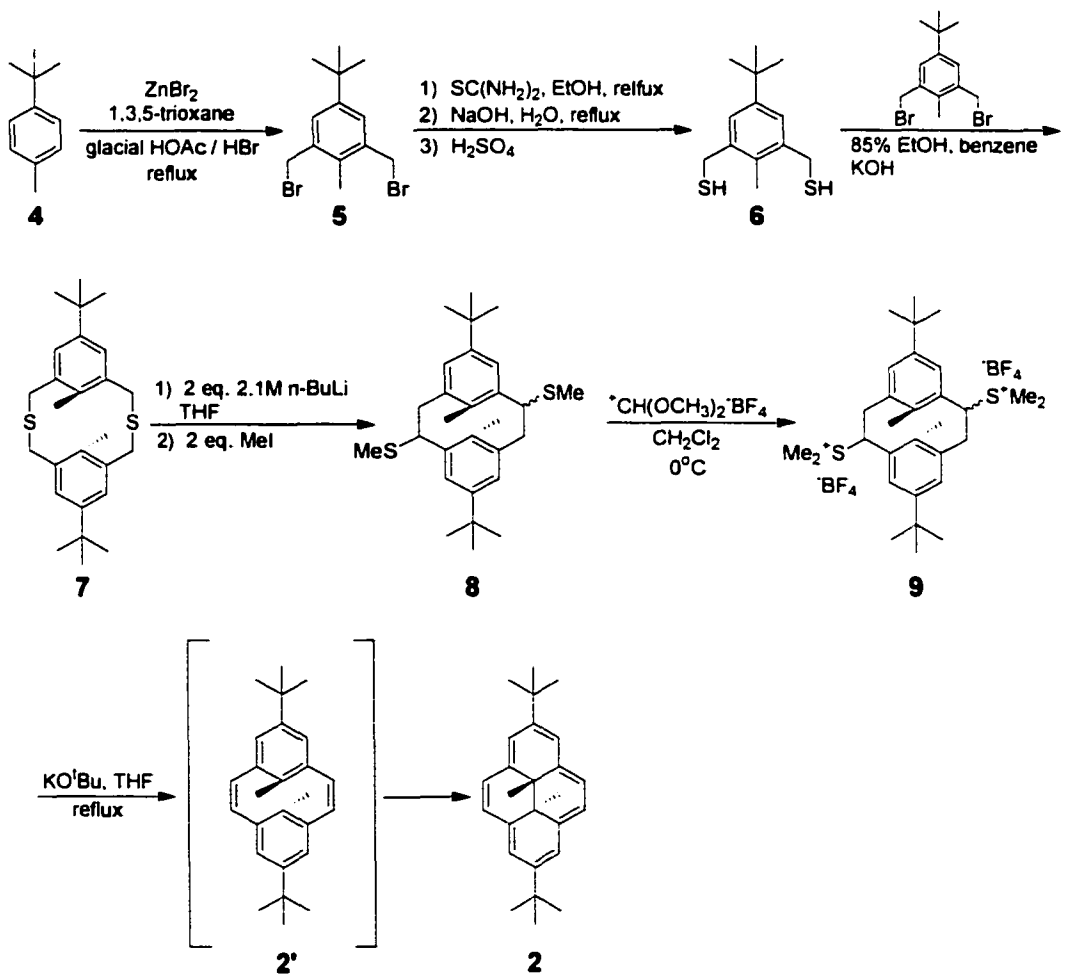

Scheme 2.1. Synthesis of 2,7-di-*t*-butyl-*trans*-10b,10c-dimethyl-10b,10c-dihydropyrene.[80]

corresponding cyclophane salts (**9**). Using the Hoffmann elimination on **9** gives the metacyclophanediene product (**2'**), which spontaneously converts to the dimethyldihydropyrene, **2**.

2.2 Single DMDHP Compounds

Very few dimethyldihydropyrenes have been studied in detail photochemically. An investigation into several simple substituted DMDHPs would provide the groundwork for an in depth study of more complicated structures containing multiple DMDHPs. In order to provide a comparison with other substituted DMDHPs previously synthesized,[69] the synthesis of several acetylene substituted dimethyldihydropyrenes was undertaken.

2.2.1 Iodination

Efficient coupling of a variety of groups to arenes can be achieved through a metal catalyzed halide coupling.[3,84] Generally, iodides are more reactive than bromides. In the case of **2**, the bromide is easily obtained using N-bromosuccinimide (NBS) in dimethylformamide (DMF) or dichloromethane.[78,85] However, the more useful iodide was unknown. Iodination of **2** was accomplished using I^+ generated from silver collidine hexafluorophosphate and iodine.[86] Careful control of the stoichiometry gives iodide **10** in 97% yield with a melting point of 156-157°C, but removal of the last traces of unreacted **2** was difficult. The structure of **10** is evident from the correct high resolution mass spectrum and the loss of I (M^+-127), and the two methyls (i.e. M^+-15, M^+-30) in the low resolution mass spectrum. The proposed structure is also supported by the differentiation of the internal methyl (-3.97 and –3.98 ppm) and t-butyl protons (1.66 and 1.70 ppm) in the NMR spectra.

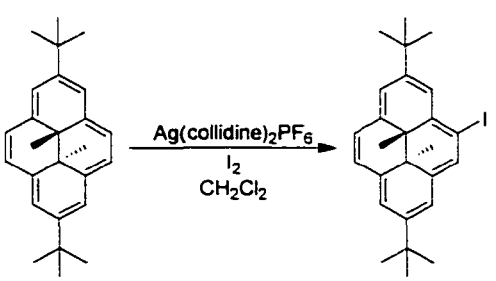

2 **10**

Scheme 2.2. Iodination of DMDHP.

2.2.2 Substitution with *i*-PrOH

When an alcohol group was directly attached to the DMDHP framework, the product was shown to be unstable. However, it was expected that a benzylic type alcohol would be isolable.[87] Thus, to determine the effect of such an alcohol on the photochemistry of the DMDHP system, the isopropyl substituted DMDHP-**11** was synthesized.

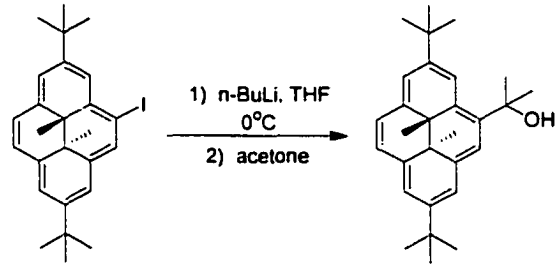

10 **11**

Scheme 2.3. Addition of acetone to DMDHP.

Lithiation of iodide **10** with n-butyl lithium (n-BuLi), followed by reaction with acetone gave the tertiary alcohol **11** in 45% yield. The structure was confirmed by high resolution mass spectrometry where a peak was seen at 402.2928 $g \cdot mol^{-1}$ corresponding to the mass calculated for $C_{29}H_{38}O$ of 402.2923 $g \cdot mol^{-1}$. The proton NMR showed the presence of the internal methyl groups at –3.90 and –3.97 ppm. The relatively large difference in chemical shift for the internal methyls indicates that an electronegative group has been incorporated in close proximity to the DMDHP framework. Peaks for the methyls adjacent to the alcohol (2.12 and 2.14 ppm) and the alcohol peak itself (2.41 ppm) were also seen in the proton NMR spectrum. The IR showed a characteristic alcohol peak at 3418 cm^{-1}. The absorption spectrum was not seen to change significantly from that of compound **2**. The melting point was found to be 165-166°C.

2.2.3 Acetylene Substitution

Acetylenes were chosen as rigid conjugating spacer groups to compare with other arene spacer groups. They were also chosen to determine the substituent effects of the

acetylene on the photochemistry of DMDHPs. This would afford a preliminary indication of the effect that incorporation of this type of species into a larger conjugated system, such as molecular wire type structures,[83] would have on the photochemistry.

2.2.3.1 Reaction with Phenylacetylene

The coupling of acetylenes to halogen substituted DMDHPs was accomplished via a Sonogashira coupling.[88,89] Phenylacetylene was used initially to determine the conditions required for the coupling. The reaction was carried out using 4-bromo- and 4,9-dibromo-DMDHP (Scheme 2.4, **12** & **13**). When phenylacetylene was used, 2.5 mole% $Pd(PPh_3)_2Cl_2$ (based on **12** / **13**) was used along with 2 mole% CuI (based on phenylacetylene) and the bromides **12** and **13**. The reaction was carried out in DMF and heated to 90°C for approximately 24 h. The coupled products were purified by column chromatography using hexanes as the eluant. The yields for compounds **14** and **15** were 64 and 66% respectively.

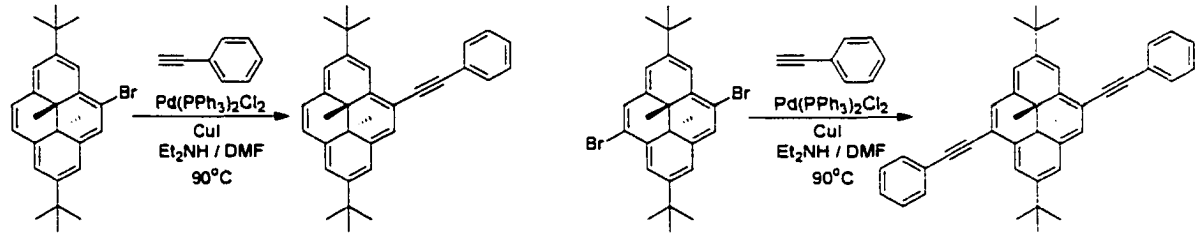

12 **14** **13** **15**

(a) (b)

Scheme 2.4. Sonogashira coupling of phenylacetylene with (a) 4-bromo-DMDHP (**12**) and (b) 4,9-dibromo-DMDHP (**13**).

High resolution mass spectrometry showed mass peaks at 444.2822 and 544.3140 g/mol^{-1} for compounds **14** and **15** as expected for $C_{34}H_{36}$ (444.2817 g·mol^{-1}) and $C_{42}H_{40}$ (544.3130 g·mol^{-1}). Proton NMR showed peaks for the internal methyl groups at –3.86 (**14**) and –3.70 ppm (**15**). It is interesting to note that there is only one internal methyl signal for **14** in the ^{1}H NMR, indicating that the shielding cone of the acetylene affects both internal methyl groups to a similar extent within the resolution of the instrument. Signals for the acetylene carbons were found at 90.45 and 94.72 ppm for **14** and at 90.10 and 95.24 ppm for **15** in the ^{13}C spectrum. The infrared spectra showed acetylene

stretches at 2191 cm^{-1} for compound **14** and at 2193 cm^{-1} for compound **15**. The melting point for **14** was found to be 180-181°C. Compound **15** had a melting point of 217-218°C. Elemental analysis for compound **14** confirmed the proposed product.

In the case of compound **15**, the NMR suggested the presence of about 15% of a byproduct, possibly where only one of the bromides reacted (Figure 2.1, **16**), which could not be separated from the product. Elemental analyses for compound **15** were calculated assuming the 15% impurity discussed above, and the elemental analysis obtained experimentally agreed with the calculations.

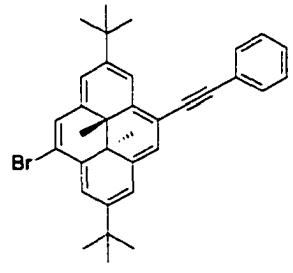

16

Figure 2.1. Possible byproduct from the Sonogashira coupling of bromide **13** and phenylacetylene.

The absorption spectrum for compound **14** showed a red shift of the major absorption bands from 341 and 387 nm (for compound **2**) to 357 and 395 nm (approximately 10 nm). The ratio of the molar absorptivity coefficient of the second major absorption band relative to the first major absorption band (0.89) was seen to increase when compared to the parent **2** (0.38). Compound **15** showed a similar shift in its absorption spectrum of approximately 20 nm to 369 nm and 411 nm. The molar absorptivity coefficient ratio (ε_{411} / ε_{369}) was seen to increase to 1.40. Perhaps the most significant effect in the absorption spectrum was seen with the long wavelength band that was found to shift to 667 (**14**) and 687 (**15**) nm from 641 nm (**2**). The molar absorptivity coefficients were also seen to increase from 900 $M^{-1}cm^{-1}$ for the parent (**2**) to 2130 and 3310 $M^{-1}cm^{-1}$ for compounds **14** and **15**.

2.2.3.2 Reaction with Methylbutynol

The incorporation of acetylene substituted DMDHPs into larger systems required a protected acetylene that could be reacted with the halogenated DMDHP, then deprotected and reacted at the other end with another compound. An isopropyl substituted acetylene was chosen as the first protected acetylene to be tested.

When 2-methylbut-3-yn-2-ol was used as the acetylene, the ratios of Pd(II) and Cu(I) were modified to 14% and 10% respectively (based on mole quantities of **12**/**13** and methylbutynol). The reactions with 4-bromo (**12**) and 4,9-dibromo-DMDHP (**13**) were preformed in the same manner as the phenylacetylene reactions and yielded similar results. The yields for compounds **17** and **18** were 35 and 60% respectively.

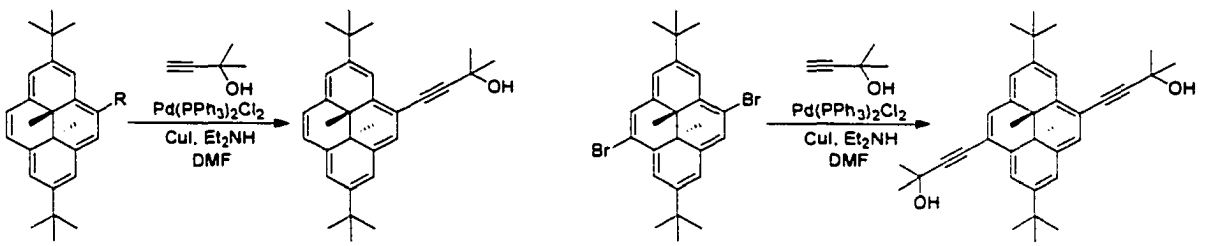

Scheme 2.5. Sonogashira coupling of methylbutynol with (a) 4-halo-DMDHP (**10**) and (b) 4,9-dibromo-DMDHP (**13**).

The proposed structures of the compounds were supported by mass spectrometry with mass peaks at 426.2928 and 508.3349 $g \cdot mol^{-1}$ corresponding to the calculated molecular weights of compounds **17** ($C_{31}H_{38}O$: 426.2923 $g \cdot mol^{-1}$) and **18** ($C_{36}H_{44}O_2$: 508.3341 $g \cdot mol^{-1}$) respectively. Proton NMR showed peaks for the internal methyls of compound **17** at –3.93 ppm. Signals were also detected at 1.851 and 1.854 ppm for the methyls of the protecting group and at 2.24 ppm for the alcohol. The internal methyls for compound **18** were found to produce a signal at –3.84 ppm while the signals for the methyls and alcohol of the protecting group were seen at 1.84 and 2.24 ppm respectively. Signals for the acetylene carbons were found to occur at 82.77 and 98.78 ppm for **17** and at 82.40 and 99.24 ppm for **18**. The IR for both compounds showed the characteristic alcohol peak at 3340 (**17**) and 3300 cm^{-1} (**18**). The acetylene stretches were also visible in the infrared spectrum at 2206 cm^{-1} for both compounds. Elemental analyses also

supported the proposed products. The melting points for compounds **17** and **18** were found to be 160-161°C and 199-200°C respectively.

The absorption spectra for compounds **17** and **18** showed similar trends as those seen for compounds **14** and **15**, namely a red shift of the major absorption bands. In the case of compound **17**, a shift to 353 (95800 $M^{-1}cm^{-1}$) and 391 (59000 $M^{-1}cm^{-1}$) nm was seen for the addition of an acetylene. Compound **18** showed a red shift to 361 (58700 $M^{-1}cm^{-1}$) and 399 (54400 $M^{-1}cm^{-1}$) nm. The ratio of the molar absorptivity coefficients for the second and first bands increased with the addition of methylbutynol (**17**: 0.62; **18**: 0.93), although the increase in ratios was more significant with the addition of phenylacetylene. The long wavelength absorption band for the methylbutynol substituted DMDHPs was also seen to shift to 663 nm (1740 $M^{-1}cm^{-1}$) for compound **17** and to 679 nm (2260 $M^{-1}cm^{-1}$) for compound **18**.

The reaction to produce compound **17** was repeated using 4-iodo-DMDHP (**10**, Scheme 2.5a). In this case, the reaction proceeded at room temperature so diethylamine was used as both the base and the solvent. The reaction proceeded cleanly and yielded 90% of the desired green isopropyl protected acetylene **17**. The work up for this reaction was the same as for the reaction of **12** and methylbutynol. The analysis and spectra were consistent with those previously mentioned.

2.2.4 Acetylene Deprotection

The deprotection of the acetylene substituted compound **17** was attempted next. Deprotection of methylbutynol with refluxing sodium iso-propoxide / isopropanol had been shown to be successful in the past although the yields were only about 57% and the reaction would not go to completion.[90] An alternative route for deprotection that used

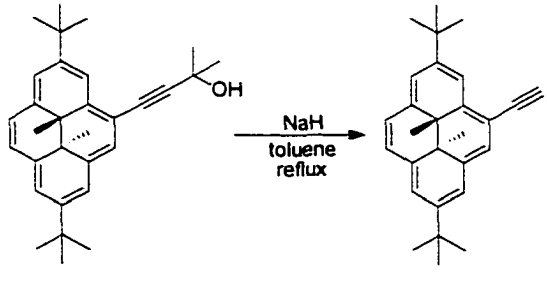

17 **19**

Scheme 2.6. Removal of acetone protecting group on the acetylene.

sodium hydride in refluxing toluene was found in the literature to work for systems such as **17**.[91] Although the conditions involved were quite harsh, the method was attempted to see if it resulted in improved yields over *i*-PrONa / *i*-PrOH deprotection.

When **17** was heated at 90°C in toluene with NaH for 4 hours, and then left for 12 hours at 20°C, deprotection was successful and gave 95% of **19** as green microcrystals. Confirmation of the product structure was obtained by elemental analysis and high resolution mass spectrometry, which showed a mass peak at 368.2501 $g \cdot mol^{-1}$ as expected for $C_{28}H_{32}$ (368.2504 $g \cdot mol^{-1}$). NMR spectra were run in benzene-d_6 to minimize decomposition. The proton spectrum showed signals for the internal methyl groups at –3.632 and –3.639 ppm. The acetylene proton was found at 3.50 ppm. The acetylene carbons gave signals at 82.52 and 84.67 ppm in the ^{13}C spectrum. The infrared spectrum showed the characteristic terminal acetylene stretch at 2085 cm^{-1} and the acetylene C-H stretch at 3282 cm^{-1}. The melting point was found to be 155-156°C.

The absorption spectrum of the deprotected product was essentially the same as that found for compound **17**. The first two absorption bands were found to shift to 351 and 389 nm and the molar absorptivities were slightly lower for **19** than those found for compound **17**. The long wavelength band for **17** was unaffected by the deprotection to give compound **19**.

2.3 Compounds Containing Bridged DMDHPs

The effect of having more than one DMDHP unit within a given compound was also of interest. Several compounds have been synthesized with fused aromatic spacers.[81] The draw back of such spacers is that there is an increased steric repulsion between the hydrogens on the arene spacer and the 3- and 6-hydrogens of the DMDHP portion (**20**, Figure 2.2) causing the molecule to twist and strain. This is similar to what is seen with biphenyl (**21**, Figure 2.2), although biphenyl can rotate to relieve the strain[84] while DMDHP cannot. Functionalization of such DMDHP systems has also been found to be more difficult and certain derivatives are sensitive to oxidation.

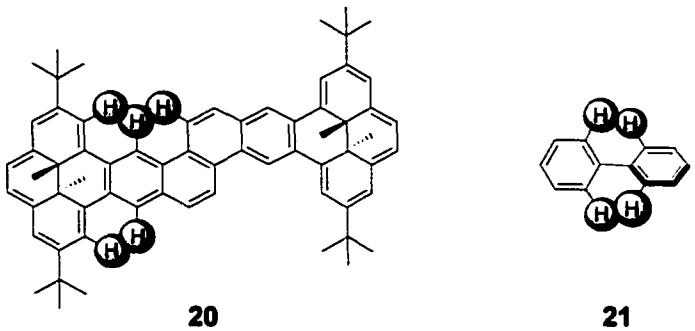

20 **21**

Figure 2.2. Illustration of possible steric repulsions in compounds containing DMDHPs fused together with arene spacer groups such as crysene (**20**). Also shown is the analogous steric interactions seen in biphenyl (**21**) for comparison.

Acetylenes alleviate steric repulsions and allow the possibility of the two DMDHP portions to adopt a planar configuration with respect to each another. However, the DMDHPs are not restricted to a planar configuration. The acetylenes still allow for extended conjugation despite the relative orientation of the DMDHP fragments.

2.3.1 Synthesis of DMDHP-(acetylene)$_2$-DMDHP

The easiest way of incorporating two DMDHP units separated by acetylenes into a single compound is through the homocoupling of compound **19**. Eglinton conditions, where a copper(II) catalyst is used, are useful for these types of couplings.[92] Compound **19** and copper acetate were stirred in pyridine at room temperature for about 24 hours. The reaction mixture was then subjected to an aqueous workup and chromatographed using 1:1 hexanes/CH_2Cl_2. Recrystallization of the orange-brown solid in hexane gave dark brown microcrystals of **22**.

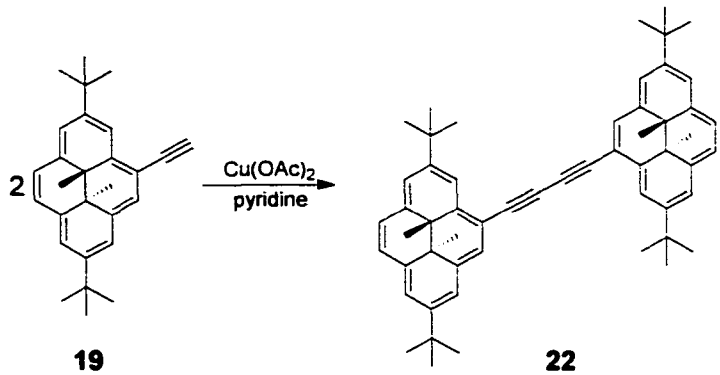

19 **22**

Scheme 2.7. Homocoupling of acetylene substituted DMDHPs.

The structure of **22** was confirmed by elemental analysis and electron impact mass spectrometry. An M^+ peak was seen at 735 as expected. The proton NMR spectrum showed a signal for the internal methyls at –3.81 ppm. The acetylene peaks could be found in the carbon spectrum at 80.11 and 84.55 ppm. A peak at 2131 cm^{-1} in the infrared spectrum corresponded to the acetylene stretch. The melting point of **22** was found to be 206-207°C.

The absorption spectrum was seen to be different from compound **19**, indicating that there was extended conjugation in the system. The first absorption band was seen to remain at 353 nm (74500 $M^{-1}cm^{-1}$) while the second absorption band was red shifted by 30 nm to 421 nm (77600 $M^{-1}cm^{-1}$). The longest wavelength absorption band occurred at 673 nm. This was intermediate between the mono- and di-substituted acetylene compounds mentioned above. The molar absorptivity coefficient for the 673 nm band was 6840 $M^{-1}cm^{-1}$, which is significantly higher than any of the other compounds above and more than twice that of **19**.

2.3.2 Attempted DMDHP-acetylene-DMDHP Synthesis

The synthesis of a compound containing two DMDHPs separated by a single acetylene (**23**) was also of interest. At first glance, one would expect the Sonogashira coupling conditions that were used for the synthesis of the acetylene compounds above, to be applicable here. Unfortunately, the Sonogashira coupling conditions also lead to a large amount of homocoupled product (**22**). Compound **22** and compound **23** are inseparable by chromatographic means. Recrystallization from various solvent systems was also unsuccessful in separating the two compounds.

The synthesis of the above compound was abandoned as it was shown from the photochemical studies on compound **22** (vide infra) that photoisomerization is shut down. This is either due to a significant increase in the thermal rate or a decrease in the quantum yield of ring opening.

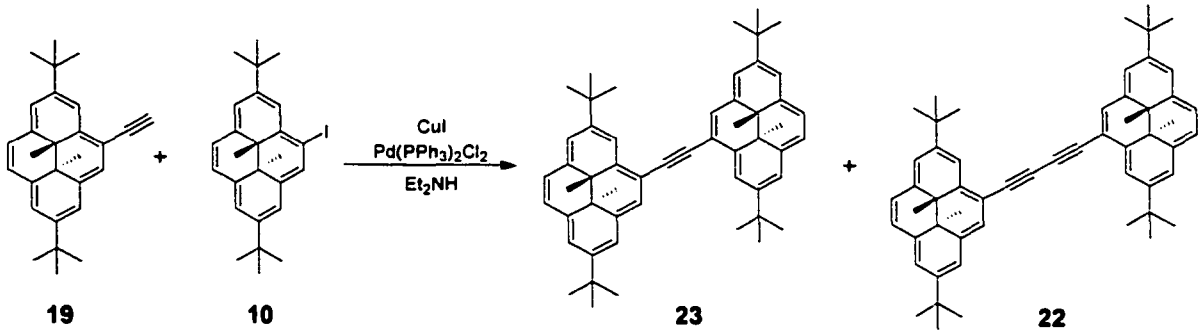

19 10 23 22

Scheme 2.8. Attempted synthesis of compound **23** using the conditions for the Sonogashira coupling of **10** and **19**. Also shown is the byproduct **22**.

2.4 Experimental

2.4.1 Equipment

Melting points were determined on a Reichart 7905 melting point apparatus integrated to an Omega Engineering Model 199 chrome-alumel thermocouple. Infrared spectra were recorded on a Perkin Elmer Spectrum One FT-IR spectrometer.

Proton and carbon NMR spectra were recorded using $CDCl_3$ as solvent (unless otherwise specified) on a Bruker AMX 360 (^1H, 360 MHz; ^{13}C, 90.6 MHz) spectrometer. Spectra were calibrated using the residual solvent peaks. ^1H NMR assignments were made on the basis of 2D COSY and NOESY experiments. Expanded data sets were obtained in order to determine coupling constant data where applicable. ^{13}C NMR assignments were made based on HETCOR and DEPT experiments.

Mass spectra were recorded on a Finnigan 3300 gas chromatography-mass spectroscopy system using methane gas for chemical ionization. Exact mass measurements were obtained on a Kratos Concept-H instrument using perfluorokerosene as the standard. Canadian Microanalytical Services Ltd., Vancouver, BC, carried out elemental analyses.

Extracts were dried with anhydrous magnesium sulphate unless otherwise stated and evaporations were carried out on a rotary evaporator or a vacuum line equipped with an oil pump and dry ice condenser. The silica gel (SiGel, Merck) used was 60-200 mesh.

2.4.2 Synthesis

2,7-Di-*t*-butyl-4-iodo-*trans*-10b,10c-dimethyl-10b,10c-dihydropyrene (10). Iodine (383 mg, 1.5 mmol) was added to a stirred solution of $Ag(collidine)_2PF_6$ (740 mg, 1.5 mmol) in anhydrous CH_2Cl_2 (120 mL) under argon. Once precipitation of AgI was complete, DMDHP **2** (500 mg, 1.45 mmol) was added and the reaction was allowed to stir at room temperature for 24 h. Aqueous $NaHSO_4$ (10%, ~100 mL) was then added and the reaction mixture was stirred for an additional 5 min. The mixture was filtered through Celite, and hexanes (150 mL) was added to the filtrate. The organic layer was separated, washed with aqueous HCl (10%, 4 × 100 mL) followed by H_2O (2 × 100 mL), dried over $MgSO_4$ and concentrated under reduced pressure to yield (660 mg, 97%) of iodide **4** as dark green crystals, mp 156-157°C. ^1H NMR ($CDCl_3$): δ 8.89 (s, 1H, H-3), 8.64 (s, 1H, H-5), 8.54 (s, 2H, H-1, 6), 8.46 (s, 2H, H-9, 10), 8.44 (s, 1H, H-8), 1.70 (s, 9H, $-C(CH_3)_3$), 1.66 (s, 9H, $-C(CH_3)_3$), -3.97 (s, 3H, $CH_{3\ INT}$), -3.98 (s, 3H, $CH_{3\ INT}$) ppm. ^{13}C NMR ($CDCl_3$): δ 147.60, 146.67, 137.78, 137.45, 135.29, 132.46, 126.14, 123.68, 123.40, 122.65, 121.84, 121.48, 120.15, 92.28, 36.20, 36.01, 31.95, 31.87, 29.75, 14.58, 13.98. UV (cyclohexane): λ_{max}, nm (ε, $M^{-1}cm^{-1}$) 348 (8.58×10^4), 387 (4.82×10^4), 482 (1.13×10^4), 650 (1.40×10^3). IR (KBr): 2957 (s), 1377 (m), 1229 (m), 882 (s), 671 (m) cm^{-1}. CI MS *m/z* 471 (MH^+). HRMS, calculated for (M^+) 470.1471. Found, 470.1475.

2-(2,7-Di-*t*-butyl-*trans*-10b,10c-dimethyl-10b,10c-dihydropyren-4-yl)propan-2-ol (11). n-BuLi (43μL, 0.11 mmol, 2.5M in hexane) was added dropwise to a stirred solution of iodide **10** (50 mg, 0.11 mmol) in dry THF (100 mL) at 0°C under argon. After the addition was complete, the solution was stirred for 20 minutes. Acetone (excess) was then added to the solution, the ice bath was removed and the solution was stirred at room temperature overnight. Hexanes (100 mL) and H_2O (100 mL) were added to the reaction mixture. The organic layer was separated, washed with H_2O (3 × 100 mL), dried over $MgSO_4$ and concentrated under reduced pressure. The resulting green solid was chromatographed (SiGel, CH_2Cl_2) and yielded 20 mg (45%) of alcohol **11** as a green powder, mp 165-166°C. ^1H NMR ($CDCl_3$): δ 9.45 (d, 1H, J=1.1 Hz, H-3), 8.62 (s, 1H, H-5), 8.48 (br s, 1H, H-1), 8.438 (AB, 1H, J=5.8 Hz, H-9 or H-10), 8.434 (AB, 1H,

J=5.8 Hz, H-9 or H-10), 8.34 (s, 2H, H-6, 8), 2.41 (s, 1H, OH), 2.14 (s, 3H, CH_3), 2.12 (s, 3H, CH_3), 1.67 (s, 9H, $-C(CH_3)_3$), 1.66 (s, 9H, $-C(CH_3)_3$), -3.90 (s, 3H, $CH_{3\ INT}$), -3.97 (s, 3H, $CH_{3\ INT}$) ppm. ^{13}C NMR ($CDCl_3$): δ 145.50, 144.64, 138.50, 137.67, 136.46, 136.03, 131.63, 122.68, 122.29, 121.55, 121.29, 121.13, 120.43, 120.23, 76.65, 36.17, 35.85, 32.83, 32.67, 31.92, 31.88, 29.39, 14.52, 14.39. UV (cyclohexane): λ_{max}, nm (ε, $M^{-1}cm^{-1}$) 344 (7.73×10^4), 383 (3.57×10^4), 483 (9.09×10^3), 649 (8.42×10^2). IR (KBr): 3418 (m), 2957 (s), 1593 (w), 1462 (w), 1360 (m), 1232 (m), 882 (m), 796 (w), 666 (m). HRMS, calculated for (M^+) 402.2923. Found, 402.2928. Anal. Calc'd for $C_{29}H_{38}O \cdot H_2O$: C, 82.81; H, 9.59. Found: C, 82.79; H, 9.61.

2,7-Di-*t*-butyl-4-(2-phenylethynyl)-*trans*-10b,10c-dimethyl-10b,10c-dihydropyrene (14). Phenyl acetylene (65 μL, 60 mg, 0.59 mmol), CuI (3 mg, 0.012 mmol) and $Pd(PPh_3)_2Cl_2$ (4 mg, 0.0059 mmol) were added to a stirred solution of bromide **12** (100 mg, 0.24 mmol) in anhydrous DMF/Et_2NH (30/5 mL) under argon. The reaction was heated to 90°C for 24 h. The reaction mixture was cooled to room temperature and hexanes/CH_2Cl_2 (6:1, 50 mL) was added. The organics were separated and washed with H_2O (6 × 100 mL), dried over $MgSO_4$ and concentrated under reduced pressure. The resulting green powder was subjected to chromatography (SiGel, hexanes) to afford 10 mg (0.024 mmol) of unreacted bromide **12** and 60 mg (64%) of acetylene substituted **14** as a pale green powder, mp 180-181°C. ^1H NMR ($CDCl_3$): δ 9.10 (d, 1H, J=1.2 Hz, H-3), 8.63 (s, 1H, H-5), 8.52 (d, 1H, J=1.4 Hz, H-1), 8.50 (s, 2H, H-6, 8), 8.45 (AB, 1H, J=8.4 Hz, H-9 or 10), 8.42 (AB, 1H, H-9 or 10), 7.77-7.74 (m, 2H, Ph-H_o), 7.46-7.35 (m, 3H, Ph-H_m, Ph-H_p), 1.72 (s, 9H, $-C(CH_3)_3$), 1.67 (s, 9H, $-C(CH_3)_3$), -3.86 (s, 6H, $CH_{3\ INT}$) ppm. ^{13}C NMR ($CDCl_3$): δ 147.20, 146.26, 138.31, 137.58, 136.98, 135.84, 131.52, 128.49, 127.90, 125.32, 124.30, 123.90, 123.36, 121.79, 121.36, 121.00, 119.59, 114.06, 94.72, 90.45, 36.26, 35.95, 31.94, 31.87, 30.42, 29.54, 14.98, 14.63. UV (cyclohexane): λ_{max}, nm (ε, $M^{-1}cm^{-1}$) 309 (1.68×10^4), 357 (7.45×10^4), 395 (6.60×10^4), 495 (1.08×10^4), 667 (2.13×10^3). IR (KBr): 2959 (s), 2191 (w), 1594 (m), 1358 (m), 1343 (m), 882 (s), 757 (s), 691(m), 665 (m) cm^{-1}. HRMS, calculated for (M^+) 444.2817. Found, 444.2822. Anal. Calc'd for $C_{34}H_{36}$: C, 91.84; H, 8.16. Found: C, 89.43; H, 7.76.

2,7-Di-*t*-butyl-4,9-bis-(2-phenylethynyl)-*trans*-10b,10c-dimethyl-10b,10c-dihydropyrene (15). Phenyl acetylene (106 μL, 114 mg, 1.12 mmol), CuI (4 mg, 0.022 mmol) and $Pd(PPh_3)Cl_2$ (5 mg, 0.0073 mmol) were added to a stirred solution of dibromide **13** (150 mg, 0.29 mmol) in anhydrous DMF/Et_2NH (40/5 mL) under argon. The reaction was heated to 90°C for 24 h. The reaction mixture was cooled to room temperature and hexanes/CH_2Cl_2 (6:1, 50 mL) was added. The organics were separated and washed with H_2O (6 × 100 mL), dried over $MgSO_4$ and concentrated under reduced pressure. The resulting brown powder was subjected to chromatography (SiGel, hexanes) to give a 15:85 mixture of bromide **16** and bis-acetylene **15** (104 mg, 66 %), mp 217-218°C. ^1H NMR ($CDCl_3$): δ 9.09 (d, 2H, J=1.4 Hz, H-3, 8), 8.65 (d, 2H, J=0.5 Hz, H-5, 10), 8.52 (br s, 2H, H-1, 6), 7.77-7.73 (m, 4H, Ph-H_o), 7.47-7.38 (m, 6H, Ph-H_m, Ph-H_p), 1.71 (s, 18H, -$C(CH_3)_3$), -3.70 (s, 6H, CH_3 $_{INT}$) ppm. ^{13}C NMR ($CDCl_3$): δ 147.70, 137.49, 137.35, 131.57, 128.54, 128.10, 126.17, 124.09, 121.83, 120.83, 115.35, 95.24, 90.10, 36.24, 31.90, 30.29, 15.20. UV (cyclohexane): λ_{max}, nm (ε, $M^{-1}cm^{-1}$) 297 (1.87×10^4), 369 (4.38×10^4), 411 (6.13×10^4), 520 (1.26×10^4), 687 (3.31×10^3). IR (KBr): 3042 (w), 2957 (s), 2193 (w), 1593 (m), 1488 (m), 1436 (m), 1385 (m), 1357 (m), 1232 (m), 893 (m), 751 (s), 686 (s), 663 (m), 526 (m). HRMS, calculated for (M^+) 544.3130. Found, 544.3140. Anal. Calc'd for $0.85(C_{42}H_{40})\cdot 0.15(C_{34}H_{35}Br)$: C, 90.48; H, 7.31. Found: C, 90.07; H, 7.76.

4-[2,7-Di-*t*-butyl-*trans*-10b,10c-dimethyl-(10b,10c-dihydropyren-4-yl)]-2-methylbut-3-yn-2-ol (17). To a stirred solution of iodide **10** (400 mg, 0.85 mmol) in degassed Et_2NH (150 mL) was added 2-methylbut-3-yn-2-ol (612 mg, 572 μL, 6.8 mmol), CuI (130 mg, 0.68 mmol) and $Pd(Ph_3)_2Cl_2$ (84 mg, 0.12 mmol) under argon. The reaction was stirred at room temperature and monitored by thin layer chromatography. Upon completion, H_2O (150 mL) and hexanes/CH_2Cl_2 (1:1, 200 mL) were added to the reaction mixture. The organics were separated, washed with H_2O (6 × 100 mL), dried over $MgSO_4$ and concentrated under reduced pressure. The resulting oil was chromatographed (SiGel, CH_2Cl_2) to give 299 mg (90%) of acetylene **17** as a green solid, mp 160-161°C.

10^3), 662 (1.71 × 10^3). IR (KBr): 3282 (s), 3042 (w), 2962 (s), 2085 (w), 1596 (w), 1380 (m), 1229 (m), 885 (s), 788 (m), 683 (m), 660 (m), 600 (m). HRMS, calculated for (M^+) 368.2504. Found, 368.2501. Anal. Calc'd for $C_{28}H_{32}$: C, 91.25; H, 8.75. Found: C, 90.90; H, 8.55.

4-[2,7-Di-*t*-butyl-9-(3-hydroxy-3-methylbut-1-ynyl)-*trans*-10b,10c-dimethyl-10b,10c-dihydropyren-4-yl]-2-methylbut-3-yn-2-ol (18). 2-Methylbut-3-yn-2-ol (323 mg, 345 μL, 3.84 mmol), CuI (72 mg, 0.38 mmol) and $Pd(PPh_3)_2Cl_2$ (48 mg, 0.067 mmol) were added to a stirred solution of dibromide **13** (240 mg, 0.48 mmol) in DMF/Et_2NH (50/5 mL) under argon. The reaction mixture was heated to 90°C and monitored by TLC (~21 h). Upon completion, the solution was cooled to room temperature and hexanes/CH_2Cl_2 (6:1, 200 mL) were added. The organics were washed with H_2O (6 × 100 mL), dried over $MgSO_4$ and concentrated under reduced pressure. The resulting brown oil was chromatographed (SiGel, 1:1 hexanes/CH_2Cl_2 → 1:1 CH_2Cl_2/EtOAc, 10% polarity intervals (100 mL)) and yielded, upon recrystallization in hexanes/CH_2Cl_2 (50:1), 146 mg (60 %) of **18** as dark orange crystals, mp 199-200°C. ^{1}H NMR ($CDCl_3$): δ 8.915 (s, 1H, H-3), 8.911 (s, 1H, H-8), 8.50 (s, 2H, H-5, 10), 8.46 (s, 2H, H-1, 6), 2.24 (s, 2H, OH), 1.84 (s, 12H, CH_3), 1.67 (s, 18H, -$C(CH_3)_3$), -3.84 (s, 6H, CH_3 $_{INT}$) ppm. ^{13}C NMR ($CDCl_3$): δ 147.56, 137.39, 137.06, 126.13, 121.73, 120.54, 114.69, 99.24, 82.40, 66.16, 36.18, 31.90, 31.83, 29.99, 14.88. UV (cyclohexane): λ_{max}, nm (ε, $M^{-1}cm^{-1}$) 361 (5.87 × 10^4), 399 (5.44 × 10^4), 503 (8.49 × 10^3), 679 (2.26 × 10^3). IR (KBr): 3300 (br, m), 2959 (s), 2206 (w), 1380 (m), 1358 (m), 1255 (m), 1166 (m), 952 (m), 890 (m), 661 (m) cm^{-1}. HRMS, calculated for (M^+) 508.3341. Found, 508.3349. Anal. Calc'd for $C_{36}H_{44}O_2 \cdot 0.5(CH_2Cl_2)$: C, 79.53; H, 8.23. Found: C, 79.96; H, 8.47.

2,7-Di-*t*-butyl-4-[4-(2,7-di-*t*-butyl-*trans*-10b,10c-dimethyl-10b,10c-dihydropyren-4-yl)buta-1,3-diynyl]-10b,10c-dihydropyrene (22). A solution of acetylene **19** (100 mg, 0.271 mmol) and $Cu(OAc)_2$ (50 mg, 0.28 mmol) in pyridine (30 mL) was stirred at room temperature and monitored by TLC (~ 24 h). Upon completion, the reaction was poured onto H_2O (100 mL) and extracted with hexanes (100mL). The organic layer was then washed with aqueous HCl (3 × 100 mL), aqueous $NaHCO_3$ (3 × 100 mL) and H_2O (6 ×

100 mL), separated, dried over $MgSO_4$ and concentrated under reduced pressure. The resulting orange-brown solid was subjected to column chromatography (SiGel, 1:1 hexanes/CH_2Cl_2), which, upon recrystallization in hexanes yielded 86 mg (86%) of acetylene **22** as dark brown microcrystals, mp 206-207°C. ^{1}H NMR ($CDCl_3$): δ 9.14 (d, 2H, J=1.3 Hz, H-3, 3'), 8.70 (s, 2H, H-5, 5'), 8.55 (d, 2H, J=1.2 Hz, H-1, 1'), 8.53 (s, 4H, H-6, 6', 8, 8'), 8.47 (AB, 2H, J=8.1 Hz, H-9 or H-10, H-9' or H-10'), 8.44 (AB, 2H, H-9 or H-10, H-9' or H-10'), 1.77 (s, 18H, -C(CH_3)$_3$), 1.68 (s, 18H, -C(CH_3)$_3$), -3.81 (s, 12H, CH_3 $_{INT}$) ppm. ^{13}C NMR ($CDCl_3$): δ 148.09, 146.45, 139.48, 138.98, 137.06, 135.76, 125.83, 124.31, 123.53, 122.24, 121.51, 121.21, 119.77, 112.93, 84.45, 80.11, 36.37, 35.98, 32.01, 31.88, 30.74, 29.56, 15.12, 14.80. UV (cyclohexane): λ_{max}, nm (ε, $M^{-1}cm^{-1}$) 282 (2.10×10^4), 353 (7.45×10^4), 421 (7.76×10^4), 479 (2.50×10^4), 611 (1.36×10^3), 673 (6.84×10^3). IR (KBr): 2945 (s), 2131 (w), 1630 (m), 1590 (m), 1459 (m), 1439 (m), 1382 (m), 1343 (m), 1229 (m), 1115 (m), 893 (m), 794 (w), 680 (m), 660 (m). EI MS *m/z* 735 (M^+). Anal. Calc'd for $C_{56}H_{62}$: C, 91.50; H, 8.50. Found: C, 91.54; H, 8.60.

CHAPTER 3: PHOTOPHYSICAL / PHOTOCHEMICAL EXPERIMENTAL

3.1 Common Reagents and Equipment

Spectrograde cyclohexane (CHX), acetonitrile (ACN), and toluene (Caledon Laboratories Ltd.) were used without further purification. All compounds were tested for purity using a HP Series 1100 High Performance Liquid Chromatography (HPLC) spectrometer using a Zorbax biphenyl column. The HPLC was equipped with an auto-sampling unit, a diode array detector (DAD) and a fluorescence detector (FLD). Peak purity was determined by comparing the degree of overlap of the absorption spectrum determined at different times within a peak. All data acquisition, instrument control, and data analysis was carried out with HP Chemstation software operating under a Microsoft Windows environment.

3.2 Absorption

A Varian Cary 1 or Cary 5 spectrometer was employed to measure UV-Vis absorption spectra at room temperature. The scan rate was set to 1200 nm/min and baseline corrections were always performed.

3.2.1 Molar Absorptivity Coefficient Determinations

Molar absorptivity coefficients were determined by preparing serial dilutions of a stock solution and measuring the corresponding absorbance for each major absorption band. At least three concentrations per absorption band were measured. By plotting the absorption measured against the concentration of the solution (Beer-Lambert law, equation (1.2)), it was possible to determine the molar absorptivities for the absorption bands of each compound.

3.2.2 Isomerization Quantum Yields

Isomerization quantum yields were performed using an Oriel 200 W high-pressure mercury lamp with a monochromator for irradiation. The cell holder is held at a constant position from the lamp for all measurements. A shutter, controlled by a timer, was used to accurately irradiate the samples for specific periods of time. The potassium

ferrioxalate actinometer was used as a primary standard [5-7] and compound **1** was used as a secondary standard.

Unknown solutions of DMDHP were prepared in CHX with an absorbance of at least 2 at the excitation wavelength so that all photons incident on the sample were absorbed. The excitation had to be kept above 350 nm to ensure that the CPD formed would not absorb. Potassium ferrioxalate solutions were prepared as indicated in the literature.[6,7] Exactly 3.00 mL of solution were placed in each 1.00 cm × 1.00 cm quartz cell. Every quantum yield value is the average of two independent experiments, each of which consists of at least 2 individual measurements. The solutions were bubbled with oxygen or nitrogen for at least 30 min.

Solutions for the measurement of the ring closing isomerization quantum yields were prepared by irradiating samples of the DHP isomer until conversion to the CPD isomer was greater than 90% as monitored by UV-Vis absorption spectroscopy.

All samples of DMDHPs or CPDs were irradiated such that the conversion being measured was kept below 20%. Standard and unknown solutions were alternated in their irradiation to account for any fluctuation in lamp emission intensity. This ensured that an accurate value for the photon flux was measured.

Quantum yields of isomerization were calculated by measuring the change in absorption at a given wavelength before and after irradiation. Equation (3.1) shows how the change in absorption is related to the quantum yield of isomerization.[6,7,9]

$$\phi_u = \frac{\phi_s \varepsilon_s \Delta A_u V_u t_s}{\varepsilon_u \Delta A_s V_s t_u} \qquad \textbf{Equation (3.1)}$$

where ϕ is the quantum yield for the standard (s) and the unknown (u), ε is the molar absorptivity at the monitoring wavelength, ΔA is the change in absorbance at the monitoring wavelength, V is the volume of solution in the cell, and t is the irradiation time.

When potassium ferrioxalate is used as the standard, a dilution is needed after the initial irradiation.[6,7] Substitution of V_s by (V_1V_3/V_2) gives equation (3.2).

$$\phi_u = \frac{\phi_s \varepsilon_s \Delta A_u V_u V_2 t_s}{\varepsilon_u \Delta A_s V_1 V_3 t_u}$$ **Equation (3.2)**

where V_1 is the initial volume in the 1.00 × 1.00 cm cell (3.00 mL), V_2 is the volume of solution taken from the irradiated sample (1.00 mL) and V_3 is the final dilution volume (10.00 mL).

3.3 Fluorescence

3.3.1 Steady-State Measurements

Steady-state fluorescence measurements were collected with a Photon Technology International (PTI) QuantaMaster (QM-2) Luminescence spectrofluorimeter. The sample compartment was maintained at (20.0 ± 0.5)°C using a Haake F3 temperature control bath. A 75 W Xenon lamp was used for excitation. The slits were set such that the bandpass was 3 nm. Felix software was used to obtain the spectra. The step size used was 0.5 nm and the integration time was set to 0.25 s. Low temperature fluorescence measurements were recorded with the same parameters as the room temperature measurements.

3.3.1.1 Emission and Excitation

Solutions for room temperature fluorescence emission and excitation spectra were prepared in aerated CHX with an absorbance of approximately 0.1 at the excitation wavelength. The excitation wavelengths used for all DMDHP isomers were between 470 and 550 nm. The emission scans were recorded between at least 580 and 800 nm and were corrected for Raman artifacts from the solvent and baseline. The metacyclophanediene (CPD) isomers were excited between 250 and 300 nm with the emission being scanned between at least 330 and 500 nm. Measurements were performed using 1.00 cm × 1.00 cm quartz fluorescence cells.

Solutions for low temperature measurements were prepared in toluene with an absorbance at the excitation wavelength of 0.1 (in a 1.00 cm ×1.00 cm cell). All solutions were de-oxygenated by bubbling nitrogen for at least 30 min. A 2 mm (internal

diameter) pathlength cylindrical quartz cell containing the compound in solution was slowly inserted into a custom quartz Dewar filled with liquid nitrogen to form a low temperature glass. Care was taken to ensure that no cracks in the glass were formed.

3.3.1.2 Fluorescence Quantum Yields

Fluorescence quantum yields were measured using $Ru(bipy)_3Cl_2$ as a primary standard.[93] Compound **2** was then used as a secondary standard. All solutions for the quantum yield measurements were prepared to give a matched absorbance (± 0.002) of approximately 0.1 in aerated CHX at the wavelength of excitation in a 1.00 cm × 1.00 cm quartz fluorescence cell. At least two matched serial dilutions were made to obtain a minimum of three data points for each measurement. Equation (3.3) shows the relationship between the fluorescence quantum yield and emission area.[94]

$$\phi_f = \frac{\phi_s A_s F_u \eta_u^2}{A_u F_s \eta_s^2} \qquad \textbf{Equation (3.3)}$$

where ϕ_x is the fluorescence quantum yield of the standard (s) or unknown (f), A is the absorbance at the excitation wavelength, F is the area of the emission spectrum and η is the refractive index of the solvent.

3.3.2 Time-Resolved Measurements

Fluorescence lifetimes were measured using two different methods. The first was using a Ti:sapphire picosecond system equipped with a Hamamatsu streak camera detection system, which simultaneously collects the decay and emission spectra. The cells used were 1.00 × 1.00 cm quartz cells. The excitation wavelength was (414 ± 4) nm, and the polychrometer slit was set at 100 μm. All measurements were carried out at (20 ± 2°C). The binarization mode on the streak camera, with a threshold of 12, was employed for data collection. The counts per cycle were kept below 0.1 for the sample and the instrument response function (IRF) to avoid the collection of more than one photon per pixel. The IRF was obtained by collecting the scattering of the laser light by a sample containing only CHX. The number of acquisition cycles was set to obtain at least

10^4 counts for the intensity maximum between the wavelengths integrated. The lifetimes were obtained by deconvoluting the IRF from the decay of the sample using the Hamamatsu analysis software. A χ^2 value of less than 6.0 was acceptable, since a photon detected by the streak camera target covers more than one pixel.[95]

Time-correlated single photon counting (SPC) was also used to obtain lifetimes. The lifetimes were measured using a Photon Technology International LS-1 time-correlated single photon counter. A hydrogen plasma lamp was used as the nanosecond excitation source. A Lauda Super RMS-6 temperature control unit maintained the sample compartment at (20.0 ± 0.1)°C. Slit widths were set such that the scatterer (aqueous silica gel solution) led to less than 2% of stop events compared to the number of start events. The scatterer was used to obtain a lamp profile. This lamp profile was deconvoluted from the decay trace. Scans were collected until 10^4 counts in the channel of maximum intensity were obtained. Lifetimes were measured in custom-made Suprasil quartz cells (approximately 1 cm × 1 cm). Excitation and emission wavelengths were set according to data obtained for each compound by steady-state methods. The traces were analyzed and fit to single exponential decays using the PTI software. Satisfactory fits were determined by examination of the residuals as well as the fit statistics. Three statistical parameters were used: the Durbin-Watson Parameter (DW), which should be greater than 1.7; the Runs Test Parameter (Z), which should be greater than -1.96 for a 95% confidence level; the Chi squared (χ^2) value, which should be in the range of 0.9-1.2. The residuals gave an indication of how close the data points lie to the fit line.

3.4. Laser Flash Photolysis

3.4.1 Experimental Setup

Transient kinetics and spectral data were recorded using pulses from a Nd:YAG laser (GCR-12) at 266, 355 or 532 nm, from an Infinity OPO tunable laser, or from a Lumonics (EX-510) excimer laser at 308 nm. Full details on signal detection, monitoring and data processing have been previously published.[96] Figure 3.1 shows the experimental setup for the LFP systems.

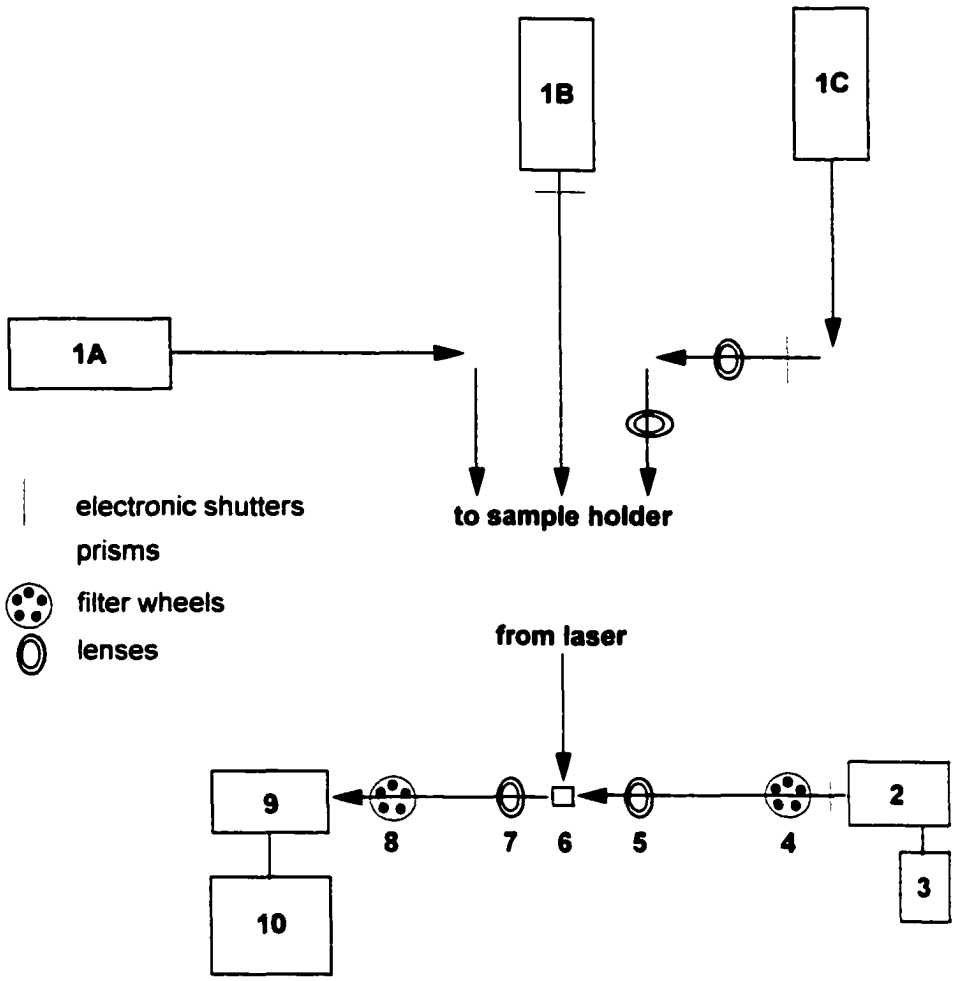

Figure 3.1. Schematic setup of the laser flash photolysis systems. The top of the figure illustrates the OPO Infinity (1A), the YAG (1B) and the excimer (1C) laser setups. The bottom shows the lamp, sample holder and detection setup (2-10).

The monitoring beam is a 150 W Xenon lamp (2) contained in an Oriel housing (model 66057) and uses a PTI power supply (model LPS-220). A custom built pulser (3) is used to produce a 4 ms high intensity burst from the lamp upon triggering. The lasers (1) are set up to fire the excitation shot 1.6 ms after the start of the lamp pulse. The monitoring beam passes through a filter wheel (4) containing cut-off filters that ensure no degradation of the sample signal takes place due to irradiation during the data accumulation period. The light then passes through a lens (5) and then the sample holder (6). The lens serves to place the beam's focal point just beyond the sample holder. A

second lens is used to collimate the beam (7) and another filter wheel (8) serves to block out any scattered laser light and overtones. Detection of the monitoring beam is accomplished using a Hamamatsu R446 photomultiplier tube (PMT), which is coupled to a CVI Digikrom 240 monochromator (9). This allows one to monitor specific wavelengths. Signals from the PMT are sent to a baseline compensation unit, which offsets the light intensity before the laser pulse. The signal is then transferred to a Tektronix TDS 520 oscilloscope and the computer (10).

Laser pulse energies can be varied for the excimer laser system by placing neutral density filters between the laser and the first prism (63%, 40%, 25% and 10%). On the YAG laser setup, a dial on the control unit of the laser serves to dial down the laser power. The software that runs the systems is written in Labview 6.0 (National Instruments, L. Netter).

3.4.2 Methods

The solutions were prepared in CHX with an absorbance between 0.15-0.25 at the irradiation wavelength. The transient absorption spectra were recorded using a flow system to avoid interference from any photodecomposition products that may result from several laser shots. This was accomplished by pumping the solution through a custom designed Suprasil quartz cell (7 × 7 mm) at a rate of 1.0 mL/min under a nitrogen or oxygen atmosphere. The flow system ensured that each laser pulse irradiated a fresh solution. Kinetic measurements were conducted in Suprasil quartz cells (7 × 7 mm) sealed with rubber septa. The solutions were purged with nitrogen or oxygen for at least 30 minutes.

Isomerization quantum yield measurements were also performed using the laser flash photolysis system with either 308 nm (CPD) or 355 nm (DHP) excitation. The triplet formation of benzophenone (BPh) was used as the standard to which the isomerization reactions were compared. Solutions of the unknown compounds were made in CHX and matched to within 0.002 absorption units at the excitation wavelength with BPh solutions in acetonitrile (ACN). The transient kinetics were measured for both compounds, at the wavelengths where the compounds were known to have a signal, at varying pulse energies.

3.4.3 Data Analysis

The transient kinetic decay traces were fit using a routine based on Levenberg-Marquardt algorithm written in Labview 6.0 (National Instruments, L. Netter).

The isomerization quantum yields were determined by comparing the absorption maximum of the BPh triplet (ΔA_{max}) to the magnitude of the residual absorption of the DHP or CPD isomer (ΔA_{res}) as measured from the transient decay kinetics traces at varying laser power. Equation (3.4) illustrates the relation between the transient absorptions and the isomerization quantum yields.

$$\Delta A_{BPh} = \frac{\varphi_{ISC} \cdot \varepsilon_{BPh}}{\varphi_{DMDHP \rightarrow CPD} \varepsilon_{DHP}} |\Delta A_{res}| \qquad \textbf{Equation (3.4)}$$

where ϕ_x refers to the quantum yield of triplet formation for BPh (*ISC*) or the isomerization quantum yield (*DMDHP→CPD*), and ε is the molar absorptivity at the monitoring wavelength. The equation is also valid for the measurement of the CPD to DMDHP isomerization (i.e. substitute *DMDHP→CPD* with *CPD→DMDHP*). The intersystem crossing quantum yield can be measured in the same manner except the magnitude of the triplet absorption (ΔA_{max}) is measured instead of ΔA_{res} and the ϕ_{T1} is calculated instead of $\phi_{DMDHP \rightarrow CPD}$.

CHAPTER 4: SIMPLE SUBSTITUTED DIMETHYLDIHYDROPYRENES

4.1 Introduction and Perspective

Preliminary work was done on the parent DMDHP, **1**, using laser flash photolysis and steady state fluorescence techniques.[97] Fluorescence experiments showed a very sharp emission centered at 640 nm with no measurable Stokes shift. Laser flash photolysis indicated the presence of two transients, upon 355 nm excitation. A bleaching was seen in the transient absorption spectrum above 300 nm and a positive absorption was observed in the 250-320 nm region. At shorter timescales (i.e. delays ≤ 50 ns), evidence of the first transient was seen. On longer timescales, only the second transient was visible since it was longer lived than the first transient. The first of the two transients showed a maximum absorption at 310 nm while the second transient was seen to blue shift to 280 nm. Lifetimes for the transients were determined from their kinetics. The lifetimes obtained from the kinetics for both the growth and decay at different wavelengths gave the same lifetimes. The short-lived component had a lifetime within the time resolution of the system (i.e. < 10 ns) while the second transient was longer lived (microseconds). Quenching experiments indicated that the longer-lived transient had a triplet energy between 22 (E_T oxygen)[9] and 38 kcal·mol^{-1} (E_T ferrocene).[98] It was proposed that the short-lived transient was a singlet biradical while the longer-lived component was assigned as the triplet excited state of the metacyclophanediene (CPD).

In order to expand on those preliminary studies, a combination of spectroscopic techniques along with quantum yield measurements were used to determine the mechanism of isomerization. This included an investigation into the effect of various substituents on the efficiency of switching.

The parent DMDHP (**1**[99,100]) was used as a comparison for the other compounds. The effect of alkyl and carbonyl substitution at the 2-position of **1** was accomplished using the 2,7-bis-*t*-butyl substituted **2**[80] and 2-acetyl-**1** (**24**[101]). The relative ease of synthesis of **2** over the parent (**1**) prompted an investigation into the effect of substitution on the 4- and 4,9-positions of compound **2**. A benzylic alcohol (**11**) was prepared to investigate the effect of nonconjugating groups as well as heavy atoms (oxygen) on the isomerization. The effect of conjugating groups on the switching efficiency was

examined using ethynyl, aryl and carbonyl substituents. The 4-acetyl substituted DMDHP (**25**[82]) was examined to investigate the effect of a conjugated heavy atom on the system. Substitution with aryl groups in which extended conjugation is only maintained when the molecule is planar was studied using phenyl substituted DMDHP, **26**.[102] Ethynyl substitution was extensively studied (**14**, **17**, **18**, **22** & **27**[103]), as these types of systems were models for DMDHPs within molecular wire frameworks.[83] Acetylenes are useful conjugating spacers due to their ability to maintain extended conjugation even when the molecules are twisted (i.e. not planar, **14** & **22**).

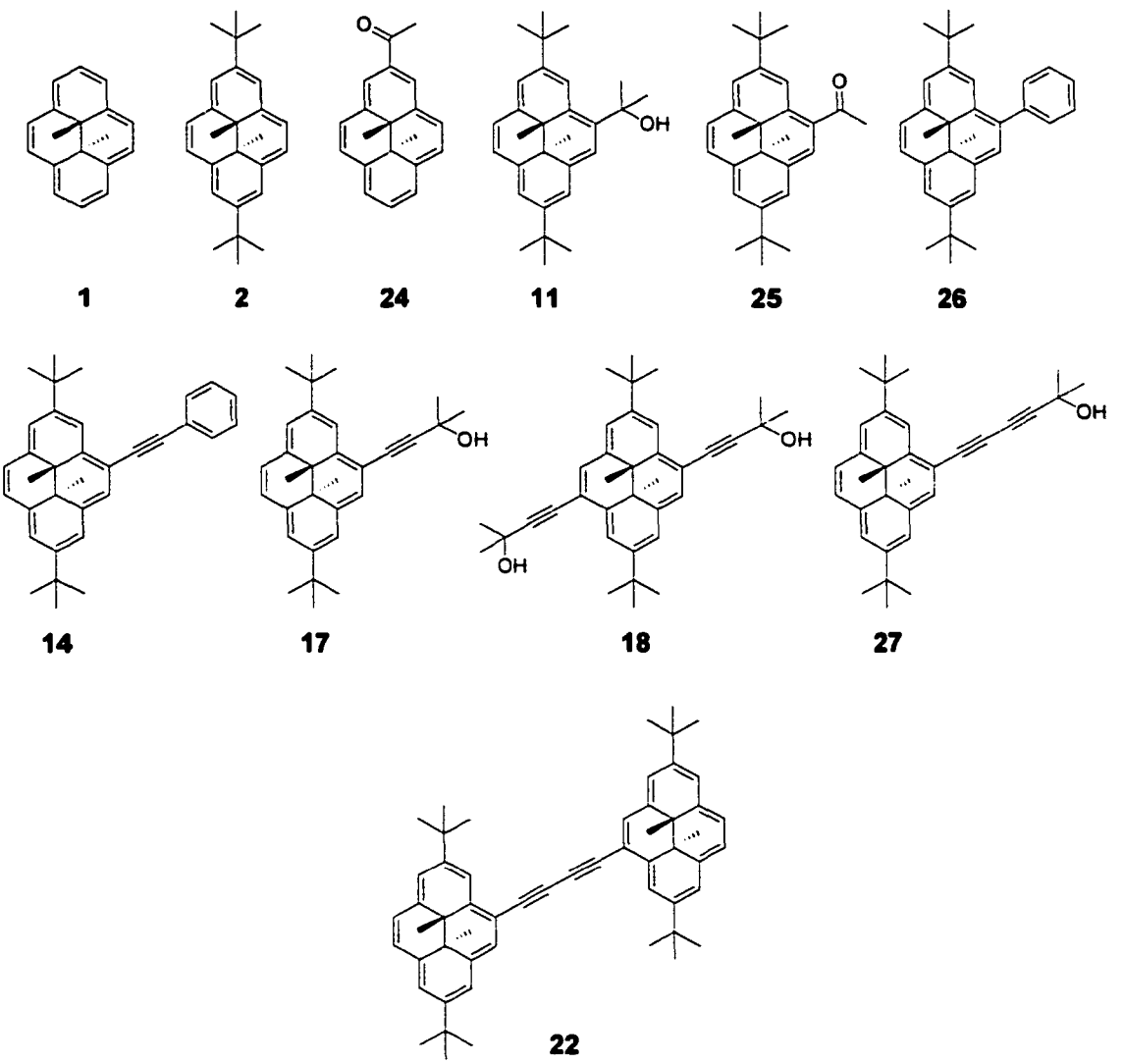

Figure 4.1. Compounds used in the investigation into the photoisomerization mechanism and the effect substituents play on the efficiency of the photoswitching reaction.

4.2 Absorption

As previously mentioned, dimethyldihydropyrenes are aromatic 14-π electron hydrocarbons. Their absorption spectra span most of the visible spectrum and consist of four major bands (Figure 4.2). The most intense absorptions occur between 320 and 420 nm consisting of two bands with molar absorptivities of about 10^6 $M^{-1}cm^{-1}$ for the first band and 10^5 $M^{-1}cm^{-1}$ for the second. A third band is seen in the region of 450 to 550 nm ($\varepsilon = 10^4$ $M^{-1}cm^{-1}$), which is broader than the first two and shows some structure. The lowest energy absorption band occurs between 640 and 690 nm and is relatively weak with molar absorptivity coefficients between 10^2 and 10^3 $M^{-1}cm^{-1}$ (Appendix A, Figures A1-3, Table A1).

Substitution with conjugating groups such as acetylenes (Figure 4.2) and acetyl groups leads to a red shift of all the absorption bands as expected due to the increased conjugation. Increasing the conjugation also results in an increase of the molar absorptivity coefficient for the longest wavelength band. This can be seen if one examines the series **2** (900 $M^{-1}cm^{-1}$), **17** (1740 $M^{-1}cm^{-1}$), **14** (2130 $M^{-1}cm^{-1}$), **27** (3980 $M^{-1}cm^{-1}$) and **22** (6840 $M^{-1}cm^{-1}$).

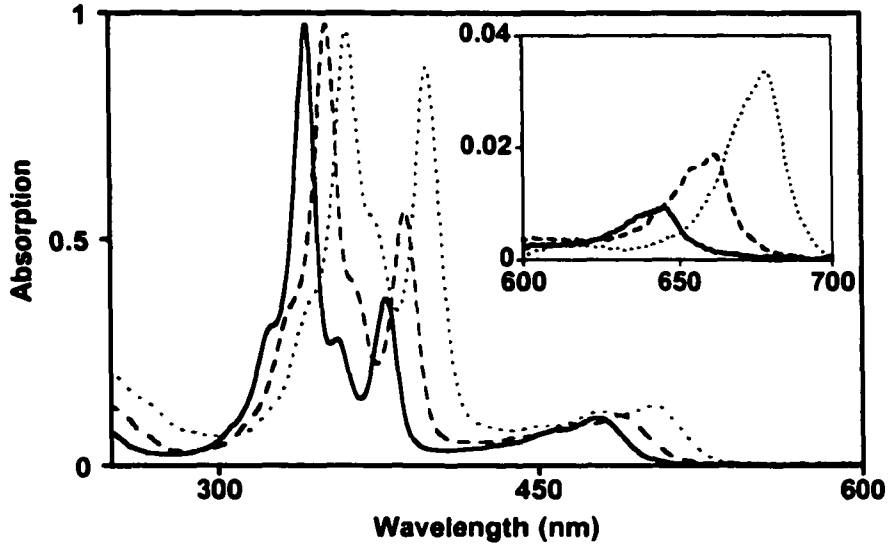

Figure 4.2. Overlay of the normalized absorption spectra of compounds **2** (——), **17** (– – –) and **18** (·····) from 250-600 nm. Inset shows the lowest energy absorption for each compound between 600-800 nm.

4.3. Fluorescence

4.3.1 Emission Spectra

Fluorescence was seen for all compounds (Appendix B). The fluorescence for simple substituted DMDHPs was observed as a single sharp band that was relatively weak in intensity (Figure 4.3a). No Stokes shift was seen for any of the compounds studied as the lowest energy absorption band and the emission were seen to overlap exactly. The 2-acetyl substituted DMDHP (**24**) showed a shoulder off the main emission band that was consistent with the mirror image of the lowest energy absorption band in the ground state absorption spectrum (Figure 4.3b). The energies of the first excited state were calculated from the highest energy band of the emission using Equation (1.1) and are shown in Table 4.1.

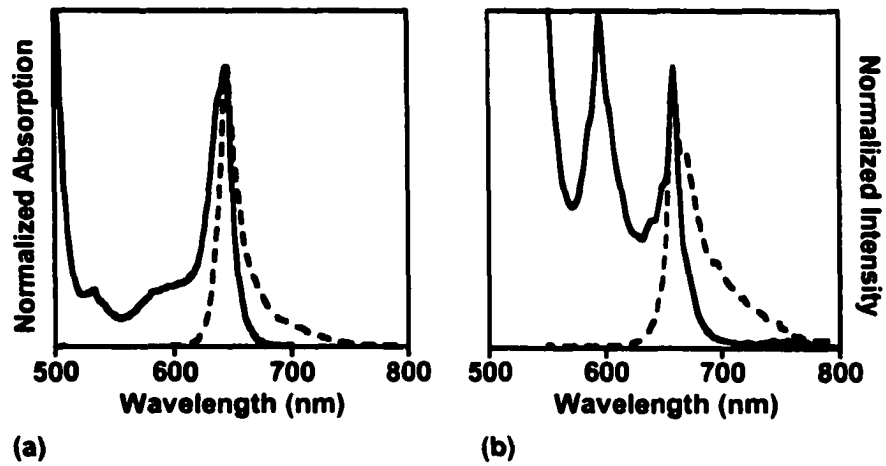

Figure 4.3. Overlay of the absorption (——) and emission (---) spectra of (a) **2** and (b) **24**, between 500-800 nm.

The lack of a Stokes shift implied that the equilibrium internuclear distance was the same in the ground and singlet excited electronic states. The sharpness of the spectrum implied that the molecule was rigid in the excited state. If the molecule was not rigid, it should have been able to sample a variety of conformations. This generally leads to a broader emission spectrum. The fact that the spectra were so sharp implied that a single transition was involved from the lowest vibrational level of the singlet excited electronic state to one vibrational level of the ground electronic state.

The effect of oxygen on the fluorescence intensity was examined. This was done by preparing solutions with matched absorptions at the excitation wavelength with varying concentrations of oxygen. The fluorescence spectrum was then measured and the ratio of the fluorescence intensity in the presence and absence of oxygen (I_o/I) was related to the oxygen concentration using Equation (1.15). It was found that oxygen quenched the fluorescence of **2** in a diffusional process with a quenching rate constant of $(1.1 \pm 0.1) \times 10^{10}$ $M^{-1}s^{-1}$ ($K_{SV} = 70 \pm 2$ M^{-1}, $\tau_s = 5.6$ ns (Table 4.1)). Since the overall difference in fluorescence intensity under nitrogen and air conditions was only 15%, all fluorescence spectra were obtained under aerated conditions.

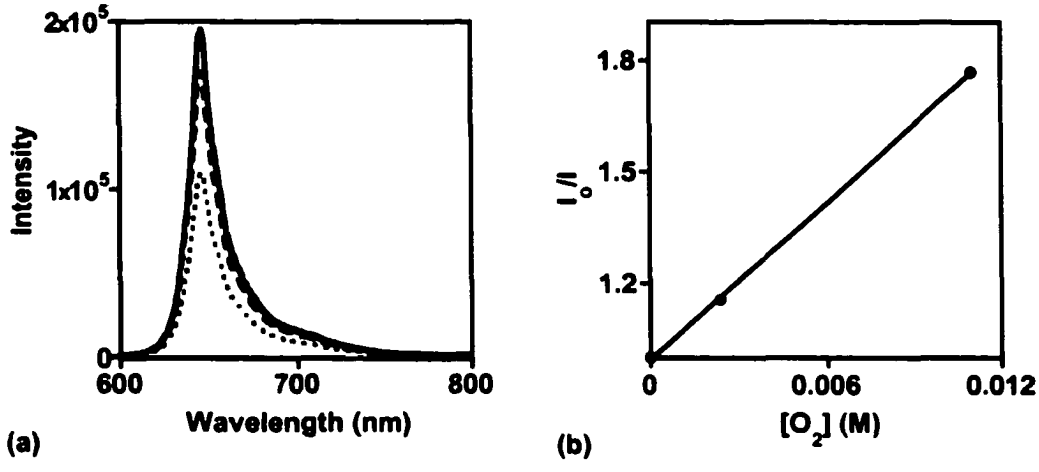

Figure 4.4. (a) Overlay of emission spectra of **2** under nitrogen (——), air (---) and oxygen (·····) purged conditions. (b) The Stern-Volmer quenching plot for **2** with oxygen.

In an attempt to resolve the room temperature emission spectra, low temperature experiments were performed. The DMDHP solutions were prepared in toluene and slowly placed in liquid nitrogen to form a low temperature glass. The fluorescence spectra were then measured. The low temperature spectra were not seen to change appreciably as no additional vibrational structure was seen when the samples were cooled. The spectra did become sharper and more intense upon cooling (Figure 4.5). The sharpening of the spectrum implied that the molecule was indeed rigid in the excited state. If it were not rigid then one would expect the emission to be resolved and vibrational structure to be evident in addition to the sharpening. An increase in the

intensity was expected as the sample was cooled since the solution would become more viscous. The interactions between the molecules and the surrounding solvent would decrease, thereby decreasing the probability of internal conversion. This would leave a greater number of excited molecules to undergo fluorescence. In other words, other deactivation pathways would be slowed down so they could not compete as efficiently with fluorescence.

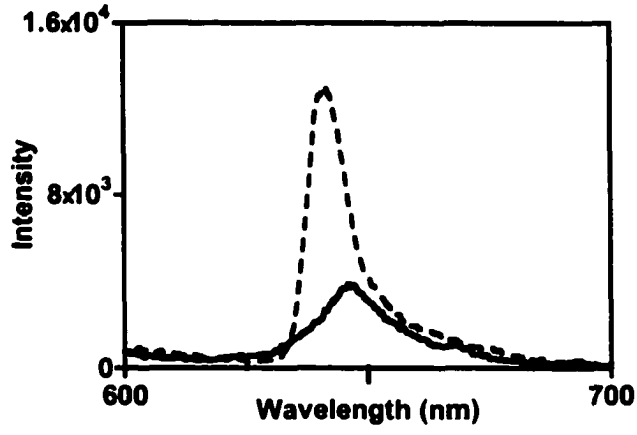

Figure 4.5. Overlay of the emission spectra for **2** at room temperature (——) in cyclohexane and at 78 K (---) in toluene with matched absorption at the excitation wavelength (470 nm).

4.3.2 Fluorescence Quantum Yields

A fluorescence quantum yield is the measure of the efficiency of the radiative decay from the singlet excited state (S_1) to the ground electronic state relative to all other deactivation pathways (i.e. radiative, nonradiative, chemistry) that the S_1 state can undergo. Fluorescence quantum yields (Table 4.1) were obtained by comparing the fluorescence of the DMDHPs with that of $Ru(bipy)_3Cl_2$ (ϕ_F = 0.042; λ_{ex} = 436 nm)[93] using Equation (3.3). $Ru(bipy)_3Cl_2$ was chosen as the standard for two main reasons. Firstly, the complex was one of the few compounds that emit in the 500-800 nm region (Figure 4.6) that had been well studied. Secondly, since the fluorescence of the DMDHPs was fairly weak, a standard with a low quantum yield was needed so that both could be accurately measured with the same instrument parameters (i.e. slit widths). The

fluorescence quantum yield for $Ru(bipy)_3^{2+}$ was sufficiently low that an accurate comparison could be made.

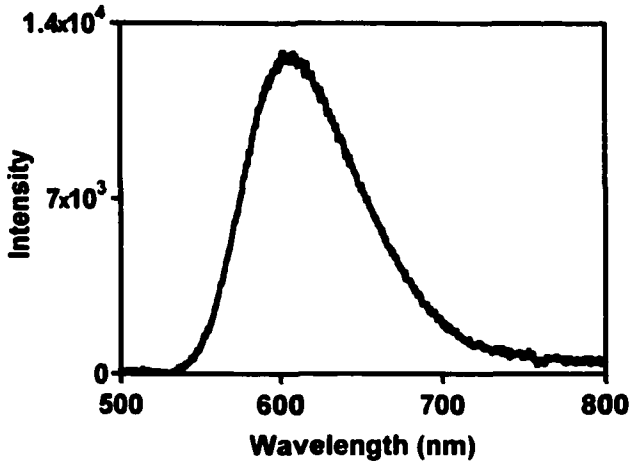

Figure 4.6. Emission spectrum of $Ru(bipy)_3Cl_2$ in water (λ_{ex} = 436 nm).

All fluorescence quantum yields were found to be between 0.0006 and 0.005. These values were low when compared to other aromatic hydrocarbons such as naphthalene (0.19), anthracene (0.3) and pyrene (0.65).[9] The parent compound, **1**, and the 2-acetyl substituted DMDHP (**24**) had the lowest fluorescence quantum yields (~ 0.0006) while the multichromophoric **22** and 4-acetyl substituted DMDHP (**25**) had the most efficient fluorescence (~ 0.005). The other derivatives had similar fluorescence quantum yields (~ 0.002). There was no correlation between substituents and fluorescence efficiency except that a very small increase was noted with increasing conjugation (i.e. **2**: 0.00203; **17**: 0.00229; **14**: 0.00252; **27**: 0.0029; **22**: 0.00389).

4.3.3 Fluorescence Lifetimes and Rate Constants

The decay of the fluorescence was found to be mono-exponential (Figure 4.7), therefore, the lifetimes for the singlet excited state could be obtained by monitoring the change in fluorescence intensity with time. The decay that was recovered was fit by Equation (4.1),

$$[S_1] = [S_1]_o e^{-k_f t} \qquad \textbf{Equation (4.1)}$$

where the fluorescence lifetime, τ_s, is the inverse of the k_f (sum of the rate constants for all possible deactivation pathways).

Table 4.1. Emission maxima (λ_{max}), singlet excited state energies (E_{S1})[a], fluorescence quantum yields (ϕ_f), singlet excited state lifetimes (τ_s), and fluorescence rate constants (k_f^o)[b] for various simple substituted DMDHP derivatives.

Compound	λ_{max} (nm)	E_{S1} (kcal·mol^{-1})	ϕ_f (10^{-3})	τ_s (10^{-9} s)	k_f^o (10^5 s^{-1})
1	641	44.6 ± 0.1	0.61 ± 0.03	5.4 ± 0.1	1.13 ± 0.06
2	641	44.6 ± 0.1	2.03 ± 0.07	5.6 ± 0.1	3.6 ± 0.1
24	660	43.3 ± 0.1	0.64 ± 0.07	4.4 ± 0.2	1.5 ± 0.2
11	649	44.1 ± 0.1	2.17 ± 0.05	5.4 ± 0.2	4.0 ± 0.2
25	666	42.94 ± 0.09	4.61 ± 0.05	4.2 ± 0.1	11.0 ± 0.3
26	649	44.1 ± 0.1	2.11 ± 0.02	5.3 ± 0.2	4.0 ± 0.2
14	667	42.87 ± 0.08	2.52 ± 0.09	c)	c)
17	663	43.1 ± 0.1	2.29 ± 0.03	4.6 ± 0.1	5.1 ± 0.1
18	679	42.12 ± 0.05	2.2 ± 0.2	3.8 ± 0.1	5.8 ± 0.5
27	669	42.74 ± 0.07	2.9 ± 0.3	4.5 ± 0.2	6.4 ± 0.3
22	673	42.48 ± 0.06	3.89 ± 0.09	3.9 ± 0.2	10.0 ± 0.5

[a] The singlet excited state energies were calculated from the emission maxima. [b] The fluorescence rate constants were calculated from the fluorescence quantum yields and lifetimes (ϕ_f / τ_s). [c] The lifetime was not measured.

The lifetimes obtained under aerated conditions were between 3.8 - 5.6 ns for all compounds. The lifetimes for other aromatic hydrocarbons under aerated conditions in cyclohexane were calculated from the lifetimes in the absence of oxygen (k_o), the singlet quenching rate constants for oxygen (k_q) and the concentration of oxygen dissolved in cyclohexane under aerated conditions ($[O_2]$ = 2.4 mM) using Equation (1.20).[9] The calculated lifetimes for naphthalene (13 ns), triphenylene (13 ns) and pyrene (16 ns) were found to be twice as long as the DMDHPs under identical conditions. However, the singlet lifetimes for DMDHPs are significantly longer than other photochromic

compounds such as fulgides,[12,26] diarylethenes[38,46,47] and spirooxazines,[104,105] which have lifetimes shorter than a picosecond.

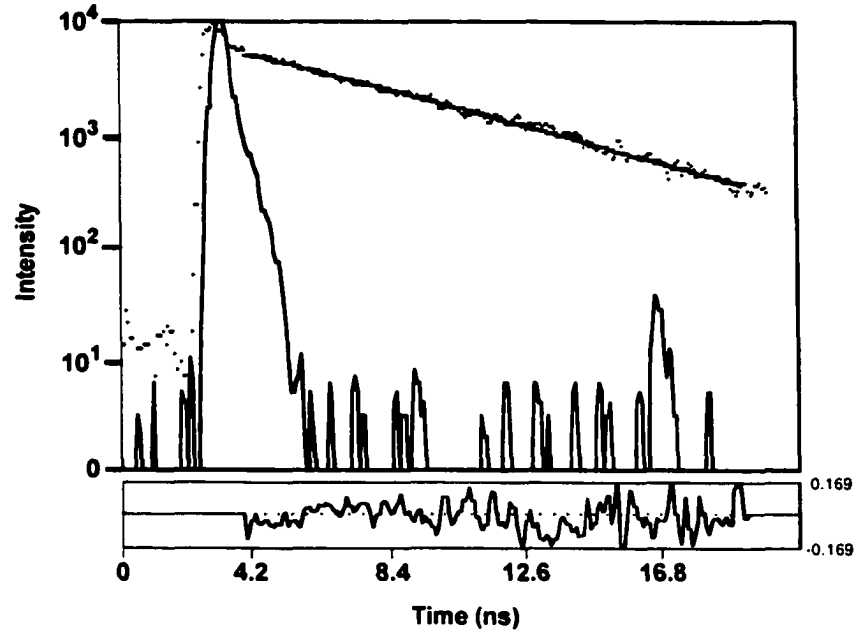

Figure 4.7. Example of a fluorescence decay trace fit to a mono-exponential function. The residuals indicating the quality of the fit are shown below the decay.

The lifetime of the singlet excited state of **2** was determined under aerated conditions to be 5.6 ns while under nitrogen purged conditions it was found to be 6.5 ns. An approximate quenching rate constant for oxygen of 10^{10} $M^{-1}s^{-1}$ was calculated using Equation (1.20). This quenching rate constant was consistent with the value obtained from steady state measurements (above).

Fluorescence rate constants could be determined from the fluorescence quantum yields and lifetimes (Equation (4.2)). The values for all compounds were on the order of 10^5 s^{-1} (Table 4.1). These fluorescence rate constants were lower than seen for other aromatic compounds such as naphthalene, anthracene and pyrene, which have rate constants of $10^6 - 10^7$ s^{-1}.[9]

$$k_f^o = \frac{\varphi_f}{\tau_s} \qquad \textbf{Equation (4.2)}$$

4.4 Quantum Yields of Isomerization

Ring opening isomerization quantum yields are a measure of the number of excited molecules that undergo isomerization when compared to the total number of molecules excited. Isomerization quantum yields for the ring opening process were obtained using the potassium ferrioxalate actinometer as a primary standard.[6,7] For compounds with extended conjugation, the CPD absorption was found to interfere with measurements made with excitation below 400 nm. Compound **1** was used as a secondary standard for those compounds that needed to be excited above 400 nm. The values reported were the average of two experiments, each of which consists of at least two data points. The isomerization quantum yields were measured under oxygen and nitrogen purged conditions and were found to be the same within error. This implied that the isomerization goes through the singlet excited state of the DMDHPs. If the triplet excited state was involved in the isomerization, a larger decrease in the quantum yield would be expected in the presence of oxygen (see below). The fact that no difference between oxygen and nitrogen purged conditions was observed for these results, when the singlet excited state was seen to be quenched by steady state and time resolved fluorescence studies, was a result of the large errors associated with the measurements (as much as 25%).

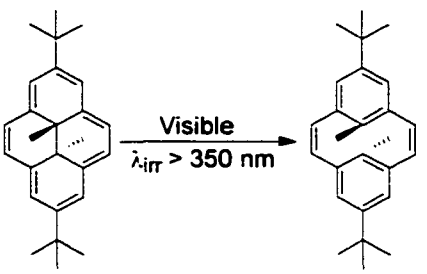

2 **2'**

Scheme 4.1. Ring opening isomerization for DMDHP **2**.

4.4.1 Substitution of 1

The ring opening isomerization quantum yield for the parent **1** was found to be 0.006. This was three times less than the reported literature values of 0.015[82] and 0.018 [76]. It was unclear from the literature what techniques were used to measure those

isomerization quantum yields. Incorporation of an alkyl group on the 2- and 7-positions (i.e. *t*-butyl substitution, **2**) showed a four-fold decrease in the isomerization efficiency when compared to **1**. The value of 0.0015 agreed well with the isomerization quantum yield reported in the literature for **2** (0.0018).[82]

Substitution with a carbonyl group, such as formyl or benzoyl, in the 2-position of **1** had been reported to increase the quantum yield to 0.25.[76] This was an order of magnitude increase in efficiency when compared to the literature value reported for **1** in the same paper.[76] Substitution with an acetyl group was expected to yield similar results. It was found that the acetyl group did in fact increase the quantum yield relative to **1** but only a 2-fold increase to 0.012 was measured.

4.4.2 Substitution of 2

Although *t*-butyl substitution (**2**) was seen to decrease the isomerization efficiency, the effect of substitution on this framework was also studied as this system was more easily synthesized. Incorporation of an alkyl group, such as the *iso*-propyl alcohol substituted **11**, was found to have no effect on the isomerization relative to **2**. This suggested that incorporation of DMDHPs into frameworks connected by non-conjugating alkyl spacers would not significantly affect the isomerization.

Substitution of **2** with an acetyl group in the 4-position (**25**) was found to have the same effect as the 2-substitution had on **1**. That is, there was a two-fold increase in the isomerization quantum yield for **25** (0.0038) relative to **2** (0.0015). The literature value for **25** of 0.0047-0.0060 agreed relatively well with the values obtained in this work.[82]

The incorporation of an aryl group directly onto the DMDHP framework was not expected to result in a planar molecule due to steric interactions. These interactions were similar to those observed in biaryls, such as biphenyl and binaphthyl[84], between the hydrogens on the aryl group and those on DMDHP (Figure 4.8). The result of these interactions was that the aryl group would twist with respect to the DMDHP framework and would not be fully conjugated with the DMDHP system. When the aryl group was a phenyl (**26**), the isomerization quantum yield was seen to decrease by an order of magnitude (0.00018) when compared to **2**. A similar effect was reported with ethenyl substitution.[82]

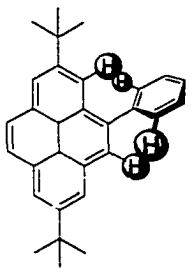

26

Figure 4.8. Illustration of the steric interactions between the protons on the phenyl group and the DMDHP moiety of compound **26** on the planarity of the molecule.

As previously mentioned, ethynyl substitution was important because it should provide insight into how the isomerization efficiency of the DMDHP would be affected in a molecular wire type system based on acetylene. Extended conjugation of acetylenes with DMDHP was expected regardless of the angle of the acetylene moiety with respect to DMDHP. Substitution with acetylenes was found to have a similar effect as the incorporation of a phenyl group. A three-fold decrease in isomerization efficiency was seen for compounds **17**, **18** and **27** as compared with **2**. The ring opening isomerization pathway was sufficiently inefficient in the multichromophoric **22** that it was not possible to accurately measure a quantum yield. It was estimated that the ring opening quantum yield for **22** was on the order of 10^{-6} to 10^{-7}. The notable exception to these results was the case where phenylacetylene was substituted onto the DMDHP framework (**14**). In that case, the isomerization efficiency was found to be comparable with that of **2** (i.e. 0.0027).

4.4.3 Ring Opening Isomerization Rate Constants

Rate constants for the ring opening isomerization were also calculated using Equation (4.2). Isomerization quantum yields ($\phi_{DMDHP\rightarrow CPD}$) were used in place of the fluorescence quantum yield and the isomerization rate constant ($k_{DMDHP\rightarrow CPD}$) was determined instead of the fluorescence rate constant (i.e. $k_{DMDHP\rightarrow CPD} = \phi_{DMDHP\rightarrow CPD}/\tau_S$). The ring opening rate constants were found to be of the same order of magnitude as the fluorescence rate constants (i.e. $k_{DMDHP\rightarrow CPD} \sim 10^5\ s^{-1}$, Table 4.2). The parent compound

1, 2-acetyl substituted **24** and 4-acetyl substituted **25** were found to have ring opening rate constants of 1.1×10^6, 2.7×10^6 and 9×10^5 s^{-1} respectively while the phenyl substituted **26** gave an isomerization rate constant of 3.4×10^4 s^{-1}. All other compounds had ring opening isomerization rate constants between 1.2×10^5 and 2.7×10^5 s^{-1}. The *t*-butyl substituted **2** and *iso*-propyl alcohol substituted **11** had almost identical rate constants while incorporation of an acetylene resulted in a 2-fold decrease in rate constants relative to **2**.

Table 4.2. Ring opening isomerization quantum yields ($\phi_{DMDHP \rightarrow CPD}$) and rate constants ($k_{DMDHP \rightarrow CPD}$) for various simple substituted DMDHPs as measured by actinometry.

Compound	$\phi_{DMDHP \rightarrow CPD}$ (10^{-3})	$k_{DMDHP \rightarrow CPD}$ (10^5 s^{-1})
1	6 ± 2	11 ± 4
2	1.5 ± 0.1	2.7 ± 0.2
24	12 ± 2	27 ± 5
11	1.4 ± 0.1	2.6 ± 0.2
25	3.8 ± 0.5	9 ± 1
26	0.18 ± 0.05	0.34 ± 0.02
14	2.7 ± 0.9	a)
17	0.56 ± 0.09	1.2 ± 0.2
18	0.52 ± 0.08	1.4 ± 0.2
27	0.7 ± 0.3	1.6 ± 0.2
22	0[b]	b)

[a] No lifetime was measured for this compound. [b] The quantum yield was estimated to be between 10^{-6} and 10^{-7}, which would lead to a rate constant of between 3×10^1 and 3×10^2 s^{-1}.

4.5 Laser Flash Photolysis

4.5.1 Transient Absorption Spectra

The transient absorption spectra (Appendix C) for all compounds showed a bleaching in the 350-600 nm region that corresponded to the ground state absorption of

Table 4.3. Transient absorption maxima for the short lived transient (TI) and the longer lived transient (TII) obtained from laser flash photolysis.

Compound	λ_{max} (nm)	
	TI	TII
1	310	285
2	315	290
24	310 (sh)	275
11	315	290
25	325 (sh)	290
26	310	295
14	325	300
17	330	300
18	345	310
27	325	300
22	310	295

4.5.2 Transient Kinetics

The transient kinetics showed the presence of two transients. The first of these transients (TI) was shorter lived than the time resolution of the system (i.e. $\tau \leq 10$ ns). The kinetics trace that was recovered for this transient corresponded to the time profile of the laser pulse as a consequence of the lifetime being short (Figure 4.10a). The first transient was followed by a second longer-lived transient (TII), which had a microsecond lifetime ($\tau \sim 5$ μs, Figure 4.10b). The decay of the shorter lived transient was seen in the kinetics trace of the longer lived transient as a spike at the beginning of the decay. The long lived transient did not decay back to the baseline but instead led to a residual absorption that was constant for the time-resolution of the equipment (i.e. 10 ns). The lifetimes obtained from the growths ($\lambda_{mon} \leq 310$ nm) and decays ($\lambda_{mon} \geq 310$ nm) were identical (inset, Figure 4.10b).

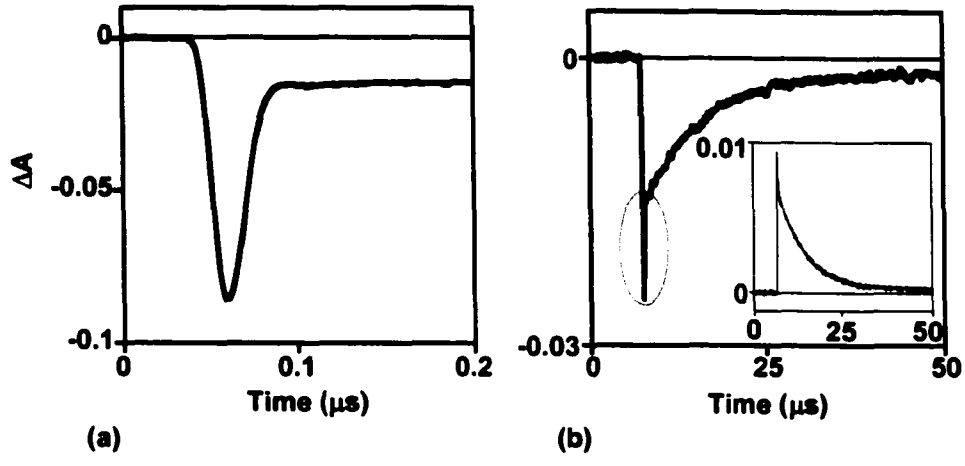

Figure 4.10. Transient kinetics for compound **2** (λ_{irr} = 470 nm) on (a) short and (b) long time scales as measured at 340 nm. The oval indicates where the fast decay seen in (a) was seen within the decay at longer timescales. The inset shows the kinetics on long timescales for the growth as measured at 280 nm giving rise to the same lifetime as the kinetics at 340 nm.

4.5.2.1 Quenching

Quenching studies with various quenchers for triplet excited states were performed to determine the identity of the longer-lived transient. The quenchers were chosen so that they did not absorb at the excitation wavelength to avoid direct excitation of the quencher. The quenchers were also chosen to have triplet excited state energies (E_T) that were expected to be lower than the transient of the DMDHP. This ensured that energy transfer between the triplet excited states was possible if the DMDHP transient was in fact a triplet. The kinetics of the DMDHP were then taken in the absence of quencher and with specific volumes of quencher added. Using Equation (1.20) it was possible to obtain quenching rate constants by relating the rate constants obtained from the DMDHP kinetics and the concentration of quencher added.

Oxygen (E_T = 22 kcal·mol^{-1})[9] was found to quench the longer lived transient with a rate constant typical for triplet quenching of (1.9 ± 0.2) × 10^9 $M^{-1}s^{-1}$. Similar results were obtained with β-carotene (E_T = 21 kcal·mol^{-1})[9], yielding a quenching rate constant of (1.4 ± 0.1) × 10^{10} $M^{-1}s^{-1}$. β-Carotene was an especially useful triplet quencher since it does not intersystem cross upon direct excitation. It also showed triplet excited state kinetics at 520 nm where the DMDHP transient did not. This allowed for two

independent measurements of the quenching efficiency when the DMDHP kinetics were measured at 280 nm.

Attempts to quench the longer-lived transient with ferrocene (E_T = 38 kcal·mol^{-1})[94] were unsuccessful. The fact that the transient was quenched by oxygen (singlet and triplet excited state quencher) and β-carotene (triplet excited state quencher) implied that the longer-lived transient was a triplet excited state. Since the transient was quenched by oxygen and not quenched by ferrocene the energy of this triplet excited state must lie between 22 kcal·mol^{-1} and 38 kcal·mol^{-1}.

Sensitization experiments were also performed using DMDHP. Sensitization experiments are similar to quenching experiments in that energy transfer from the excited state of one molecule to another is accomplished. In this case, a compound was chosen that has a triplet excited state energy that was known to be higher than the energy of the DMDHP triplet excited state. Sensitization of the triplet excited state of **2** with benzophenone (BPh, E_T = 69 kcal·mol^{-1})[9] was attempted. This was accomplished by exciting a solution of BPh at 266 nm where **2** does not significantly absorb. The benzophenone solution was then quenched with specific volumes of a concentrated solution of **2**. A diffusional rate constant of (1.3 ± 0.1) × 10^{10} $M^{-1}s^{-1}$ was obtained from the sensitization of **2** with BPh using Equation (1.20). At high concentrations of **2**, the same transient absorption spectrum was obtained at long delays as was seen for direct excitation of **2**, confirming that the longer-lived transient was the triplet excited state. Quenching studies involving the shorter-lived transient were not possible due to the initial lifetime of the transient and the lack of suitable equipment with the required time resolution.

4.5.2.2 Relative Isomerization Quantum Yields

The kinetics discussed above did not decay to zero (baseline) but instead led to a residual absorption that did not recover within the timescale of the equipment (1 ms). This residual absorption was previously assigned to be proportional to the amount of DMDHP converted to CPD.[97] If this was the case, then by measuring and comparing the residual absorption of various DMDHP derivatives, it should be possible to obtain relative isomerization quantum yields (Figure 4.11).

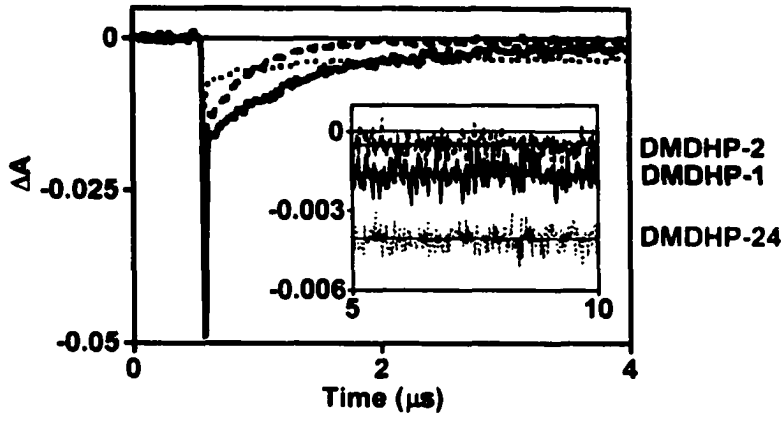

Figure 4.11. Overlay of the transient kinetics for compounds **1** (——), **2** (---), and **24** (·····) measured at 465 nm qualitatively illustrating the use of residual absorptions for determining the relative quantum yields of DMDHP photoconversion to CPD. Inset shows an expansion of the residual absorption at longer time scales (lines are included for clarity).

For an accurate comparison, the absorption of the compounds examined at the excitation wavelength (480 nm) had to be matched to within 0.002 absorption units. Measurement of the kinetics of the compounds at the same wavelength (i.e. 465 nm) gave the magnitude of the residual absorption. A quantitative measurement required taking into account the molar absorptivity coefficient for each compound at 465 nm (Appendix A, Table A3). This gave the concentration of CPD created upon excitation. Normalization of the [CPD] relative to **1** allowed for a direct comparison with the normalized quantum yields (relative to **1**) obtained from actinometry (Table 4.4). The values obtained by LFP were found to be in good agreement with those recovered from actinometry.

Table 4.4. Metacyclophanediene concentrations ([CPD])[a] and relative [CPD] obtained from LFP compared with relative ring opening isomerization quantum yields (relative $\phi_{DMDHP \rightarrow CPD}$) obtained from actinometry for various DMDHP derivatives.

Compound	[CPD] (10^{-7} M)	Relative [CPD]	Relative $\phi_{DMDHP \rightarrow CPD}$
1	2.6 ± 0.5	1	1
2	0.7 ± 0.1	0.26 ± 0.05	0.25 ± 0.08
24	7 ± 1	2.8 ± 0.6	2.0 ± 0.8
11	0.8 ± 0.2	0.30 ± 0.06	0.23 ± 0.07
25	2.0 ± 0.4	0.8 ± 0.2	0.6 ± 0.2
26	1.3 ± 0.3[b]	ca. 0.5	0.03 ± 0.01
14	1.2 ± 0.2	0.46 ± 0.09	0.5 ± 0.1
17	0.5 ± 0.1	0.19 ± 0.04	0.09 ± 0.03
18	1.4 ± 0.3[b]	ca. 0.5	0.09 ± 0.03
27	0.7 ± 0.1	0.27 ± 0.05	0.12 ± 0.05
22	0.033 ± 0.007	0.013 ± 0.003	~ 0

[a] A 20% error was estimated for all ΔA measurements used in the CPD concentration calculations. [b] [CPD] were overestimated since kinetics traces did not fully decay.

4.5.2.3 Intersystem Crossing Quantum Yields and Rate Constants

The longer-lived transient was assigned to a triplet excited state. The efficiency of intersystem crossing from the singlet excited state to the triplet excited state was of interest. It was possible to determine the concentration of the triplet excited state ($[T_1]_{DMDHP}$) produced by measuring the magnitude of the DMDHP bleaching from its kinetics on long timescales. The [DMDHP] bleached was assumed to be directly proportional to the $[T_1]_{DMDHP}$ formed (i.e. $\varepsilon_{T1} = 0$ at λ_{mon}). Comparing the $[T_1]_{DMDHP}$ obtained from the DMDHP kinetics to a compound which had a process with a known quantum yield, made it possible to obtain a value for the efficiency of intersystem crossing for the DMDHP isomer using Equation (4.3):

$$\Delta A_{BPh} = \frac{\phi_{ISC}\epsilon_{BPh}}{\phi_{T1}\epsilon_{DMDHP}}|\Delta A_{T1}| \qquad \textbf{Equation (4.3)}$$

where ΔA is the magnitude of the triplet absorption measured from the kinetics of *BPh* or **2** (*T1*), ϕ_{ISC} is the intersystem crossing quantum yield of BPh, and ϕ_{T1} is the quantum yield of triplet formation for **2**.

Benzophenone (BPh) was used as the standard to which DMDHP **2** was compared. BPh (λ_{irr} = 355 nm) has an intersystem quantum yield of unity and a maximum absorption for the triplet transient at 520 nm (6500 $M^{-1}cm^{-1}$)[9] in acetonitrile. Since **2** was one of the few compounds examined whose CPD did not absorb at 355 nm, the intersystem crossing quantum yield was measured relative to BPh (Figure 4.12) and was then used as a secondary standard for the other DMDHP derivatives.

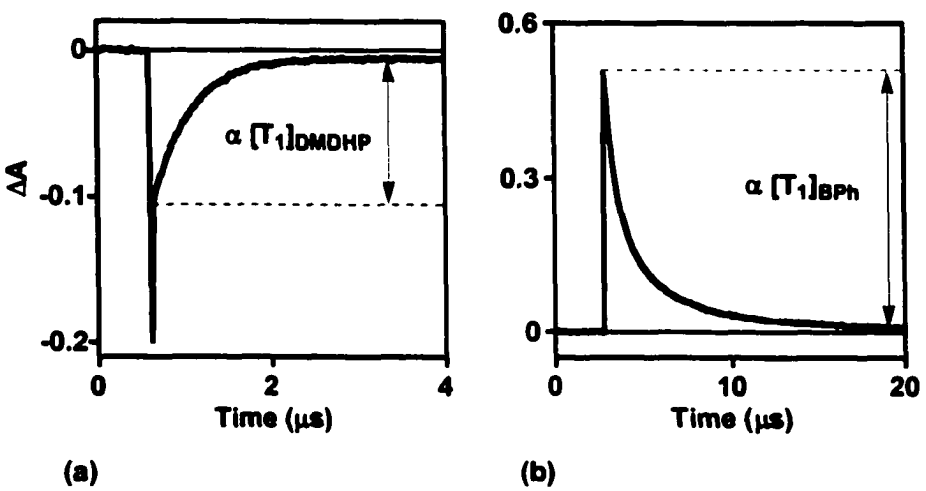

Figure 4.12. Comparison of the triplet transient kinetics of (a) DMDHP **2** at 465 nm and (b) benzophenone at 520 nm for measuring intersystem crossing quantum yields.

The intersystem crossing quantum yield measured for **2** was found to be 0.005 ± 0.001. This was used, along with the kinetics data obtained for the relative quantum yield measurements (above), to obtain efficiencies for triplet formation for other DMDHP derivatives. All triplet quantum yields were found to be in the range of 0.0009 to 0.018.

These values were of the same magnitude as the fluorescence and isomerization quantum yields obtained.

Table 4.5. Triplet excited state concentrations ($[T_1]$)[a], intersystem crossing quantum yields (ϕ_{ISC}) and rate constants (k_{ISC}) for various DMDHP derivatives.

Compound	$[T_1]$ (10^{-6} M)	ϕ_{ISC} (10^{-3})	k_{ISC} (10^5 s^{-1})
1	2.5 ± 0.5	6 ± 1	11 ± 2
2	1.9 ± 0.4	5 ± 1	9 ± 2
24	0.5 ± 0.1	1.3 ± 0.3	3.0 ± 0.6
11	2.6 ± 0.5	7 ± 1	13 ± 3
25	7 ± 1	18 ± 4	43 ± 9
26	2.1 ± 0.4[b]	5 ± 1	10 ± 2
14	0.39 ± 0.08	1.0 ± 0.2	c
17	1.6 ± 0.3	4 ± 1	9 ± 2
18	1.5 ± 0.3[b]	4 ± 1	11 ± 2
27	1.3 ± 0.3	3.5 ± 0.7	8 ± 2
22	0.33 ± 0.7	0.9 ± 0.2	2.2 ± 0.4

[a] A 20% error was estimated for all ΔA values used in determining the triplet excited state concentrations. [b] $[T_1]$ were underestimated since kinetics traces did not fully decay. [c] τ was not measured.

Intersystem crossing rate constants were calculated based on the corresponding quantum yields and singlet lifetimes (i.e. $k_{ISC} = \phi_{ISC}/\tau_s$). These were found to be on the order of 10^6 s^{-1} (Table 4.5). These values were slightly higher than the rate constants for fluorescence and isomerization indicating that this process should predominate over the other two processes in the absence of another more efficient deactivation pathway.

4.6 Proposed Photophysical / Photochemical Mechanism

Upon irradiation DMDHP was excited to the first excited singlet state (S_1). The fluorescence spectra were found to be sharp and exhibited no Stokes shift, indicating that the excited state was rigid. The fluorescence efficiency was found to be on the order of

10^{-3}, resulting in fluorescence rate constants of 1×10^5 to 1×10^6 s^{-1}. The lifetimes were determined to be between 3.8-5.6 ns. These lifetimes were much longer than for other photochromic molecules, which exhibit excited state lifetimes of less than a picosecond.[12,26,38,46,47,104,105] The longer lifetime found for the DMDHPs suggests than the isomerization step was slow.

Laser flash photolysis data indicated the presence of two transients on different timescales. The shorter-lived transient detected by laser flash photolysis was most likely the singlet excited state of DMDHP since the singlet lifetimes obtained from fluorescence were similar to the pulse width of the laser (10 ns). However, the results obtained do not rule out the existence of another short-lived species that was formed and decayed within the laser pulse. Such a species could be a singlet biradical ($BR^{1\bullet}$) formed from the S_1 state of DMDHP. The singlet biradical could be thought of as the DMDHP in which the transannular bond was broken and two spin paired radical centers are placed on the sp^3 carbons. Bond formation to give back DMDHP would be highly favourable unless the molecule rearranged sufficiently to prevent it. Either way, the biradical would be short-lived. The conjugation of such a species might be expected to be intermediate between that of DMDHP and CPD since the radicals are capable of rearrangement to less conjugated species than DMDHP or of losing planarity. The transient absorption spectra obtained indicated that the short-lived transient was less conjugated than DMDHP but exhibited a greater degree of conjugation than CPD.

The efficiency of the ring opening process was found to be low (i.e. $10^{-2} - 10^{-4}$) giving rate constants between 3×10^4 and 3×10^6 s^{-1}. Substituents were found to modulate this value to some extent. The rate constants were low considering that the ring opening process was photochemically allowed according to the Woodward-Hoffmann rules. A possible explanation for the low reactivity was that the ring opening reaction was an activated process. Examples of such processes have been reported previously with hexamethyl substituted DMDHPs.[76] If an activated process was occurring, the isomerization rate constants would be expected to increase with the increasing energy of the singlet excited state (as calculated from the emission maximum). This process was ruled out since compounds **17** and **18** have different excited singlet state energies (by ca. 1 kcal·mol^{-1}) but have similar ring opening isomerization rate constants. A 5-fold

difference in rate constants would be expected for **17** and **18** if an activation barrier existed for the isomerization reaction.

There also exists the possibility that the isomerization was not a concerted process but proceeded through an intermediate, which would account for the low cleavage rate constants for the singlet excited state of DMDHP. As previously mentioned, a singlet biradical, formed from the singlet excited state of DMDHP, was a possibility. If a singlet biradical was involved, it was possible that the S_1 to BR^{1*} process was very efficient but the BR^{1*} to CPD reaction was the inefficient step. Reformation of the transannular bond would be expected to compete efficiently with isomerization, since the singlet multiplicity of the biradical makes this an allowed process. Intersystem crossing to the triplet biradical would not be expected since the proximity of the radical centers to one another would cause the energy difference between the singlet and triplet biradical to be large.[4.106.107]

Assuming that all the excited molecules that do not undergo fluorescence, intersystem crossing or isomerization, proceed to the singlet biradical, one can estimate an upper limit on the rate constant for this process between 1.7×10^8 and 2.5×10^8 s^{-1} ($k_{BR1*} = 0.95/\tau_s$). Formation of BR^{1*} from S_1 would be much faster than the other deactivation pathways and as such, the other deactivation pathways (i.e. fluorescence, internal conversion, intersystem crossing) could not compete with it. It should be noted that even the formation of the singlet biradical would be much slower than similar processes observed with other photochromic compounds.[12.26.38.46.47.104.105] The upper limit on the rate constant assumes that there was no internal conversion occurring. In reality, a combination of the two processes would most likely be occurring, if the biradical was formed. Even though the S_1 to BR^{1*} process could potentially be more efficient than the other deactivation pathways for S_1, the BR^{1*} deactivation to the ground state DMDHP would still be the predominant deactivation pathway for the biradical.

Differentiation between a concerted mechanism and a mechanism involving the formation of a singlet biradical was not possible from the current data. A potential explanation for the low isomerization quantum yield may be that the rigidity of the molecular framework of DMDHP makes it impossible for the reactive species (singlet excited state or biradical) to investigate a variety of nuclear motions on the reaction

surface. This could restrict the efficiency of isomerization for either mechanism by not having different reaction modes available for the molecule to sample. In the case of other photochromic molecules such as spirooxazines,[104,105] fulgides,[12,26] and diarylethenes,[38,46,47] a much larger change in geometry was permitted during the cycloreversion process. The reaction efficiency was much higher for these types of compounds possibly due in part to the fact that these compounds were free to spatially rearrange and explore various reaction modes.

It was determined that the longer-lived transient observed by laser flash photolysis was the triplet excited state whose energy was between 22 and 38 kcal·mol^{-1}. The triplet was most likely the first triplet excited state of DMDHP. The intersystem crossing quantum yield was determined to be on the order of 10^{-3} which led to intersystem crossing rate constants (k_{isc}) of 10^5 to 10^6 s^{-1}. These rate constants were comparable with those measured for fluorescence and isomerization.

The ring opening isomerization occurred through the singlet excited state and although the triplet was formed upon excitation, it was not involved in the switching. The isomerization quantum yields measured were the same within error in the presence and absence of oxygen. If the triplet excited state was involved, one would have expected a significant difference in the quantum yield under oxygen purged conditions. Assuming a diffusional rate constant for the quenching of the triplet state by oxygen obtained from LFP studies (1.9×10^9 $M^{-1}s^{-1}$), a rate constant in the absence of quencher of 2×10^5 s^{-1} (k_o) and an oxygen concentration of 11.5 mM in CHX[9], an observed rate constant (k_{obs}) of 2.1×10^7 s^{-1} was calculated using Equation (1.20). This translated into a change in isomerization quantum yield from 0.006 to 0.00006 for compound **1**. The same quenching involving the singlet excited state ($k_o = 1 \times 10^8$ s^{-1}) would only result in a change from 0.006 to 0.0048, which was observed for this compound.

Scheme 4.13 summarizes the possible pathways the excited molecules may follow. Once excited, the molecules returned to the ground state by fluorescence, intersystem crossing or isomerize to CPD. The combined efficiencies for these three processes accounted for less than 5% of all excited molecules. The other 95% of the excited molecules must have decayed nonradiatively to the ground state DMDHP. This

might have been as a result of internal conversion (IC) or decay from the singlet biradical.

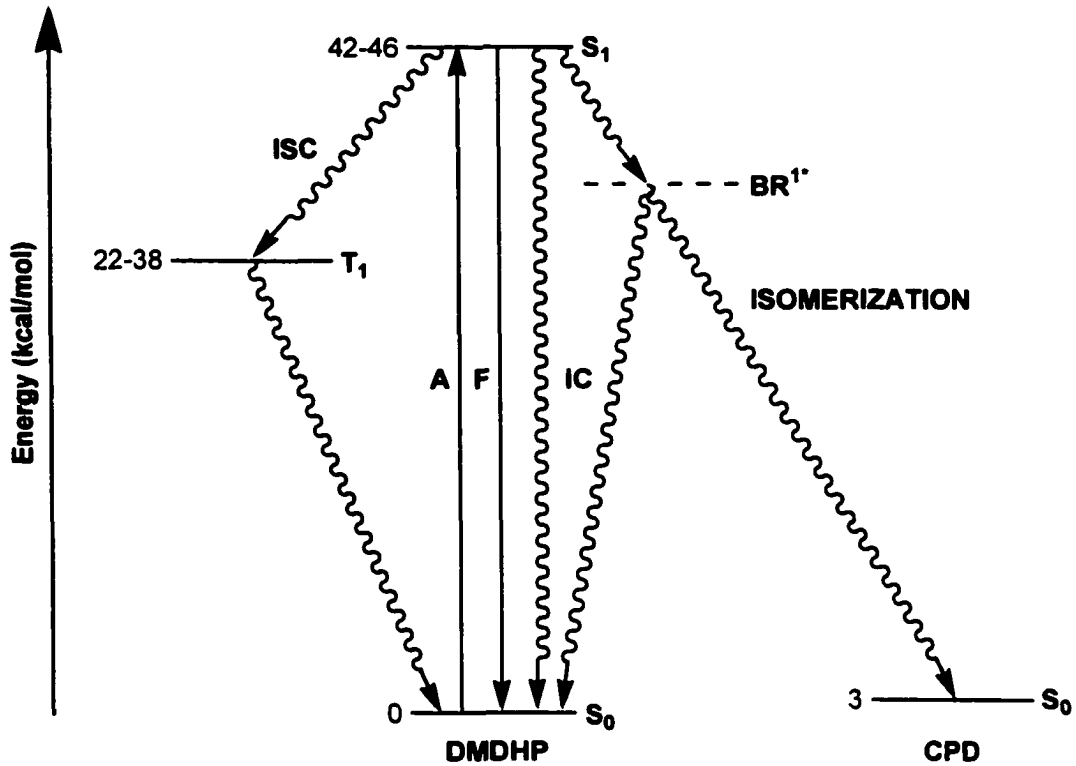

Figure 4.13. Proposed mechanism for the possible deactivation pathways (fluorescence (F), internal conversion (IC), intersystem crossing (ISC) and isomerization) of DMDHP following excitation (absorption (A)) to the excited singlet state (S_1). The isomerization reaction may occur directly from S_1 of DMDHP to S_0 of CPD or proceed via a singlet biradical (BR^{1*}).

CHAPTER 5: [e]-ANNELATED DMDHP SYSTEMS

5.1 Introduction

Preliminary studies qualitatively showed that the dimethyldihydropyrene derivative where a benzene group was fused on the [e] face (**3**) bleached almost completely within five minutes, upon irradiation using a tungsten lamp.[108] Irradiation of the same sample with a UV lamp was seen to return the coloured solution. This was unlike the simple substituted DMDHPs, where irradiation for several hours at lower temperatures was still not able to produce a colourless solution. As a result of these preliminary findings, a more thorough investigation into the photophysics of arene fused compounds was initiated to determine if the mechanism of isomerization was different from that of the simple DMDHP systems. To this end, a series of [e]-annelated dimethyldihydropyrenes were studied.

Compound **3** was used as the standard to which the other annelated systems were compared. The effect of adding substituents at the 4-position of compound **3** was also studied to see if the same effects were seen in the benzo-fused system as with the simple DMDHPs. Although it was found for the simple substituted DMDHPs that incorporation of an acetylene at the 4-position (**17**, section 4.42, table 4.2) lead to at least a 3-fold decrease in ring opening efficiency, an acetylene substituted version of compound **3** (**28**[103]) was studied to determine if the same effect was seen with the [e]-benzo fused compound. Since substitution with an acetyl group was seen to double the ring opening efficiency in the simple DMDHP systems (**24**, **25**, section 4.4, table 4.2), an acetyl substituted analog (**29**[102]) of the [e]-benzo fused compound was studied.

The effect that changing the fused arene might have on the isomerization was also of interest. For this series, the benzene fused **3** was used as the standard to which the naphthalene (**30**[74]) and triphenylene (**31**[102]) fused compounds were compared. Due to the instability of the anthracene fused system[108], a detailed photophysical study was not possible.

The [e,l]-dibenzo fused compound (**32'**[78]) was also studied as part of the series. Compound **32'** was found to exhibit positive photochromism unlike the other DMDHP derivatives studied. This meant that the CPD isomer (colourless, denoted with prime)

was the more stable of the two isomers and was converted to the DMDHP isomer upon UV irradiation. The half life of the DMDHP isomer at room temperature was found to be ca. 1-2 ms,[78] therefore, examination of the CPD isomer was only possible in that case.

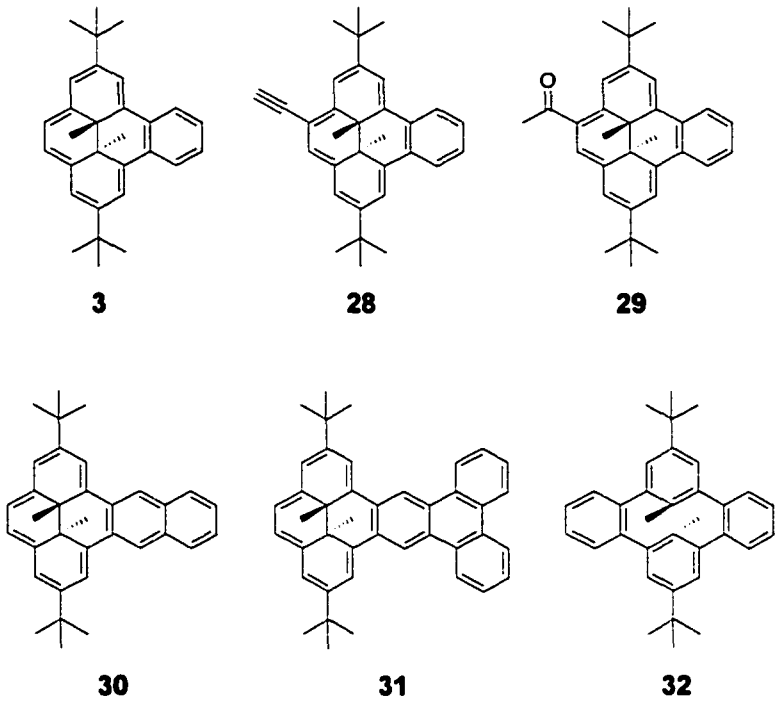

Figure 5.1. Compounds used in the investigation into the photoisomerization mechanism of [e]-fused derivatives of dimethyldihydropyrene.

5.2 Dimethyldihydropyrene Isomers

5.2.1 Absorption

The absorption of annelated DMDHPs spanned from the ultraviolet (~ 260 nm) to the visible (650 nm, Appendix A, Table A2, Figure A3). The longest wavelength band absorbed in the region of 450 to 600 nm and often had a visible shoulder above 600 nm. The same band in the simple substituted DMDHPs was much less broad and a second distinct band was clearly visible above 600 nm. The molar absorptivity coefficients of the longest wavelength band for the annelated compounds were about 10^3 $M^{-1}cm^{-1}$. There were several bands between 280 and 420 nm with molar absorptivities of 10^4 $M^{-1}cm^{-1}$. The two most intense bands occur between 380 and 420 and were associated with

the DMDHP moiety while the other higher energy bands resembled the red shifted ground state absorption spectra of the arene moieties.

Substitution of compound **3** with conjugating groups such as acetylene and acetyl caused the bands associated with the DMDHP moiety to be red shifted by 10 nm for **28** and 15 nm for **29**. There appeared to be no significant difference in the molar absorptivity coefficients upon simple substitution (Appendix A, Table A2).

Changing the fused arene group lead to an even greater shifting of the DMDHP absorption bands. The longest wavelength band was red shifted by 25 nm for **31** and by 50 nm for **30**. No significant change in the molar absorptivity coefficients was seen for this band.

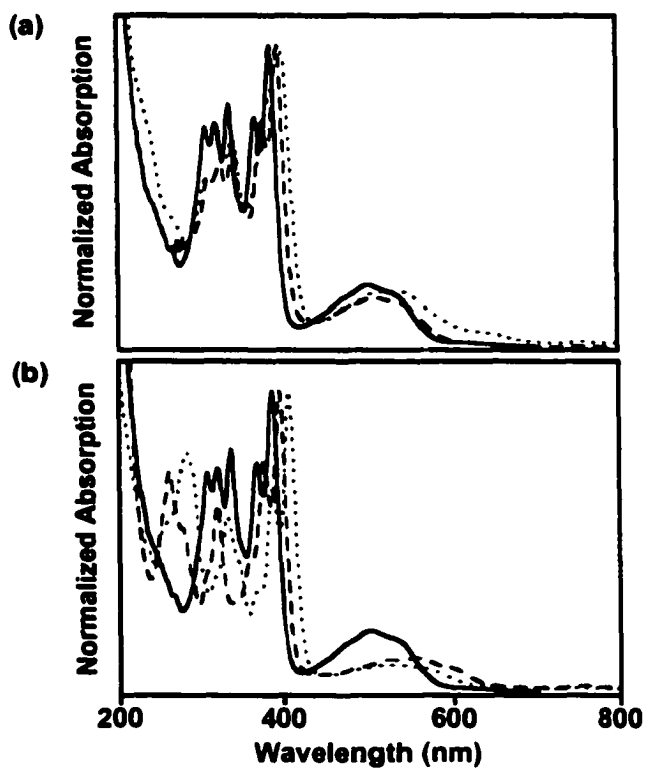

Figure 5.2. Overlay of the absorption spectra (normalized for the maximum intensity absorption) of [e]-annelated DMDHP isomers of (a) **3** (——), **28** (– – –) and **29** (·····), and (b) **3** (——), **30** (– – –) and **31** (·····).

5.2.2 Fluorescence

5.2.2.1 Emission Spectra

Fluorescence was seen for all compounds except **29**. The emission for the annelated DMDHP derivatives was weaker and broader than the simple DMDHPs but still exhibited no structure. A noticeable Stokes shift was present at room temperature. The maxima of the room temperature fluorescence spectra were in the 670 to 700 nm region and the emission spanned from about 600 to 800 nm.

At low temperature (77 K) the spectra for compounds **3**, **28** and **31** were seen to resolve into two distinct bands and were blue shifted when compared with the room temperature spectra. It was not possible to see if the emission of the naphtho-substituted **30** was resolved as the emission was too weak to accurately differentiate it from the baseline noise. At low temperature there was no real Stokes shift since the emission overlapped with the shoulder of the longest wavelength band.

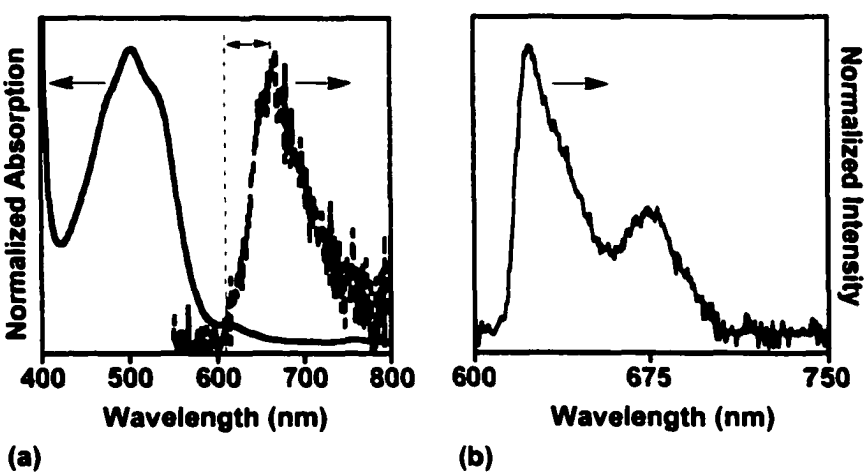

Figure 5.3. (a) Overlay of the absorption (——) and emission (---) spectra for **3** at room temperature. The difference between the dashed lines indicates the Stokes shift between the emission maximum and the longest wavelength shoulder (believed to be the (0,0) band) in the ground state absorption spectrum. (b) The emission spectrum of **3** at 77 K between 600 and 750 nm in cyclohexane.

The fact that the emission was seen to resolve into two bands at low temperature implies that the annelated DMDHPs were less rigid than the simple DMDHPs, which exhibited sharp emissions that did not change at low temperature (Section 4.3.1). At

Table 5.1. Emission maxima (λ_{max})[a], singlet excited state energies (E_{S1})[b], fluorescence quantum yields (ϕ_f), singlet excited state lifetimes (τ_s), and fluorescence rate constants (k_f^o)[c] for various [e]-annelated DMDHP derivatives.

Compound	λ_{max} (nm)	E_{S1} (kcal·mol^{-1})	ϕ_f (10^{-3})	τ_s (10^{-9} s)	k_f^o (10^5 s^{-1})
3	620	46.1 ± 0.2	0.9 ± 0.1	2.4 ± 0.1	3.8 ± 0.5
28	633	45.2 ± 0.2	0.48 ± 0.01	2 – 5[f]	1 – 2.4[h]
30	690[d]	ca. 41[d]	≤ 0.01[e]	g)	i)
31	630	45.4 ± 0.2	0.35 ± 0.01	2 – 5[f]	0.7 – 1.8[h]

[a] The fluorescence maxima were determined from the low temperature fluorescence spectra. [b] The singlet excited state energies were calculated from the λ_{max} of the low temperature emission spectra. [c] The fluorescence rate constants were calculated from the fluorescence quantum yields and the lifetimes obtained from time-resolved fluorescence. [d] The fluorescence maximum was determined from the room temperature fluorescence spectrum. [e] The fluorescence quantum yield was estimated from a single measurement. [f] Only a range of lifetimes could be estimated from the lifetime data. [g] Lifetime data could not be obtained due to the weak fluorescence intensity. [h] A range of rate constants was calculated from the range of lifetimes. [i] A rate constant could not be calculated due to lack of lifetime data.

5.2.2.3 Fluorescence Lifetimes and Rate Constants

The decay of the fluorescence with time was mono-exponential for **3** and a lifetime for the singlet excited state of 2.4 ns under aerated conditions was recovered using Equation (4.1). Due to the weak fluorescence for compounds **28** and **31**, an absolute lifetime could not be determined since the number of counts at maximum intensity obtained was only 2000-5000 as opposed to the 10000 required for an accurate measurement. Instead, a range of lifetimes (2-5 ns) was given for this parameter. No lifetime could be measured for **30** since the fluorescence intensity was too weak for the decay to be distinguished from the background noise.

The lifetime of **3** was slightly shorter than the lifetimes measured for the simple substituted DMDHPs. The lifetimes for the annelated DMDHPs were still much longer than the sub-nanosecond lifetimes seen for other photochromic compounds.[12,38,105] The lifetimes for the annelated DMDHPs were shorter than the corresponding lifetimes for the arene group itself. For example, benzene has a lifetime of 12 ns in aerated cyclohexane while naphthalene and triphenylene have lifetimes of 13 ns.[9]

Fluorescence rate constants (or ranges) were determined from the singlet excited state lifetimes and fluorescence quantum yields (i.e. Equation (4.2)). The rate constants

were found to be in the range of 0.7×10^4 to 3.8×10^5 s^{-1}. These were comparable with the fluorescence rate constants obtained for the simple substituted dimethyldihydropyrenes but were about an order of magnitude lower than those calculated for the arene moieties by themselves.[9]

5.2.3 Ring Opening Isomerization Quantum Yields

The CPD isomers for all annelated DMDHPs absorbed to some extent at 380 nm. Therefore, the potassium ferrioxalate actinometer was not used to avoid the potentially larger errors associated with this system when used above 400 nm.[5.109] As a result, the ring opening quantum yields were obtained relative to compound **1** ($\phi_{DMDHP \rightarrow CPD} = 0.006 \pm 0.002$) and were measured with irradiation at 480 nm. The values reported were the average of two experiments, each of which consisted of the average of at least two individual measurements. Oxygen was found to have no effect on the isomerization efficiency and as such, the measurements were carried out using freshly prepared solutions under aerated conditions.

The ring opening quantum yield for the benzo fused **3** was found to be 0.042 or in other words 4.2% of all excited molecules underwent isomerization. This was about 30 times more efficient than the *t*-butyl substituted **2** and 7 times more efficient than the parent **1**. Substitution of **3** with an acetylene (**28**) was found to improve the ring opening efficiency by another factor of two. This was in contrast to the simple substituted DMDHPs where substitution with an acetylene (**17**) was found to decrease the ring opening quantum yield by a factor of three relative to **2**.

Substitution with an acetyl (**24**) was found to double the efficiency of ring opening of the simple DMDHP **1**. For the annelated systems, a quantum yield of 0.095 was obtained for **29**, which is slightly more than twice the efficiency measured for **3**. Therefore, it can be concluded that incorporation of an acetyl on any DMDHP framework should be expected to double the ring opening efficiency.

Exchanging the benzene group for naphthalene resulted in a small increase in the ring opening quantum yield to 0.054. Substitution with a triphenylene group showed a similar efficiency of 0.039 compared with **3**. It can be concluded that changing the arene

group that was fused on the DMDHP framework did not significantly change the ring opening quantum yield.

The ring opening quantum yields obtained for the arene fused DMDHPs were comparable with other photochromic compounds as their efficiencies were only one order of magnitude less than the most efficient literature compounds. For example, the most efficient dithienylethene derivative (**33**, Scheme 5.1a) was found to have a ring opening quantum yield of 0.58[110], although most are significantly lower (≤ 0.13)[38] while one of the most efficient furylfulgides (**34**, Scheme 5.1b) had an efficiency for the ring opening of 0.28[12].

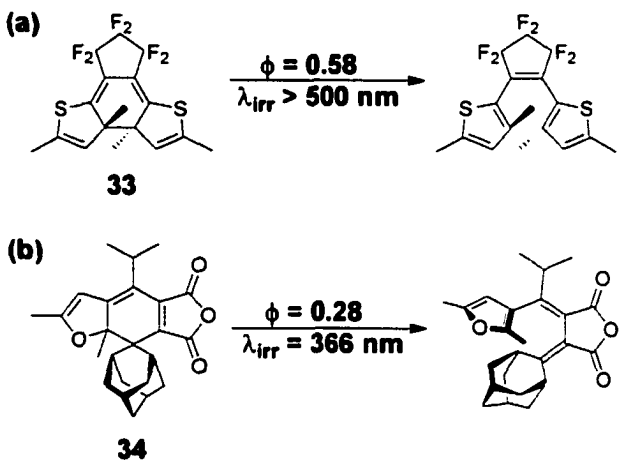

Scheme 5.1. Literature examples of the (a) diarylethene[110] and (b) furylfulgide[12] having one of the most efficient ring opening isomerization quantum yields.

The most efficient ring opening for the DMDHP derivatives studied in this project was 0.1 for the acetyl substituted benzo-fused compound, **29**. This was in contrast to the simple substituted DMDHPs, which had ring opening quantum yields that were at least an order of magnitude lower than the annelated DMDHPs.

Table 5.2. Ring opening isomerization quantum yields ($\phi_{DMDHP \rightarrow CPD}$) and rate constants ($k_{DMDHP \rightarrow CPD}$)[a] for various [e]-annelated DMDHPs as measured by actinometry.

Compound	$\phi_{DMDHP \rightarrow CPD}$ (10^{-3})	$k_{DMDHP \rightarrow CPD}$ (10^{7} s^{-1})
3	42 ± 2	1.8 ± 0.1
28	75 ± 8	1.5 – 3.8
29	95 ± 8	b)
30	54 ± 5	b)
31	39 ± 3	0.8 – 2.0

[a] Isomerization rate constants were calculated from the quantum yield of isomerization and lifetimes obtained from time-resolved fluorescence. [b] Isomerization rate constants were not be calculated because the lifetimes could not be obtained from time resolved fluorescence measurements (see above).

The isomerization rate constants were calculated from the isomerization quantum yields and the singlet excited state lifetimes using a derivative of Equation (4.1). They were found to be between 8×10^{6} and 3.8×10^{7} s^{-1}. It was important to note that for the simple DMDHPs, the ring opening isomerization rate constant and fluorescence rate constant were of similar magnitude. For the arene fused DMDHPs the isomerization rate constants were two orders of magnitude higher than the corresponding fluorescence rate constants. Therefore, the increase in isomerization efficiency for the annelated dimethyldihydropyrenes was due to the higher rate constant for this process relative to other deactivation pathways such as fluorescence.

5.2.4 Laser Flash Photolysis

5.2.4.1 Transient Absorption Spectra

The transient absorption spectra were the same for all compounds under deoxygenated conditions. Only one transient was seen that formed within the laser pulse and led to a residual absorption that was constant for the time-resolution of the equipment (see below for kinetics). The growth of the transient was seen as a positive signal below 300 nm and the maximum of the absorption was the same as that for the CPD isomer. A bleaching was seen above 300 nm where the molar absorptivity coefficients for DMDHP

were larger than those of the transient. The bleaching resembled the ground state absorption spectrum of the DMDHP isomer (Figure 5.4a).

In the presence of oxygen, a second transient was seen in the transient absorption spectrum of **3**, **28**, **30**, and **31**. This appeared as a small positive absorption in the 420 nm region for **31** (Figure 5.4b) where the molar absorptivity coefficients of the new transient were larger than those of the DMDHP. The inset in Figure 5.4b shows the difference spectrum that was obtained from subtracting the aerated transient absorption spectrum at long delays (110 ns) from the transient absorption spectrum at short delays (8.81 ns). This spectrum should correspond to the transient absorption spectrum of the new transient formed in the presence of oxygen. It was interesting to note that the absorption maximum obtained from the inset of Figure 5.4b (i.e. 430 nm) was the same as the absorption maximum for the triplet-triplet absorption of triphenylene.[111]

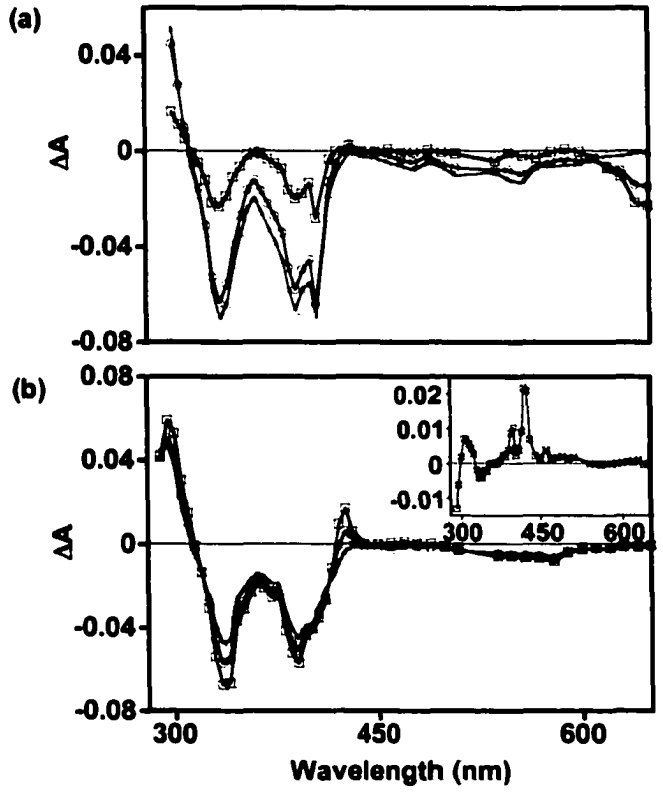

Figure 5.4. Transient absorption spectra of **31** under (a) deoxygenated conditions at 7.87 ns (□), 22.7 ns (○) and 123 ns (Δ), and 9b) oxygenated conditions at 8.81 ns (□), 42.2 ns (○) and 110 ns (Δ) obtained with 525 nm excitation. The inset shows the difference spectrum obtained from subtracting the transient spectrum at 110 ns from the spectrum at 8.81 ns shown in (b) normalized at 540 nm.

5.2.4.2 Transient Kinetics

The transient kinetics showed a single transient that grew in within the laser pulse (≤ 10 ns) under nitrogen purged conditions (Figure 5.5). This transient led to a residual absorption that was constant for the time resolution of the instrument. No transient absorption corresponding to the triplet excited state was observed under these conditions. This was in contrast with the observation for the simple substituted DMDHPs where the triplet excited state was formed with low efficiency (10^{-3}). In the presence of increasing concentrations of oxygen, a second transient was seen to grow in with a lifetime of several hundred nanoseconds for **3**, **28**, and **31**.

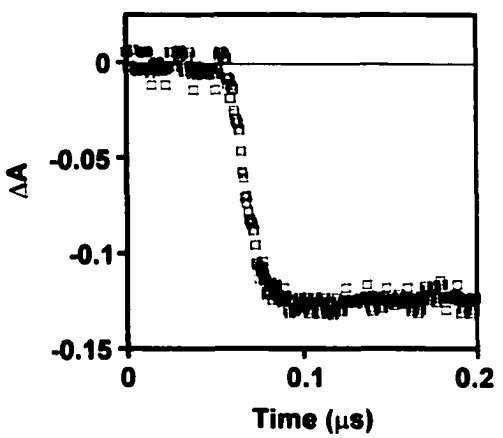

Figure 5.5. Transient kinetics for **29** at 400 nm under deoxygenated conditions in cyclohexane.

5.2.4.2.1 Oxygen Induced Intersystem Crossing

The yield of the transient formed in the presence of oxygen was proportional to the degree of bleaching of the DMDHP (ΔA_T) and it increased with increasing oxygen concentrations (Figure 5.6). At low oxygen concentrations, the new transient had a lifetime of hundreds of nanoseconds that was shortened upon increasing the oxygen concentration. These results were consistent with oxygen induced intersystem crossing from the singlet excited states of the DMDHPs to their corresponding triplet excited states.[1] The reaction outlined in Equation (5.1) then competes with other deactivation pathways.

$$DMDHP^{1*} + O_2^3 \rightarrow DMDHP^{3*} + O_2^{1*}$$ **Equation (5.1)**

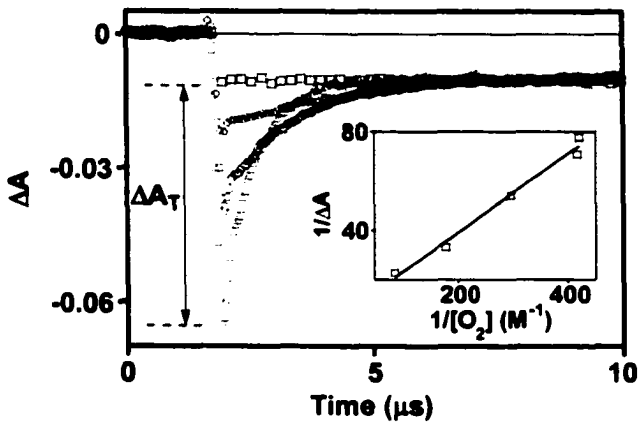

Figure 5.6. Overlay of the transient kinetics for **3** in the presence of 0 mM (□), 2.4 mM (◊), 5.6 mM (○), and 11.5 mM (Δ) oxygen as measured at 335 nm in cyclohexane. The measurement of the magnitude of the triplet absorption is illustrated for the kinetics trace in the presence of 11.5 mM oxygen. The inset shows the determination of the quenching rate constant for the singlet excited state using Equation (5.2).

Since the quenching of the singlet excited state by oxygen could not be measured directly, an alternative way of measuring it was needed. It was possible to indirectly measure the quenching by monitoring the products of the reaction of the singlet excited state of DMDHP and oxygen (i.e. triplet excited state formation). This was done by assuming that the difference between the magnitude of the bleaching of the DMDHP and the residual absorption (ΔA_T, Figure 5.6) was proportional to the triplet excited state absorption. A quenching rate constant was obtained by comparing the magnitude of the bleaching at various oxygen concentrations using Equation (5.2):[112,113]

$$\frac{1}{\Delta A_T} = \alpha + \frac{\alpha}{K_{SV}[O_2]} = \alpha + \frac{\alpha}{k_q \tau_s [O_2]}$$ **Equation (5.2)**

where ΔA_T is the magnitude of the absorbance of the triplet excited state (i.e. magnitude of bleaching of DMDHP less the residual absorption), α is a constant that incorporates

instrumental parameters, K_{SV} is the Stern-Volmer constant, k_q is the quenching rate constant and τ_s is the radiative lifetime.

The Stern Volmer constant recovered for **3** was 41 M^{-1}, which corresponded to a quenching rate constant for the singlet excited state by oxygen of 1.7×10^{10} $M^{-1}s^{-1}$ (τ_s = 2.4 ns, Table 5.1). This was consistent with the quenching rate constant obtained from steady state fluorescence measurements.

The triplet excited state that was formed from the singlet excited state was also quenched by oxygen. At low concentrations of oxygen the lifetime of the triplet excited state was hundreds of nanoseconds (Figure 5.6, ◊). With increasing oxygen concentrations the lifetime was seen to decrease down to 50 ns for a maximum oxygen concentration of 11.5 mM (Figure 5.6, Δ). A linear relationship of the lifetimes obtained from the transient kinetics of the triplet excited state at various oxygen concentrations using Equation (1.20) led to a diffusional quenching rate constant of $(1.25 \pm 0.06) \times 10^9$ $M^{-1}s^{-1}$. This quenching rate constant was consistent with the value seen for oxygen quenching of other polyaromatic triplet states.[9]

As previously mentioned, the kinetics did not decay back to baseline but instead led to a residual absorption, the magnitude of which was proportional to the amount of CPD formed upon isomerization of the DMDHP form. It should be noted that the same residual absorption was obtained in the presence and absence of oxygen. Therefore, the triplet excited state was not involved in the ring opening reaction.

It could be argued, however, that the CPD was formed from both the singlet and triplet excited states with a combined efficiency that exactly matched the efficiency of CPD formation in the absence of oxygen. That is to say that the isomerization quantum yield for the formation of CPD from the excited singlet state (i.e. $S_1 \rightarrow$CPD) was decreased in the presence of oxygen but was compensated for by an increase in the isomerization quantum yield for the formation of CPD from the triplet excited state (i.e. $T_1 \rightarrow$CPD). This explanation was unlikely since the quenching of the triplet excited state with increasing oxygen concentrations should lead to a significant decrease in the isomerization quantum yield (see above).

5.2.4.2.2 Relative Isomerization Quantum Yields

As was seen with the simple substituted dimethyldihydropyrenes, the kinetics for the annelated derivatives did not decay to zero but instead led to a residual absorption. This residual absorption (ΔA_{res}) was proportional to the concentration of metacyclophanediene formed ([CPD]), which in turn was proportional to the ring opening quantum yield ($\phi_{DMDHP \rightarrow CPD}$). The concentration of CPD was determined by comparing the kinetics for the various annelated derivatives at 465 nm obtained from excitation of solutions with matched absorptions at the excitation wavelength (480 nm, Figure 5.7). The concentrations were then calculated ($\Delta A_{res}/\varepsilon_{465\ nm}$) relative to **3** and compared with the relative ring opening isomerization quantum yields (relative to **3**, Table 5.3). The relative isomerization quantum yields obtained from laser flash photolysis were within error of those obtained through actinometric methods (Table 5.3).

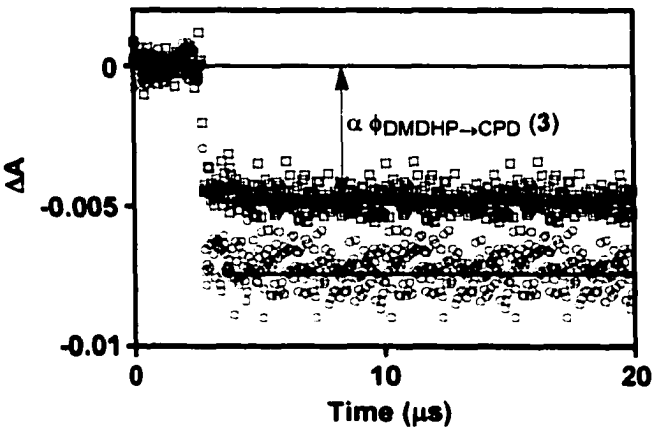

Figure 5.7. Overlay of the transient kinetics for compounds **3** (□) and **28** (○) at 465 nm qualitatively illustrating the use of residual absorptions in determining the relative ring opening isomerization quantum yields of [e]-annelated DMDHPs.

Table 5.3. Metacyclophanediene concentrations ([CPD])[a] and relative [CPD] obtained from LFP compared with relative ring opening isomerization quantum yields (relative $\phi_{DMDHP \rightarrow CPD}$) obtained from actinometry for various [e]-annelated DMDHP derivatives.

Compound	[CPD] (10^{-7} M)	Relative [CPD]	Relative $\phi_{DMDHP \rightarrow CPD}$
3	8 ± 2	1	1
28	19 ± 4	2.3 ± 0.5	1.8 ± 0.6
30	19 ± 4	2.3 ± 0.5	1.3 ± 0.4
31	14 ± 3	1.7 ± 0.3	0.9 ± 0.3

[a] Metacyclophanediene concentrations were calculated by dividing the magnitude of the residual absorption obtained from the transient kinetics at 465 nm by the molar absorptivity coefficient for each compound at 465 nm ([CPD] = $\Delta A_{res} / \varepsilon_{465}$).

5.3 Metacyclophanediene Isomers

5.3.1 Absorption

The metacyclophanediene isomers of the annelated derivatives absorbed strongly in the ultraviolet with intense bands between 230 and 290 nm that tailed out to 410 nm (Figure 5.8). No distinct absorption maxima were visible after the major absorptions bands but it was clear from the absorption spectra that there were weak absorptions at longer wavelengths (Appendix A, Figure A4). The structure of the spectrum was consistent with the overlap of an intense allowed absorption band with a weaker absorption band at lower energies. This would be expected if the higher energy absorption corresponded to the $S_0 \rightarrow S_2$ transition. The S_0 to S_2 transition is an allowed process and would be expected to have high molar absorptivity coefficients. The lower energy structured absorption most likely corresponds to the $S_0 \rightarrow S_1$ transition. This transition would be forbidden by symmetry, giving it lower molar absorptivity coefficients. Substitution did not seem to have much affect on the position of the absorption maxima.

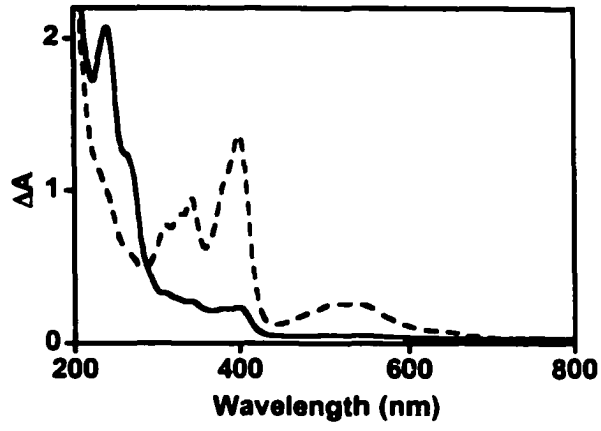

Figure 5.8. Overlay of the ground state absorption spectra for the CPD (— —) and DMDHP (- - -) isomers of **29** in cyclohexane.

5.3.2 Fluorescence

5.3.2.1 Emission Spectra

Fluorescence was seen to some extent for all metacyclophanediene derivatives except **29'** (Appendix B). The emission for **3'** was centered at 340 nm and exhibited some structure as shoulders off the main band (Figure 5.9a) over the region of 300 – 450 nm. Compounds **28'**, **31'** and **32'** showed a very structured emission spectrum, with five distinct bands, that were red shifted when compared with **3'** (Figure 5.9b) in the region of 350 – 500 nm. The emission for the naphthalene-annelated **30'** showed a broad emission (300 – 500 nm) that exhibited some structure but was much weaker in intensity than observed for the other annelated derivatives (Figure 5.9c).

The fluorescence emission for the CPD derivatives was red shifted when compared with the emission for the arene portions of the molecules. For example, the highest energy emission bands for benzene, naphthalene and triphenylene were reported as 261, 311, and 343 nm[9] while the corresponding CPDs (namely, **3'**, **30'** and **31'**) exhibited the highest energy emissions at 341, 380, and 406 nm. This implied that there was significant conjugation between the arene and the phenyl rings of the CPD moiety. This was not expected since the CPD geometry was 'stepped' (Scheme 1.10) as opposed to the DMDHP isomer where the molecule was planar and extensive conjugation was expected. Therefore, there must have been some overlap between the π-orbitals on the arene and

those on the phenyl rings of the CPD. It should be noted that there was a smaller effect of this extended conjugation on the more highly conjugated arenes. For example, the difference in energy for the highest energy emission of benzene and **3'** was 25.7 kcal·mol^{-1} while the same energy difference for triphenylene and **31'** was only 12.9 kcal·mol^{-1}. The same difference in energy (i.e. red shift in the spectrum) was seen between the ground state absorption of the arenes and the absorption bands of the annelated DMDHP isomers associated with the arene moiety.

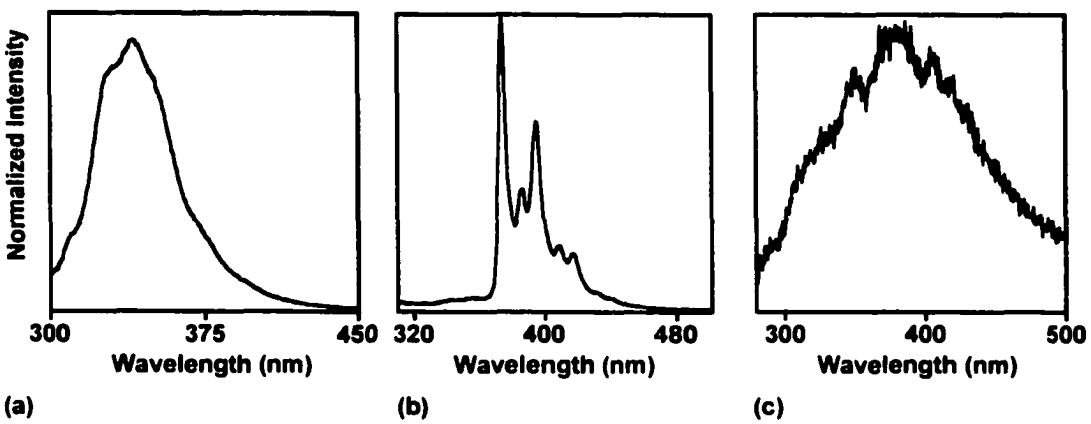

Figure 5.9. Emission spectra of (a) **3'** (λ_{ex} = 270 nm), (b) **32'** (λ_{ex} = 280 nm), as representative of the vibrational structure seen in the emission for **28'** and **31'**, and (c) **30'** (λ_{ex} = 250 nm).

All spectra seemed to exhibit a noticeable Stokes shift when compared with the lowest energy absorption maximum that was clearly visible at room temperature (i.e. $S_0 \rightarrow S_2$ transition). It was obvious from the tail of the ground state absorption spectra (Figure 5.8) that weaker absorption bands corresponding to the $S_0 \rightarrow S_1$ transition existed. Although an accurate value for the maxima of these weaker absorptions was not possible, the tail of the absorption spectra overlapped with the high energy end of the emission spectra indicating that there was probably no Stokes shift.

The fluorescence spectrum for **3'** and **30'** were less structured than the emission for the other compounds. This implies that the CPDs of **3'** and **30'** were less rigid in the excited state (see above). It was surprising that the emission for **28'** was so much more structured and red shifted than **3'**, considering the only difference between the two compounds was the addition of an acetylene group.

Oxygen was found to quench the fluorescence intensity in a diffusional process. Using Equation (1.15), a Stern-Volmer constant for **3'** of (35 ± 9) M^{-1} was recovered, giving a lower limit on the quenching rate constant of 2×10^{10} $M^{-1}s^{-1}$ ($\tau_s < 2$ ns, Table 5.4). This was consistent with the quenching seen for the DMDHP derivatives from fluorescence and laser flash photolysis data.

The singlet excited state energies were calculated from the highest energy emission maximum. They were found to be in the range of 70 – 84 kcal·mol^{-1}. This was double the energy of the DMDHP isomers.

5.3.2.2 Fluorescence Quantum Yields

The fluorescence quantum yields of the metacyclophanedienes were measured relative to naphthalene ($\phi_f = 0.19$) in cyclohexane. Naphthalene was chosen because it emitted in the same wavelength region (Figure 5.10) as the annelated CPDs. It also had a quantum yield that was sufficiently low to make an accurate comparison between the compounds using the same instrument settings on the fluorimeter for both measurements (i.e. same slits). The values reported were an average of two experiments, each consisting of three individual measurements (Table 5.4). All CPD measurements were performed under aerated conditions.

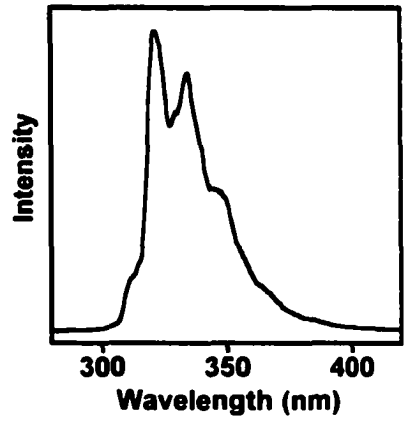

Figure 5.10. Fluorescence spectrum for naphthalene in cyclohexane.

The fluorescence quantum yield for **3'** was found to be 0.03. Substitution of **3'** with an acetylene (**28'**) at the 4-position was found to have little effect on the

fluorescence efficiency. Addition of a second fused benzene ring on the [l]-face (**32'**) decreased the emission efficiency by a factor of three. Exchange of the benzene group with another arene decreased the fluorescence quantum yield by about an order of magnitude. A fluorescence quantum yield for **30'** of 0.0037 was measured, which was an eight-fold decrease in efficiency, while a value of 0.0016, a 19-fold decrease in efficiency was measured for the triphenylene-fused **31'**. The fluorescence quantum yields measured for the CPDs were larger than the same values for the corresponding DMDHPs.

Table 5.4. Emission maxima (λ_{max}), singlet excited state energies (E_{S1})[a], fluorescence quantum yields (ϕ_f), singlet excited state lifetimes (τ_s), and fluorescence rate constants (k_f^o)[b] for various [e]-annelated CPD derivatives.

Compound	λ_{max} (nm)	E_{S1} (kcal·mol^{-1})	ϕ_f (10^{-3})	τ_s (10^{-9} s)	k_f^o (10^5 s^{-1})
3'	341	83.8 ± 0.6	30 ± 7	2.0 ± 0.5[c]	150 ± 40[c]
28'	375	76.2 ± 0.6	20 ± 1	13.7 ± 0.5	15 ± 1
30'	380	75.2 ± 0.5	3.7 ± 0.4	13 ± 1	2.9 ± 0.4
31'	406	70.4 ± 0.4	1.6 ± 0.4	17 ± 1	9 ± 2
32'	375	76.2 ± 0.6	9.4 ± 0.9	12 ± 2	7.8 ± 0.9

[a] Singlet excited state energies were calculated from the highest energy fluorescence maximum. [b] The fluorescence rate constants were calculated from the fluorescence quantum yields and lifetimes ($k_f^o = \phi_f / \tau_s$). [c] The lifetime was estimated from the quenching rate constant seen for the simple substituted DMDHPs and the Stern-Volmer constant measured for the fluorescence quenching by oxygen for **3'** since it was shorter than the time-resolution of the single photon counter. As a result, the fluorescence rate constant was calculated using the calculated lifetime.

5.3.2.3 Fluorescence Lifetimes and Rate Constants

The fluorescence intensity of the CPD isomers was found to decay mono-exponentially with time (Figure 5.11). The lifetimes recovered using Equation (4.1) were much longer than those of the corresponding DMDHPs. The notable exception was for the benzene-fused derivative (**3'**) where the lifetime was found to be less than the time resolution of the instrument. The other derivatives had comparable lifetimes between 12 and 17 ns.

The Stern-Volmer constant determined from steady state fluorescence quenching with oxygen (Section 5.3.2.1, (35 ± 9) M^{-1}) could be used to obtain an alternative estimate of the lifetime for **3'**. A fluorescence quenching rate constant for **3'** was

estimated by assuming that the fluorescence quenching was comparable to that seen for the simple substituted DMDHPs. Therefore, by using the fluorescence quenching rate constant determined for **2** of 2×10^{10} $M^{-1}s^{-1}$ (Chapter 4, Section 4.3.1), a lifetime for **3'** of (2 ± 0.5) ns was estimated.

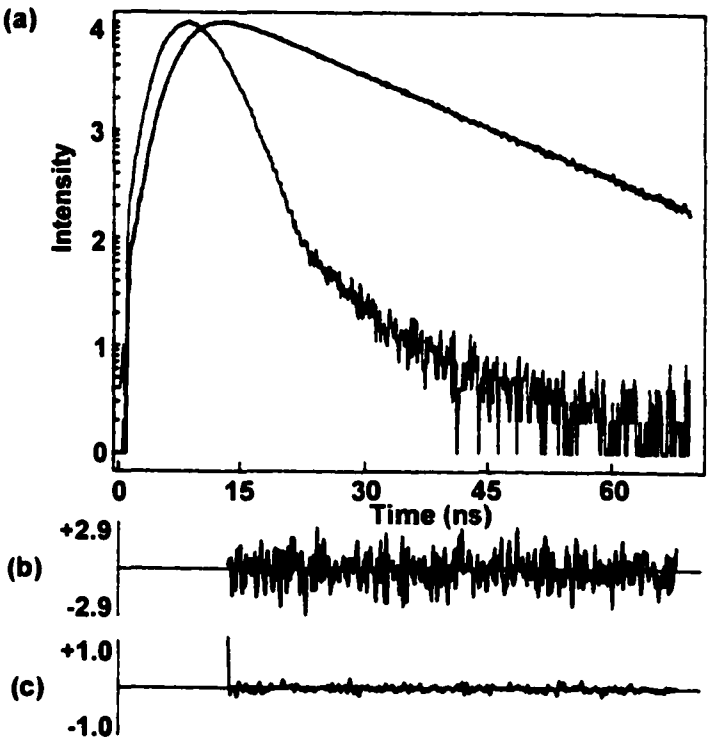

Figure 5.11. (a) Fluorescence decay for the CPD isomer of **28'** measured in cyclohexane at 395 nm using a single photon counter. (b) Residuals and (c) autocorrelation show how well the data fit to a mono-exponential function (solid line in (a)).

The fluorescence rate constants were calculated using the fluorescence efficiencies and the lifetimes (Equation (4.2)). They were found to be on the order of 10^5 s^{-1}, similar to those obtained for the DMDHP isomers. The only exception was for **3'** where the rate constant was calculated to be 2×10^7 s^{-1}. In can be concluded from the lifetime and rate constant data that the fluorescence quantum yields were increased as a consequence of the longer lifetimes and not because the fluorescence rate constants were higher than for the corresponding DMDHPs.

5.3.3 Ring Closing Isomerization Quantum Yields

The ring closing isomerization quantum yields for the annelated CPDs were measured relative to potassium ferrioxalate (ϕ = 1.25) with excitation at 254 nm[6,7] where the DMDHP isomers did not absorb. The values reported were an average of two experiments, each of which consisted of at least two individual measurements.

The ring closing efficiencies were the same within error for all compounds studied. The quantum yields for the dibenzo-annelated **32'** could not be measured since the half life of the DMDHP isomer at room temperature was only 1-2 ms.[78] The other derivatives showed efficiencies for ring closing between 0.28 and 0.39. This was almost an order of magnitude higher than the ring opening quantum yields measured for the DMDHP isomers, however, it was significantly lower than the value of unity previously suggested for the simple substituted DMDHPs.[76] The fact that the efficiencies were similar for all derivatives implied that the ring closing reaction was not significantly affected by structural changes on the CPD framework.

The ring closing efficiencies were comparable with those seen for diarylethenes and fulgides. For example, several dithienylethene[38] (Scheme 1.8) and furylfulgide[12] derivatives (Scheme 1.7) have been shown to have cyclization quantum yields in the range of 0.1-0.5.

Table 5.5. Ring closing isomerization quantum yields ($\phi_{DMDHP \rightarrow CPD}$) and rate constants ($k_{CPD \rightarrow DMDHP}$) for various [e]-annelated CPDs as measured by actinometry.

Compound	$\phi_{CPD \rightarrow DMDHP}$	$k_{CPD \rightarrow DMDHP}$ (10^7 s^{-1})
3'	0.42 ± 0.07	21 ± 5[a)]
28'	0.28 ± 0.03	2.0 ± 0.2
29'	0.39 ± 0.09	b)
30'	0.29 ± 0.04	2.2 ± 0.3
31'	0.38 ± 0.09	2.2 ± 0.5

[a)] the isomerization rate constant was calculated using the estimated lifetime for **3'** of 2 ns. [b)] the isomerization rate constant could not be calculated since the compound did not fluoresce and therefore, a lifetime could not be measured.

The ring closing rate constants were calculated from the quantum yields and lifetimes using Equation (4.2). They were found to be similar to those of the ring opening rate constants. That is, the ring closing rate constants were calculated to be in the range of 2×10^7 s^{-1} for **28'**, **30'** and **31'**. This was expected since both the ring opening and ring closing isomerizations were photochemically allowed processes and should proceed with similar rate constants. The benzo-fused derivative (**3'**) was found to have a higher ring closing rate constant of 2×10^8 s^{-1}. Although these rate constants were comparable with the ring opening rate constants, they are much lower than similar processes in other photochromic compounds (i.e. 10^{12} s^{-1}).[12,38,105]

In can be concluded that the isomerization quantum yields for the annelated DMDHPs rivaled those of other compounds even though the isomerization rate constants were much lower. This was because the lifetimes of the annelated DMDHPs were also much longer than the lifetimes of other photochromic compounds.

5.3.4 Laser Flash Photolysis

5.3.4.1 Transient Absorption Spectra

The CPD isomers of the annelated derivatives were irradiated at 308 nm. The transient spectra obtained from the irradiation of the metacyclophanediene isomers resembled the inverse of the spectra obtained upon irradiation of the DMDHPs (Appendix C). The transient absorption spectra showed a bleaching below 300 nm corresponding to the disappearance of CPD. A positive absorption was seen above 300 nm that resembled the ground state absorption of the DMDHP isomer (Figure 5.12a). Under nitrogen purged conditions, a single transient was formed within the laser pulse and led to a residual absorption that was constant for the time-resolution of the instrument (i.e. 10 ms, see below for kinetics).

Under oxygen purged conditions a second transient was clearly visible in the transient absorptions spectra of the DMDHP isomers **3**, **28**, **30** and **31**. In the transient absorption spectra of the CPD isomers, however, it was difficult to discern if a second transient was formed (Figure 5.12b). This may be due to the fact that at short delays, the

fluorescence of the CPDs occurred in the same region where the absorption for the triplet excited state might be expected to occur making it impossible to see this absorption.

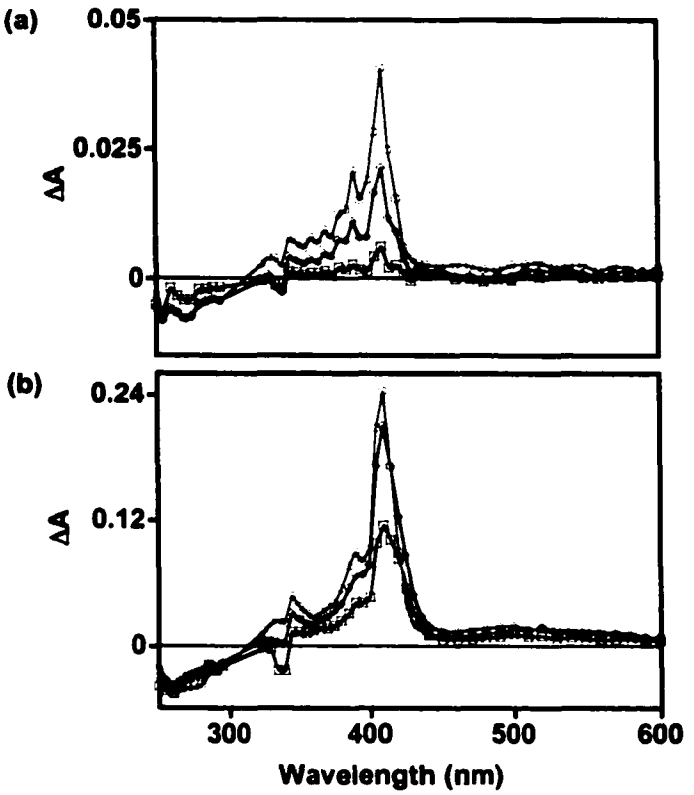

Figure 5.12. Transient absorption spectrum of **31'** under (a) deoxygenated conditions at 5.74 ns (□), 17.0 ns (◊) and 104 ns (○), and (b) oxygenated conditions at 15.3 ns (□), 55.1 ns (◊) and 116 ns (○).

5.3.4.2 Transient Kinetics

A single transient was seen in the transient kinetics that formed within the laser pulse and led to a residual absorption under nitrogen purged conditions (Figure 5.13). The positive residual absorption was constant for the time-resolution of the instrument up to 10 ms. The presence of a transient absorption corresponding to the triplet excited state was not seen under these conditions.

Under oxygenated conditions, the formation of a second transient was observed with a lifetime of hundreds of nanoseconds for **3'**, **28'** and **31'** as was seen with the corresponding DMDHP isomers. It was interesting to note that the new transient was not

observed for the CPD of **30'** even though it was seen for the corresponding DMDHP isomer.

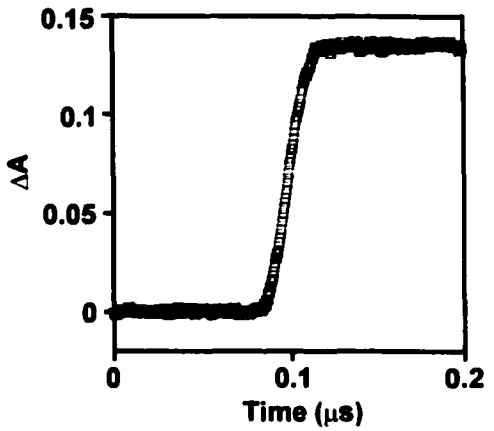

Figure 5.13. Transient kinetics for **29'** at 400 nm under deoxygenated conditions.

5.3.4.2.1 Oxygen Induced Intersystem Crossing

As previously observed for the annelated DMDHP isomers, a second transient was seen in the presence of oxygen for the CPD isomers of **3'**, **28'** and **31'** (Figure 5.14). As the concentration of oxygen was increased, the amount of the second transient formed (ΔA_T) increased as well. This indicates that the formation of the transient was induced by oxygen. The lifetime of the new transient decreased with increasing concentrations of oxygen (i.e. was quenched by oxygen). These results are consistent with the oxygen induced formation of the triplet excited state from the singlet excited state of the CPD isomers.[1]

Qualitatively the kinetics form the CPDs under aerated conditions behaved in a similar manner to the DMDHP kinetics. The rate constants for the formation and subsequent quenching of the triplet excited state were estimated to be consistent with the results obtained from the DMDHP isomers (i.e. $k_q = 10^{10}\ M^{-1}s^{-1}$).

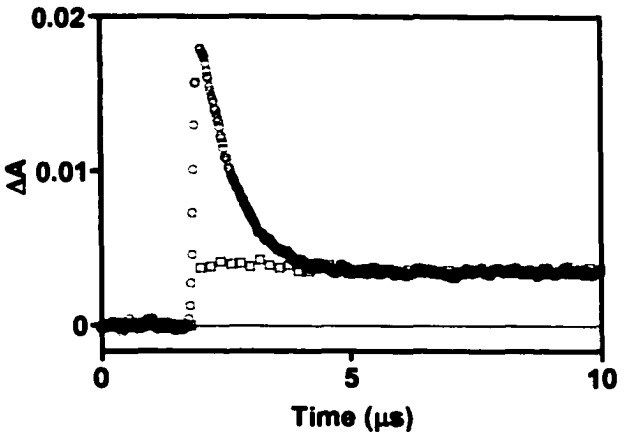

Figure 5.14. Overlay of the transient kinetics for **28'** in the presence of 0 mM (□) and 11.5 mM (○) oxygen as measured at 510 nm in cyclohexane.

5.3.4.2.2 Ring Closing Isomerization Quantum Yields

For the annelated DMDHP isomers, it was not possible to measure an absolute isomerization quantum yield because the DMDHPs could not be irradiated at the same wavelength as the standard, benzophenone (i.e. 355 nm). This was because the CPD isomers, produced upon irradiation of the DMDHP isomers, absorbed out to 400 nm. As a result, the isomerization quantum yields were measured relative to **3'** (i.e. ratios of quantum yields). In contrast, for the CPD isomers the ring closing isomerization quantum yields could be measured relative to benzophenone since irradiation of both samples could be carried out at 266 nm where the DMDHP isomers did not absorb. As with the DMDHP isomers, excitation of the CPD isomers led to a transient that did not decay to baseline but led to a residual absorption (ΔA_{res}). It was assumed that the magnitude of the residual absorption was proportional to the amount of DMDHP formed upon irradiation of the CPD isomers. The isomerization quantum yield was then estimated from a comparison of the absolute magnitude of the residual absorption ($|\Delta A_{res}|$) obtained from the kinetics of the annelated CPD isomers, measured at several wavelengths above 300 nm, to the magnitude of the triplet absorption of benzophenone (ΔA_{BPh}) in acetonitrile (Figure 5.15) using a modified version of Equation (3.4) (i.e. Equation (5.3)).

$$\Delta A_{BPh} = \frac{\phi_{isc}\epsilon_{BPh}}{\phi_{CPD\rightarrow DMDHP}\epsilon_{DMDHP}}|\Delta A_{res}| \qquad \textbf{Equation (5.3)}$$

The ring closing quantum yields obtained from laser flash photolysis (Table 5.6) were, on average, lower than those obtained by actinometry. However, the trends are consistent between the two methods and the quantum yields measured from laser flash photolysis can be thought of as being a lower limit.

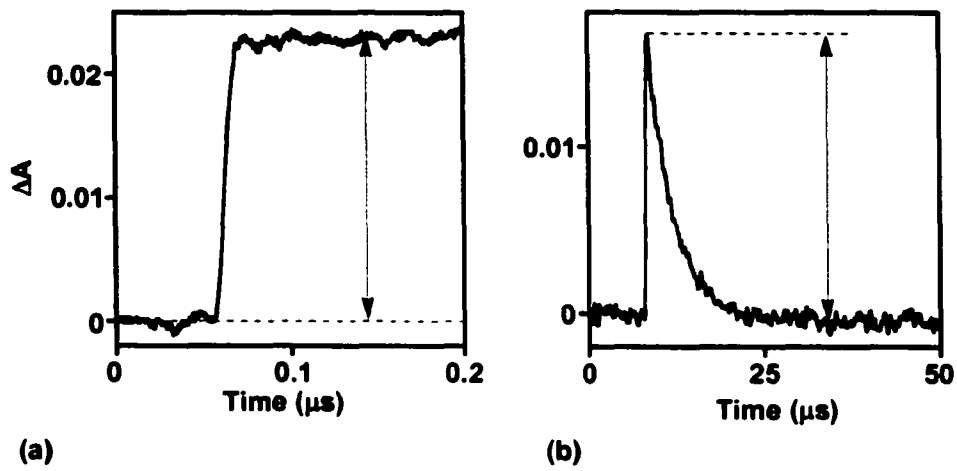

Figure 5.15. Comparison of the (a) residual absorption of **32'** at 400 nm and (b) triplet transient kinetics of benzophenone at 520 nm for measuring the ring closing isomerization quantum yield.

In the case of the [e,l]-dibenzo annelated derivative **32'**, a direct quantum yield measurement of the ring closing quantum yield by actinometry was not possible due to the half-life of the DMDHP isomer at room temperature being too short ($\tau_{1/2} \rightarrow$ 1-2 ms).[78] Laser flash photolysis was useful in this case since the timescales employed were much shorter. A comparison of the residual absorption for **32'** and the triplet absorption for benzophenone gave a value for the $\phi_{CPD\rightarrow DMDHP}\varepsilon_{DMDHP}$ of 5094 $M^{-1}cm^{-1}$. An exact value for the molar absorptivity of the DMDHP isomer of **32'** was not known. Therefore, the molar absorptivity coefficient for the 410 nm band of **32'** was estimated to be between $1.5 \times 10^5 - 4.6 \times 10^5$ $M^{-1}cm^{-1}$. The estimate was based on the molar absorptivity coefficients for the corresponding absorption band of the other annelated DMDHPs

between 369 and 392 nm. These values were used to give an estimate for the ring closing quantum yield between 0.11 and 0.33.

Table 5.6. Dimethyldihydropyrene concentrations ([DMDHP]) and ring closing isomerization quantum yields ($\phi_{CPD \rightarrow DMDHP}$) obtained from LFP compared with ring closing isomerization quantum yields obtained from actinometry for various [e]-annelated CPD derivatives.

Compound	$\phi_{DMDHP \rightarrow CPD}$	
	LFP	Actinometry
3'	0.31 ± 0.06	0.42 ± 0.07
31'	0.20 ± 0.04	0.38 ± 0.09
32'	0.11 – 0.33	

5.4 Proposed Photophysical / Photochemical Mechanisms

5.4.1 Dimethyldihydropyrene Isomers

Upon excitation the annelated DMDHPs underwent fluorescence or isomerization under nitrogen purged conditions. The fluorescence spectra were broad, weak and lacked any structure at room temperature. At low temperature, the spectra were seen to resolve into two bands. The fluorescence quantum yields were on the order of 10^{-4}, which was an order of magnitude lower than observed for the simple DMDHPs (Chapter 4). Due to the weak fluorescence, it was only possible to obtain an accurate lifetime for **3** of 2.4 ns. The lifetimes of **28** and **31** were estimated to be between 2 and 5 ns. The lifetimes for the annelated DMDHPs were similar to those obtained for the simple substituted DMDHPs (Table 4.1, Section 4.3). The fluorescence rate constants were estimated to be between 7×10^4 and 3.8×10^5 s^{-1} for the annelated DMDHPs, which was comparable with the rate constants obtained for the simple DMDHPs.

Transient absorption spectra showed a single transient under deoxygenated conditions. As with the simple substituted DMDHPs, the short lived transient (≤ 10 ns) was most likely the S_1 state of the DMDHP since the lifetimes of the singlet excited states of the annelated DMDHPs were shorter than the time-profile of the laser pulse. There

was no indication of a transient absorption corresponding to the triplet excited state of DMDHP.

The ring opening isomerization quantum yields of the arene-fused dimethyldihydropyrenes were found to be an order of magnitude higher than those measured for the simple substituted DMDHPs (Table 4.2, Section 4.4). The quantum yields of the annelated DMDHPs were not changed significantly by substitution of the fused arene group. The addition of an acetylene (**28**) was seen to increase the quantum yield by 1.8 times while addition of an acetyl group (**29**) increased the quantum yield by 2.3 times relative to **3**.

There was an increase in ring opening efficiency of two orders of magnitude between the most efficient annelated DMDHP (**29**) and the simple t-butyl substituted DMDHP (**2**). The significant increase in ring opening efficiency seen upon annelation of an arene could be attributed to the bond fixation ability of the arene groups on the DMDHP moiety. It was shown previously that fusion of an arene group served to bond fix the double bonds on the DMDHP framework.[74] It was possible that the electrocyclization reaction was more efficient when the double bonds behaved more like isolated double bonds (i.e. bond fixed) and less like delocalized double bonds (i.e. aromatic). The increase in the ring opening quantum yield that was seen upon addition of an acetylene or acetyl group was likely due to the fact that the increased conjugation can stabilize the 6-membered transition state.

The isomerization rate constants calculated for the annelated DMDHPs were found to be between 8×10^6 and 1.8×10^7 s^{-1}, which was two orders of magnitude higher than those calculated for the simple substituted DMDHPs (Chapter 4, Section 4.4.3). The isomerization rate constants were also two orders of magnitude higher than the fluorescence quantum yields. In the case of the simple substituted DMDHPs, the fluorescence and isomerization rate constants were of similar magnitude, allowing both processes to effectively compete with each other. For the annelated DMDHPs, however, the isomerization rate constants were sufficiently higher than the fluorescence rate constants that isomerization was more efficient than fluorescence for these compounds. The increase in isomerization quantum yield seen for the annelated derivatives relative to

the simple compounds was attributed to the higher isomerization rate constants since the lifetimes the simple and annelated DMDHPs were comparable.

In the presence of oxygen, a second transient was seen by LFP in the transient absorption spectra. It was concluded that this was the oxygen induced formation of the triplet excited state of the DMDHP from the singlet excited state. Since the isomerization quantum yields were the same in the presence and absence of oxygen, it was unlikely that the triplet excited state was involved in the isomerization of the annelated DMDHPs. The triplet excited state was quenched at higher concentrations of oxygen, which would have led to a corresponding decrease in the quantum yield. This was not seen.

5.4.2 Metacyclophanediene Isomers

The shape and energy of the fluorescence spectra for the annelated CPDs was found to be dependent on the substitution of the metacyclophanediene framework. The benzo-fused derivative (**3'**) was found to behave differently from the other derivatives in that its emission was shifted to higher energy and was less structured relative to the other CPD isomers. The lifetime of **3'** was found to be less than 2 ns while the lifetimes of the other annelated derivatives were between 12 and 17 ns. The lifetimes of **28'** and **30'-32'** were three to four times longer than the lifetimes for the DMDHP derivatives. The fluorescence quantum yields for the CPD isomers were found to be higher (i.e. 0.0016-0.030) than their corresponding DMDHP isomers. The fluorescence rate constants. however, were still on the order of 10^5 s^{-1} (except **3'**). This indicates that the increase in fluorescence quantum yield seen for the CPD derivatives relative to their DMDHP isomers was due to the increase in lifetime and not a change in the rate constants.

The transient absorption spectra of the annelated CPDs showed the presence of a single short lived transient under nitrogen purged conditions. This transient was most likely the singlet excited state of the CPD even though the lifetime of most of the annelated CPDs were sufficiently long that the S_1 transient absorption should have been visible in the LFP spectra. The fact that the transient absorption was not seen may be due to the fact that the fluorescence of the CPDs was relatively intense in the region in which the transient absorption of the singlet excited state was expected to occur. Therefore, the fluorescence masked the absorption of the singlet excited state.

The ring closing isomerization quantum yields were found to be insensitive to the nature of the arene ring and addition of conjugating groups at the 4-position. The quantum yields obtained were between 0.28 and 0.42, which were an order of magnitude higher than the ring opening quantum yields of the corresponding annelated DMDHPs. The isomerization rate constants were calculated to be about 2×10^7 s^{-1}. These rate constants were two orders of magnitude higher than the fluorescence rate constants. This indicated that the isomerization pathway was more efficient than fluorescence, which could not compete effectively. Therefore, the increase in the isomerization quantum yield, relative to the corresponding DMDHP isomers, was due to the longer lifetimes of the annelated CPDs since the isomerization rate constants were of the same magnitude.

Under aerated conditions a second transient was seen in the transient absorption spectrum for **3'**, **28'** and **31'**. This transient was assigned to the triplet excited state of the CPD formed from the reaction of the singlet excited state and oxygen. Compounds **29'**, **30'** and **32'** did not show the presence of a second transient. It was possible that formation of the triplet excited state did occur under aerated conditions but the intensity of the residual absorption was so large for those compounds relative to the absorption of the triplet, that the transient absorption was lost in the experimental noise. If the intersystem crossing quantum yield was assumed to be the same for the annelated CPDs as was measured for the simple substituted DMDHPs (i.e. 10^{-3}) then the absorption due to the triplet would be expected to account for less than 2% of the entire signal and may have been lost in the signal noise.[114] As with the annelated DMDHP isomers, the triplet excited state was not believed to be involved in the isomerization since the same ring closing quantum yields were seen in the presence and absence of oxygen.

5.4.3 Mechanism

Upon excitation the annelated dimethyldihydropyrene derivatives underwent fluorescence, isomerization or internal conversion. Under nitrogen purged conditions, intersystem crossing as was seen with the simple substituted DMDHPs did not occur. Isomerization to the ground state of the CPD isomer proceeded either directly from the singlet excited state of DMDHP (i.e. $DMDHP^{1*} \rightarrow CPD$) or from a singlet biradical formed from the S_1 of DMDHP (i.e. $DMDHP^{1*} \rightarrow BR^{1*} \rightarrow CPD$). It was not possible to

distinguish between a concerted process and one that involved an intermediate based on the current data.

Excitation of the arene-fused metacyclophanedienes led to fluorescence or isomerization. It was expected that the efficiency of internal conversion would be decreased due to the large energy difference between the ground state and first excited singlet state of CPD. The probability of internal conversion occurring is inversely proportional to the energy difference between the ground and excited electronic states.[1] This probably accounted for, in part, the increase in isomerization efficiency that was seen for the CPD isomers relative to the DMDHP isomers. The CPD isomers can isomerize to the ground state DMDHP isomers directly through the singlet excited state of the CPD (i.e. $CPD^{1*} \rightarrow$ DMDHP) or through some biradical intermediate (i.e. $CPD^{1*} \rightarrow BR^{1*} \rightarrow$ DMDHP). Figure 5.16 shows the possible deactivation pathways that the excited annelated DMDHP and CPD isomers can follow as well and the interconversion between the two isomers.

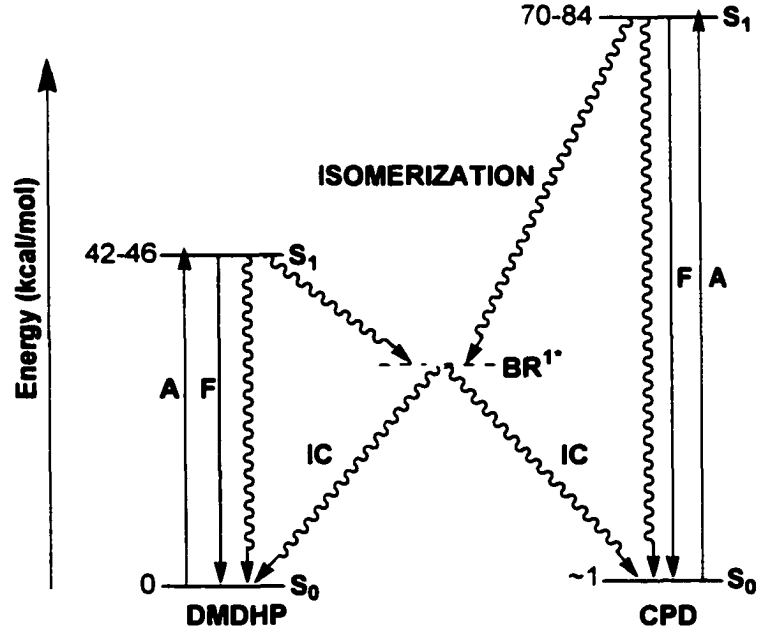

Figure 5.16. Proposed mechanism for the possible deactivation pathways (fluorescence (F), internal conversion (IC) and isomerization) of the annelated DMDHP and CPD isomers following excitation (absorption (A)) to their corresponding singlet excited states (S_1) under nitrogen purged conditions. The isomerization reaction may occur directly from the S_1 of one isomer to the S_0 of the other isomer or proceed via a singlet biradical (BR^{1*}).

CHAPTER 6: CONCLUSIONS

6.1 Isomerization Mechanism

The photoisomerization reaction was found to proceed from the ground state of the DMDHP isomer to the ground state of the CPD isomer, through the first singlet excited state of DMDHP (Scheme 6.1). The photoisomerization of the CPD to DMDHP isomer proceeded in a similar manner (i.e. CPD + hν → CPD^{1*} → DMDHP). The involvement of a singlet biradical formed from the singlet excited state was a possible intermediate whose existence can neither be proven nor disproven based on current experiments. That is to say that the data could not distinguish between a concerted reaction and one that involved an intermediate of some sort.

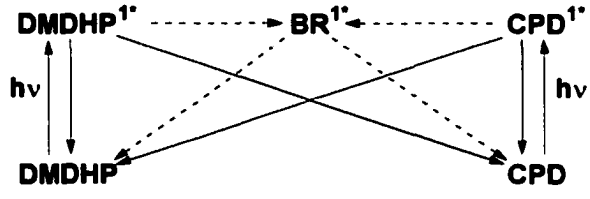

Scheme 6.1. Mechanism of isomerization for DMDHP to CPD photoconversion.

The ring opening reaction efficiencies of the simple substituted DMDHPs (Chapter 4) were seen to decrease upon the addition of conjugating acetylene (**17**, **18**, **22** and **27**) and phenyl (**26**) groups on the 4-position of the framework. Acetyl substituents on either the 2- (**24**) or 4-position (**25**) were seen to double the ring opening quantum yield relative to their unsubstituted counterparts (**1** and **2** respectively).

The ring opening isomerization quantum yields for the arene [e]-fused DMDHPs (Chapter 5) were found to be at least 4 times more efficient than the isomerization of the most efficient simple substituted DMDHP (**24**). Addition of an acetylene group in the 4-position (**28**) was found to increase the ring opening efficiency by 1.8 times relative to its unsubstituted counterpart (**3**). The addition of an acetyl on the 4-position (**29**) was found to more than double (2.3 times) the reaction efficiency compared with **3**. The nature of the arene had little effect on the ring opening quantum yield.

The efficiency of the ring closing reaction for the arene [e]-fused CPDs was found to be independent of the nature of the arene or the substitution. The efficiencies were

found to be the same, within error, for all the fused derivatives studied (i.e. 0.28-0.42). The ring closing quantum yields were at least 2 times higher than the ring opening quantum yields measured for the corresponding DMDHP isomers (0.095 for **29**).

The lifetimes of the singlet excited state for the DMDHP isomers of all derivatives were found to be relatively long for photochromic compounds (see below), between 2 and 5 ns, while the lifetimes of most CPD isomers were even longer (i.e. 12-17 ns). The isomerization rate constants for the simple substituted DMDHPs were calculated to be on the order of 10^5 s^{-1}. These rate constants are comparable with the rate constants calculated for fluorescence and intersystem crossing of the simple substituted DMDHPs (i.e. 10^5 s^{-1}).

In the case of the arene [e]-fused systems the isomerization rate constants were found to be 10^7 s^{-1}. The isomerization rate constants were two orders of magnitude higher than the rate constants calculated for fluorescence (i.e. 10^5 s^{-1}) making the ring opening reaction more competitive. The higher isomerization rate constants for the DMDHP isomers of the fused systems accounted for the higher ring opening efficiencies when compared to the simple substituted DMDHPs. This was concluded since the lifetimes were similar for both groups. The only other variable that the increase in isomerization quantum yield could then be attributed to was the higher photoisomerization rate constants ($\phi_{DMDHP \rightarrow CPD} = \tau_s \cdot k_{DMDHP \rightarrow CPD}$) for the fused DMDHPs. In the case of the annelated CPD isomers, the higher ring closing isomerization quantum yields, when compared to their corresponding annelated DMDHP analogs, could be attributed to the longer lifetimes since the isomerization rate constants were of the same order of magnitude.

6.2 Comparison With Other Photochromic Compounds

As mentioned previously, the lifetimes of the DMDHP derivatives were much longer than those of other photochromic compounds. Bond breakage in diarylethenes, for example, was shown to occur within 10 ps in both solution and solid state by picosecond and femtosecond laser flash photolysis studies.[46-51] The lifetimes for the DMDHP derivatives were found to be 2 – 5 ns and the CPD isomers were found to have lifetimes in the range of 12 – 17 ns.

The rate constants for the isomerization of diarylethenes were on the order of 10^{10} - 10^{12} s^{-1}. This was much higher than even the benzo-fused CPD derivative (**3'**), which had an isomerization rate constant of 2×10^{8} s^{-1}. It was interesting to note that although the ring opening rate constants were several orders of magnitude lower for the dimethyldihydropyrenes than the diarylethenes, in some cases the quantum yields for the ring opening reaction of the DMDHPs were of similar magnitude to those of the diarylethenes. For example, the ring opening quantum yield for **28** was 0.075 and the rate constant was around 2×10^{7} s^{-1}. The majority of bis(3-thienyl)-perfluorocyclopentenes (Scheme 6.2, **35–39**) published had ring opening (cycloreversion) efficiencies between 0.01 – 0.1 (Table 6.1) and rate constants for the process of about 5×10^{10} s^{-1}.[38] The quantum yields for the bis(2-thienyl)perfluorocylopentenes (Scheme 6.2, **33**, **40–42**) have been measured between 0.32 – 0.58 with rate constants in the range of 4×10^{11} s^{-1}.[110]

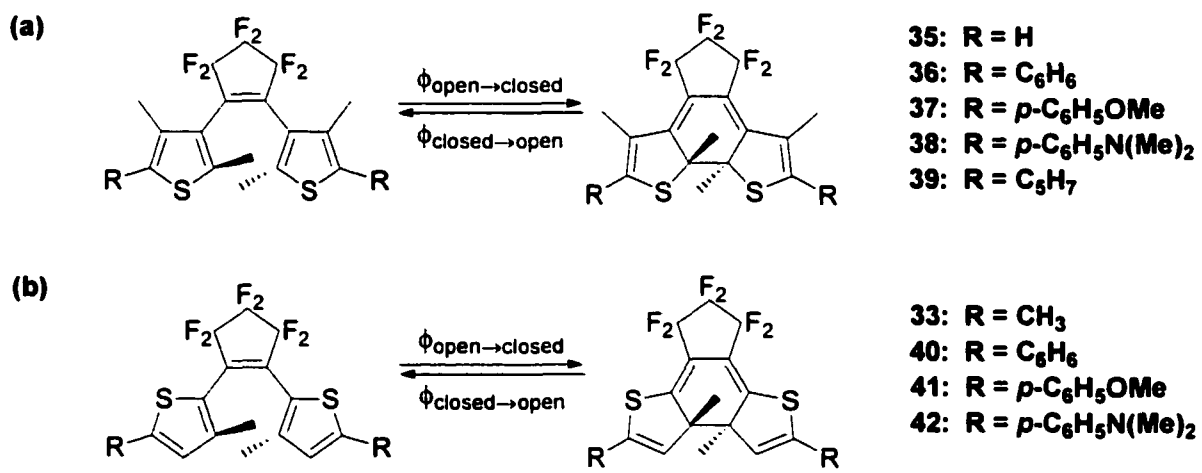

Scheme 6.2. Isomerization reactions for selected (a) bis(3-thienyl)-perfluorocyclopentenes[38] and (b) bis(2-thienyl)perfluorocyclopentenes.[110]

The CPD isomers give further evidence that the bond formation need not be fast to be efficient. The rate constants for the ring closing reaction for the CPD isomers were about 2×10^{7} s^{-1} and gave ring closing isomerization quantum yield between 0.28 and 0.42. The ring closing of the diarylethenes to the dihydrophenanthrene derivatives was found to occur with efficiencies between 0.1 and 0.5 (Table 6.1) and rate constants around 10^{11} s^{-1}.[38,110]

character on the bond, it was strengthened and was less likely to break, leading to a decrease in the ring opening quantum yield.[38]

The same stabilization phenomenon may be occurring with the transannular bond of the DMDHP derivatives as well, albeit for a different reason. Fusion of an arene ring on the [e]-face of the molecule increased the ring opening quantum yield dramatically relative to the unsubstituted system. This was attributed to the bond fixation ability of the arene. It is possible that by fixing the bonds in the DMDHP framework, the transannular bond is being weakened with respect to the unsubstituted system. This could be due to an increase in antibonding character being placed on the central bond in the excited state.

Addition of an acetyl to the 2-position of the parent DMDHP (**24**) was seen to increase the ring opening quantum yield by a factor of two relative to **1**. In contrast, any increase in conjugation on the aryl groups of the diarylethenes served to decrease the quantum yields.[38,110] A similar decrease in ring opening quantum yield was seen with 4-substitution on **2**. Adding conjugated hydrocarbons such as phenyl (**26**) or acetylene (**17**, **18** or **22**) on the 4-position of **2** decreased the ring opening quantum yield by at least a factor of four. The cyclization quantum yields of diarylethenes **35-39** are fairly insensitive to substituents.[38] This is consistent with the lack of a substituent effect seen for the ring closing reaction of the arene [e]-fused DMDHPs.

6.3 Future Directions

It is evident from the results outlined in chapters 4 and 5 that future DMDHP photoswitches should be based on the arene [e]-fused framework. The most promising DMDHP photoswitches are the 4-acetylene (**28**) and 4-acetyl (**29**) substituted benzo[e]-annelated DMDHPs. Further study into the substituent effect on these systems is required since it is unclear at this point why the isomerization quantum yields are increased upon substitution with these groups. It would be interesting to see if substitution at both the 4- and 5- positions of **3** with acetylene or acetyl groups would serve to further increase the ring opening quantum yield. The effect of incorporation of other conjugating groups such as phenyl, thienyl and ethenyl group would also be of interest. This would be important for the incorporation of such switches in molecular wire type frameworks.

A study into various fused heteroaromatic groups might also be of interest to determine if an effect of aromaticity on the ring opening quantum yields is seen. Presumably, the bond fixation is related to the aromatic stabilization energy exhibited by an aromatic ring. Therefore, by changing the aromatic group, one should see a change in the ring opening quantum yield.

REFERENCES

(1) Gilbert, A.; Baggott, J. *Essentials of Molecular Photochemistry*; Blackwell Scientific Publications: Oxford, 1991.

(2) Turro, N. J. *Modern Molecular Photochemistry*; Benjamin/Cummings Publishing Co.: Menlo Park, 1978.

(3) Solomons, T. W. G. *Organic Chemistry*; 6th ed.; John Wiley & Sons, Inc.: Toronto, 1996.

(4) Turro, N. J.; Buchachenko, A. L.; Tarasov, V. F. *Acc. Chem. Res.* **1995**, *28*, 69.

(5) Bunce, N. J. In *Handbook of Organic Photochemistry*; Scaiano, J. C., Ed.; CRC Press: Boca Raton, 1989; Vol. I, pp 241-259.

(6) Parker, C. A. *Proc. Roy. Soc. A* **1953**, *220*, 104.

(7) Hatchard, C. G.; Parker, C. A. *Proc. Roy. Soc. A* **1956**, 518.

(8) Hadel, L. M. In *Handbook of Organic Photochemistry*; Scaiano, J. C., Ed.; CRC Press: Boca Raton, 1989; Vol. I, pp 279-292.

(9) Murov, S. L.; Carmichael, I.; Hug, G. L. *Handbook of Photochemistry*; 2nd ed.; Marcel Decker: New York, 1993.

(10) Bouas-Laurent, H.; Dürr, H. *Photochromism, Molecules and Systems*; Elsevier Science Publishing Co. Inc.: New York, 1990 and references cited within. a) Fritsche, M. *Comp. Rend.* **1867**, *69*, 1035. b) ter Merr, E. *Ann. Chem.* **1876**, *181*, 1. c) Phipson, T.L. *Chem. News* **1881**, *43*, 283. d) Marckwald, W. *Z. Phys. Chem.* **1899**, *30*, 140. e) Wislicenus, W. *Ann. Chem.* **1893**, *277*, 1. f) Biltz, H. *Ann. Chem.* **1899**, *305*, 170. g) Biltz, H. *Z. Phys. Chem.* **1899**, *30*, 537. h) Biltz, H.; Wienands, A. *Ann. Chem.* **1899**, *308*, 1. i) Hirshberg, Y. *Compt. Rend.* **1950**, *231*, 903.

(11) Bouas-Laurent, H.; Dürr, H. *Pure Appl. Chem.* **2001**, *73*, 639.

(12) Yokoyama, Y. *Chem. Rev.* **2000**, *100*, 1717.

(13) Yokoyama, Y. In *Molecular Switches*; Feringa, B. L., Ed.; Wiley-VCH GmbH: Weinheim, 2001, pp 107-121.

(14) Santiago, A.; Becker, R. S. *J. Am. Chem. Soc.* **1968**, *90*, 3654.

(15) Heller, H. G.; Hart, R. J. *J. Chem. Soc. Perkin Trans. 1* **1972**, 1321.

(16) Heller, H. G.; Megit, R.-M. *J. Chem. Soc. Perkin Trans. 1* **1974**, 923.

(17) Heller, H. G.; Oliver, S. *J. Chem. Soc. Perkin Trans. 1* **1981**, 197.

(18) Heller, H. G.; Langan, J. R. *J. Chem. Soc. Perkin Trans. 2* **1981**, 341.

(19) Yoshioka, Y.; Tanaka, T.; Sawada, M.; Irie, M. *Chem. Lett.* **1989**, 19.

(20) Darcy, P. J.; Heller, H. G.; Strydom, P. J.; Whittall, J. *J. Chem. Soc. Perkin Trans. 1* **1981**, 202.

(21) Heller, H. G.; Szewczyk, M. *J. Chem. Soc. Perkin Trans. 1* **1974**, 1487.

(22) Yokoyama, Y.; Hayata, H.; Ito, H.; Kurita, Y. *Bull. Chem. Soc. Jpn.* **1990**, *63*, 1607.

(23) Suzuki, H.; Tomoda, A.; Ishizuka, M.; Kaneko, A.; Furui, M.; Matsushima, R. *Bull. Chem. Soc. Jpn.* **1989**, *62*, 3968.

(24) Kaneko, A.; Tomoda, A.; Ishizuka, M.; Suzuki, H.; Matsushima, R. *Bull. Chem. Soc. Jpn.* **1988**, *61*, 3569.

(25) Lenoble, C.; Becker, R. S. *J. Phys. Chem.* **1986**, *90*, 2651.

(26) Kurita, N.; Kashiwaga, A.; Kurita, Y.; Miyasaki, H.; Mataga, N. *Chem. Phys. Lett.* **1990**, *171*, 553.

(27) Yu, L.; Ming, Y.; Zhang, X.; Fan, M. G.; Lin, N.; Yao, S. *J. Photochem. Photobiol. A: Chem.* **1993**, *74*, 37.

(28) Zhao, W.; Ming, Y.; Zhu, Z.; Fan, M. G. *J. Photochem. Photobiol. A: Chem.* **1993**, *63*, 235.

(29) Heller, H. G. *IEEE Proc.* **1983**, *130*, 209.

(30) Matsui, F.; Taniguchi, H.; Yokoyama, Y.; Sugiyama, K.; Kurita, Y. *Chem. Lett.* **1994**, 1869.

(31) Tomoda, A.; Tsuboi, H.; Kaneko, A.; Matsushima, R. *Nippon Kaguku Kaishi* **1992**, 1071.

(32) Liang, Y.; Dvornikov, A. S.; Rentzepis, P. M. *J. Mater. Chem.* **2000**, *10*, 2477.

(33) Liang, Y.; Dvornikov, A. S.; Rentzepis, P. M. *Chem. Commun.* **2000**, 1641.

(34) Yokoyama, Y.; Shimizu, Y.; Uchida, S.; Yokoyama, Y. *Chem. Commun.* **1995**, 785.

(35) Janicki, S. Z.; Schuster, G. B. *J. Am. Chem. Soc.* **1995**, *117*, 8524.

(36) Willner, I.; Rubin, S.; Wonner, J.; Effenberger, F.; Bauerle, P. *J. Am. Chem. Soc.* **1992**, *114*, 3150.

(37) Willner, I.; Lion-Digan, M.; Rubin, S.; Wonner, J.; Effenberger, F.; Bauerle, P. *Photochem. Photobiol.* **1994**, *59*, 491.

(38) Irie, M. *Chem. Rev.* **2000**, *100*, 1685.

(39) Irie, M. In *Molecular Photoswitches*; Feringa, B. L., Ed.; Wiley-VCH GmbH: Weinheim, 2001, pp 37-61.

(40) Irie, M.; Mohri, M. *J. Org. Chem.* **1988**, *53*, 803.

(41) Nakamura, S.; Irie, M. *J. Org. Chem.* **1988**, *53*, 6136.

(42) Nakayama, Y.; Hayashi, K.; Irie, M. *J. Org. Chem.* **1990**, *55*, 2592.

(43) Nakayama, Y.; Hyashi, K.; Irie, M. *Bull. Chem. Soc. Jpn.* **1991**, *64*, 789.

(44) Irie, M.; Lifka, T.; Uchida, K.; Kobatake, S.; Shindo, Y. *Chem. Commun.* **1999**, 747.

(45) Uchida, K.; Nakayama, Y.; Irie, M. *Bull. Chem. Soc. Jpn.* **1990**, *63*, 1311.

(46) Miyasaka, H.; Araki, S.; Tabata, A.; Nobuto, T.; Mataga, N.; Irie, M. *Chem. Phys. Lett.* **1994**, *230*, 249.

(47) Tamai, N.; Saika, T.; Shimidzu, T.; Irie, M. *J. Phys. Chem.* **1996**, *100*, 4689.

(48) Owrutsky, J. C.; Nelson, H. H.; Baronavski, A. P.; Kim, O.-K.; Tsivgoulis, G. M.; Gilat, S. L.; Lehn, J.-M. *Chem. Phys. Lett.* **1998**, *293*, 555.

(49) Kaieda, T.; Kobatake, S.; Miyasaki, H.; Murakami, S.; Iwai, N.; Nagata, Y.; Itaya, A.; Irie, M. *J. Am. Chem. Soc.* **2002**, *124*, 2015.

(50) Ern, J.; Bens, A. T.; Martin, H.-D.; Mukamel, S.; Tretiak, S.; Tsyganenko, K.; Kuldova, K.; Trommsdorff, H. P.; Kryschi, C. *J. Phys. Chem. A* **2001**, *105*, 1741.

(51) Ern, J.; Bens, A. T.; Martin, H.-D.; Kuldova, K.; Trommsdorff, H. P.; Kryschi, C. *J. Phys. Chem. A* **2002**, *106*, 1654.

(52) Malval, J.-P.; Gosse, I.; Morand, J.-P.; Lapouyade, R. *J. Am. Chem. Soc.* **2002**, *124*, 904.

(53) Yagi, K.; Soong, C. F.; Irie, M. *J. Org. Chem.* **2001**, *66*, 5419.

(54) Osuka, A.; Fujikane, D.; Shinmori, H.; Kobatake, S.; Irie, M. *J. Org. Chem.* **2001**, *66*, 3913.

(55) Norsten, T. B.; Peters, A.; McDonald, R.; Wang, M.; Branda, N. R. *J. Am. Chem. Soc.* **2001**, *123*, 7447.

(56) Norsten, T. B.; Branda, N. R. *J. Am. Chem. Soc.* **2001**, *123*, 1784.

(57) Endtner, J. M.; Effenberger, F.; Hartschuh, A.; Port, H. *J. Am. Chem. Soc.* **2000**, *122*, 3037.

(58) Matsuda, K.; Irie, M. *J. Am. Chem. Soc.* **2000**, *122*, 7195.

(59) Takeshita, M.; Irie, M. *J. Org. Chem.* **1998**, *63*, 6643.

(60) Takeshita, M.; Kato, N.; Kawauchi, S.; Imase, T.; Watanabe, J.; Irie, M. *J. Org. Chem.* **1998**, *63*, 9306.

(61) Takeshita, M.; Yamada, M.; Kato, N.; Irie, M. *J. Chem. Soc., Perkin Trans. 2* **2000**, *2*, 619.

(62) Takeshita, M.; Choi, C. N.; Irie, M. *Chem. Commun.* **1997**, 2265.

(63) Denekamp, C.; Feringa, B. L. *Adv. Mater.* **1998**, *10*, 1080.

(64) Gilat, S. L.; Kawai, S. H.; Lehn, J.-M. *Chem. Eur. J.* **1995**, *1*, 275.

(65) Saika, T.; Irie, M.; Shimidzu, T. *Chem. Commun.* **1994**, 2123.

(66) Yoshida, T.; Arishima, K.; Ebisawa, F.; Hoshino, M.; Sukegawa, K.; Horikawa, Y. *J. Photochem. Photobiol. A: Chem.* **1996**, *95*, 265.

(67) Hoshino, M.; Ebisawa, F.; Yoshida, T.; Sukegawa, K. *J. Photochem. Photobiol. A: Chem.* **1997**, *105*, 75.

(68) Dietz, F.; Tyutyulkov, N. *Phys. Chem. Chem. Phys.* **2001**, *3*, 4600.

(69) Mitchell, R. H. *Eur. J. Org. Chem.* **1999**, 2695.

(70) Mitchell, R. H.; Williams, R. V.; Dingle, T. W. *J. Am. Chem. Soc.* **1982**, *104*, 2560.

(71) Mitchell, R. H.; Yan, J. S. H.; Dingle, T. W. *J. Am. Chem. Soc.* **1982**, *104*, 2551.

(72) Mitchell, R. H.; Carruthers, R. J.; Mazuch, L.; Dingle, T. W. *J. Am. Chem. Soc.* **1982**, *104*, 2544.

(73) Mitchell, R. H.; Chen, Y.; Iyer, V. S.; Lau, D. Y. K.; Baldridge, K. K.; Siegel, J. S. *J. Am. Chem. Soc.* **1996**, *118*, 2907.

(74) Mitchell, R. H.; Ward, T. R. *Tetrahedron* **2001**, *57*, 3689.

(75) Blattman, H. R.; Meuche, D.; Heilbronner, E.; Molyneux, R. J.; Boekelheide, V. *J. Am. Chem. Soc.* **1965**, *87*, 130.

(76) Blattman, H. R.; Schmidt, W. *Tetrahedron* **1970**, *26*, 5885.

(77) Schmidt, W. *Helv. Chim. Acta* **1971**, *54*, 862.

(78) Mitchell, R. H.; Chen, Y. *Tetrahedron Letters* **1996**, *37*, 5239.

(79) Schmidt, W. *Tetrahedron Letters* **1972**, *7*, 581.

(80) Tashiro, M.; Yamato, T. *J. Am. Chem. Soc.* **1982**, *104*, 3701.

(81) Mitchell, R. H.; Ward, T. R.; Wang, Y.; Dibble, P. W. *J. Am. Chem. Soc.* **1999**, *121*.

(82) Murakami, S.; Tsutsui, T.; Saito, S.; Yamato, T.; Tashiro, M. *Nippon Kagaku Kaishi* **1988**, 221.

(83) Ward, M. D. *J. Chem. Ed.* **2001**, *78*, 321.

(84) Carey, F. A.; Sundberg, R. J. *Advanced Organic Chemistry, Part A: Structure and Mechanisms*; 3rd ed.; Plenum Press: New York, 1990.

(85) Mitchell, R. H.; Chen, Y.; Zhang, J. *Org. Prep. Proc. Int.* **1977**, *29*, 715.

(86) Lemieux, R. U.; Morgan, A. R. *Can. J. Chem.* **1965**, *43*, 2190.

(87) Mitchell, R. H.; Jin, X. *Tetrahedron Letters* **1995**, *36*, 4357.

(88) Sonogashira, K.; Tohda, Y.; Hagihara, N. *Tetrahedron Letters* **1975**, 4467.

(89) Takahashi, S.; Kuroyama, Y.; Sonogashira, K.; Hagihara, N. *Synthesis* **1980**, 627.

(90) R.H. Mitchell, personal communication.

(91) Havens, S. J.; Hergenrother, P. M. *J. Org. Chem.* **1985**, *50*, 1763.

(92) Eglinton, G.; Galbraith, A. R. *J. Chem. Soc.* **1959**, 889.

(93) Van Houton, J.; Watts, R. J. *J. Am. Chem. Soc.* **1976**, *98*, 4853.

(94) Eaton, D. F. In *Handbook of Organic Photochemistry*; Scaiano, J. C., Ed.; CRC Press: Boca Raton, 1989; Vol. I, pp 231-239.

(95) Murphy, R. S.; Barros, T. C.; Barnes, J.; Mayer, B.; Marconi, G.; Bohne, C. *J. Phys. Chem. A* **1999**, *103*, 137.

(96) Liao, Y.; Bohne, C. *J. Phys. Chem.* **1996**, *100*, 734.

(97) Murphy, R. S.; Chen, Y.; Ward, T. R.; Mitchell, R. H.; Bohne, C. *Chem. Commun.* **1999**, 2097.

(98) Farmilo, A.; Wilkinson, F. *Chem. Phys. Lett.* **1975**, *34*, 575.

(99) Boekelheide, V.; Phillips, J. B. *J. Am. Chem. Soc.* **1967**, *89*, 1695.

(100) Mitchell, R. H.; Boekelheide, V. *J. Am. Chem. Soc.* **1974**, *96*, 1547.

(101) Phillips, J. B.; Molyneux, R. J.; Sturm, E.; Boekelheide, V. *J. Am. Chem. Soc.* **1967**, *89*, 1704.

(102) The synthesis will be published in the future as part of the PhD thesis of Y. Wang, University of Victoria.

(103) The synthesis will be published in the future as part of the PhD thesis of S. Bandyopadhyay, University of Victoria.

(104) Tamai, N.; Masuhara, H. *Chem. Phys. Lett.* **1992**, *191*, 189.

(105) Berkovic, G.; Krongauz, V.; Weiss, V. *Chem. Rev.* **2000**, *100*, 1741.

(106) Steiner, U. E.; Thomas, U. *Chem. Rev.* **1989**, *89*, 51.

(107) Steiner, U. E.; Wolff, H.-J. In *Photochemistry and Photophysics*; Rabek, J. F., Ed.; CRC Press: Boca Raton, 1991; Vol. 4, pp 1-130.

(108) Ward, T. R. In *Department of Chemistry*; University of Victoria: Victoria, 2001, p 177.

(109) Kirk, A. D.; Namasivayam, C. *Anal. Chem.* **1983**, *55*, 2428.

(110) Uchida, K.; Matsuoka, T.; Kobatake, S.; Yamaguchi, T.; Irie, M. *Tetrahedron* **2001**, *57*, 4559.

(111) Porter, G.; Topp, M. R. *Nature* **1968**, *220*, 1228.

(112) Wagner, P. J. *Pure Appl. Chem.* **1977**, *49*, 259.

(113) Bays, J. P.; Encinas, V.; Small, R. D.; Scaiano, J. C. *J. Am. Chem. Soc.* **1980**, *102*, 727.

(114) The percent of the transient signal corresponding to the triplet absorption can be estimated by dividing the quantum yield of intersystem crossing by the isomerization quantum yield. It should be noted that the intersystem crossing quantum yield is likely smaller for the CPDs than was measured for the DMDHPs.

APPENDIX A

Table A1. Absorption maxima (λ_{max}) and molar absorptivity coefficients (ε) for simple substituted DMDHP derivatives.

Cmpd	λ_{max} / nm ε / 10^3 $M^{-1}cm^{-1}$					
1	338 109 ± 6	377 48 ± 3	470 8.6 ± 0.6	641 0.427 ± 0.006		
2	341 103 ± 1	379 38.8 ± 0.1	477 11.1 ± 0.1	641 0.900 ± 0.003		
10	348 85.8 ± 0.6	387 48.2 ± 0.2	482 11.3 ± 0.1	650 1.40 ± 0.01		
11	344 77.3 ± 0.5	383 35.7 ± 0.2	483 9.09 ± 0.05	649 0.842 ± 0.006		
14	309 16.84 ± 0.07	357 74.5 ± 0.1	395 66.0 ± 0.3	495 10.84 ± 0.05	667 2.13 ± 0.01	
15	297 18.7 ± 0.2	369 43.8 ± 0.3	411 61.3 ± 0.6	520 12.6 ± 0.1	687 3.31 ± 0.03	
17	353 95.8 ± 0.2	391 59.0 ± 0.1	489 10.2 ± 0.1	663 1.74 ± 0.05		
18	361 58.7 ± 0.2	399 54.4 ± 0.2	503 8.5 ± 0.1	679 2.3 ± 0.1		
19	351 83.3 ± 0.4	389 48.3 ± 0.4	488 9.68 ± 0.04	662 1.71 ± 0.01		
21	282 21.0 ± 0.2	353 74.5 ± 0.4	421 77.6 ± 0.4	479 25.0 ± 0.1	611 1.357 ± 0.006	673 6.84 ± 0.01
24	343 92 ± 2	395 39 ± 1	506 15.5 ± 0.3	595 0.629 ± 0.007	660 0.529 ± 0.005	
25	346 37.8 ± 0.2	395 36.5 ± 0.2	495 7.24 ± 0.03	666 2.74 ± 0.01		
26	347 82.1 ± 0.1	387 47.4 ± 0.2	483 10.0 ± 0.1	649 1.06 ± 0.01		
27	275 16.3 ± 0.1	291 18.5 ± 0.1	358 107 ± 1	398 99.5 ± 0.6	497 16.5 ± 0.1	669 3.98 ± 0.02

Table A2. Absorption maxima (λ_{max}) and molar absorptivity coefficients (ε) for arene [e]-fused DMDHP derivatives.

Cmpd	λ_{max} / nm ε / 10^3 $M^{-1}cm^{-1}$					
3	308 22.9 ± 0.5	321 23.4 ± 0.3	337 25.4 ± 0.2	369 24.0 ± 0.4	387 30.4 ± 0.3	503 6.85 ± 0.05
28	313 13.0 ± 0.2	326 13.9 ± 0.4	343 15.4 ± 0.4	378 15.4 ± 0.1	397 21.0 ± 0.3	511 4.3 ± 0.2
29	311 16.2 ± 0.4	328 17.9 ± 0.5	342 20.2 ± 0.7	400 24.0 ± 0.5	518 5.00 ± 0.02	636 1.00 ± 0.01
30	262 28.5 ± 0.2	321 25.4 ± 0.3	378 31.7 ± 0.4	398 41.8 ± 0.1	553 4.20 ± 0.05	
31	284 43.2 ± 0.4	337 38.7 ± 0.1	374 22.2 ± 0.1	392 46.3 ± 0.2	412 72.5 ± 0.3	529 5.72 ± 0.02

Table A3. Molar absorptivity coefficients at 465 nm (ε_{465}) for selected simple substituted DMDHP derivatives.

Compound	ε_{465} / 10^3 $M^{-1}cm^{-1}$
1	8.4 ± 0.8
2	9.1 ± 0.9
11	7.1 ± 0.7
14	8.9 ± 0.9
17	8.6 ± 0.9
18	5.9 ± 0.6
21	24 ± 2
24	8.2 ± 0.8
25	5.9 ± 0.6
26	8.2 ± 0.8
27	14 ± 1

Table A4. Molar absorptivity coefficients at 465 nm for selected arene [e]-fused DMDHP derivatives.

Compound	ε_{465} / 10^3 $M^{-1}cm^{-1}$
3	4.6 ± 0.5
28	2.9 ± 0.3
30	2.5 ± 0.3
31	3.7 ± 0.4

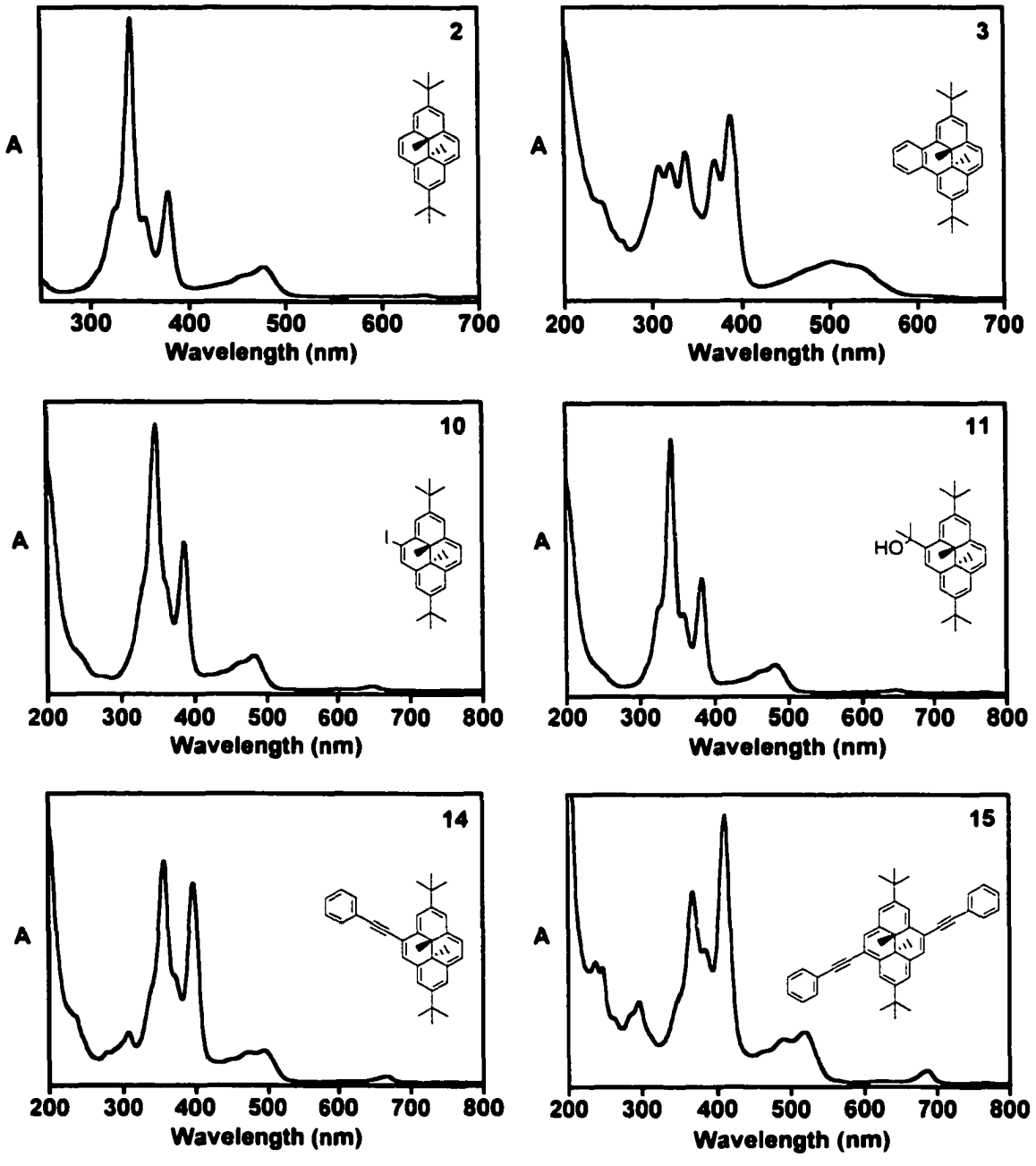

Figure A1 Ground state absorption spectra of DMDHP derivatives (for ε values see Tables A1 and A2). The structure of the compound is shown as an inset in the figure. The number for each derivative as it appears in the text is given in the top right corner.

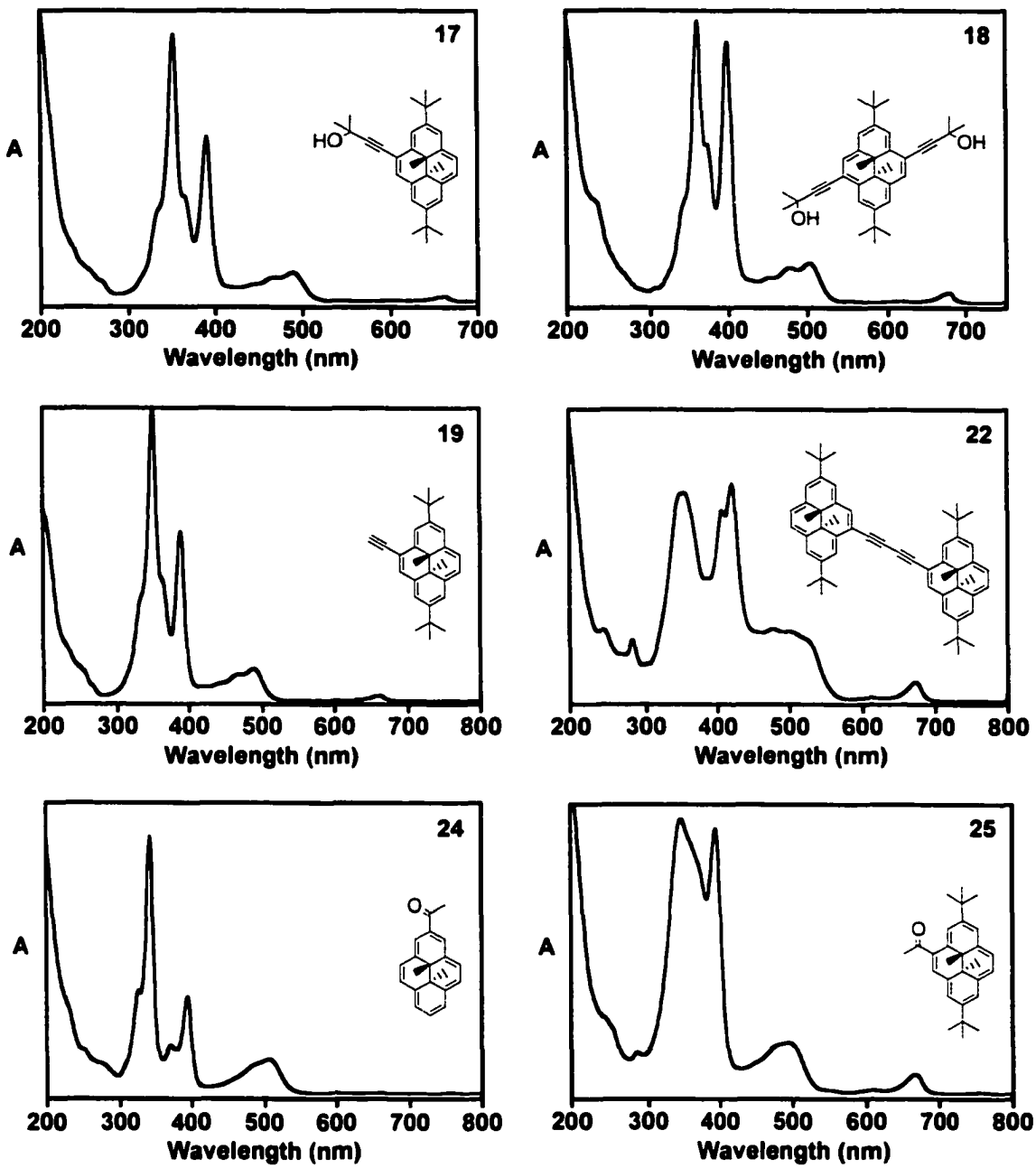

Figure A2. Ground state absorption spectra of DMDHP derivatives (for ε values see Table A1). The structure of the compound is shown as an inset in the figure. The number for each derivative as it appears in the text is given in the top right corner.

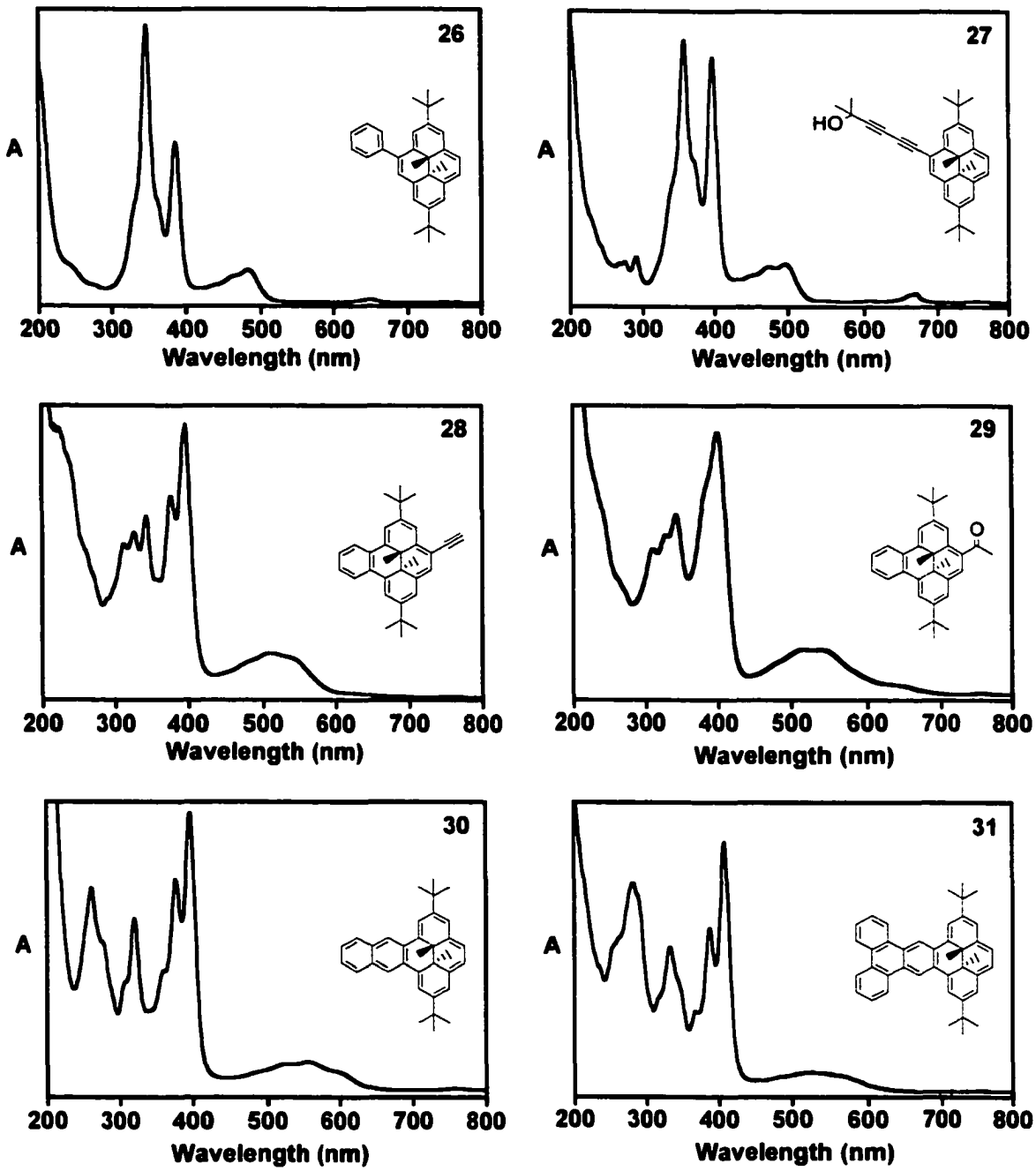

Figure A3. Ground state absorption spectra of DMDHP derivatives (for ε values see Tables A1 and A2). The structure of the compound is shown as an inset in the figure. The number for each derivative as it appears in the text is given in the top right corner.

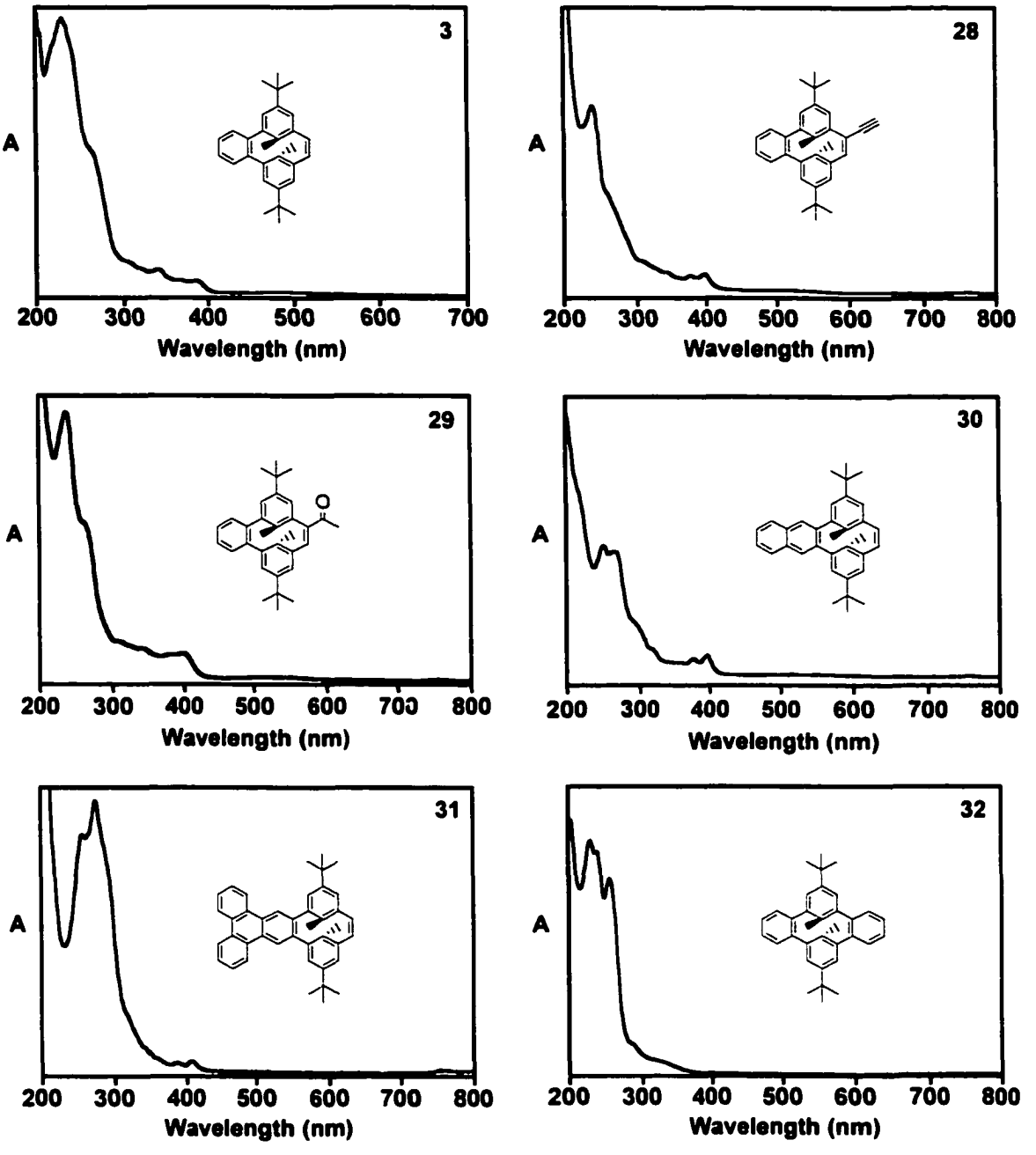

Figure A4. Ground state absorption spectra of CPD derivatives. The structure of the compound is shown as an inset in the figure. The number for each derivative as it appears in the text is given in the top right corner.

APPENDIX B

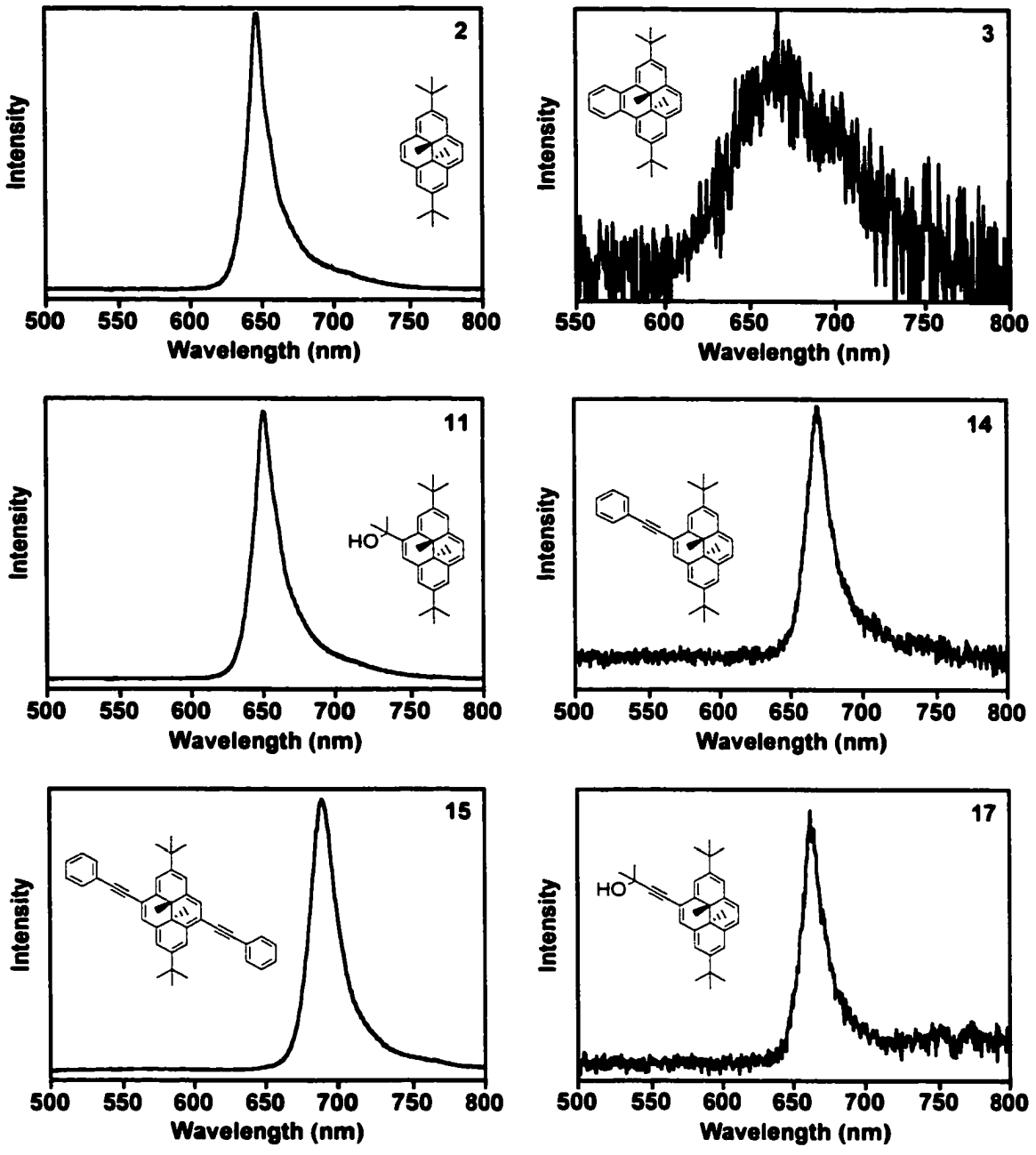

Figure B1. Room temperature fluorescence spectra of DMDHP derivatives. The structure of the compound is shown as an inset in the figure. The number for each derivative as it appears in the text is given in the top right corner.

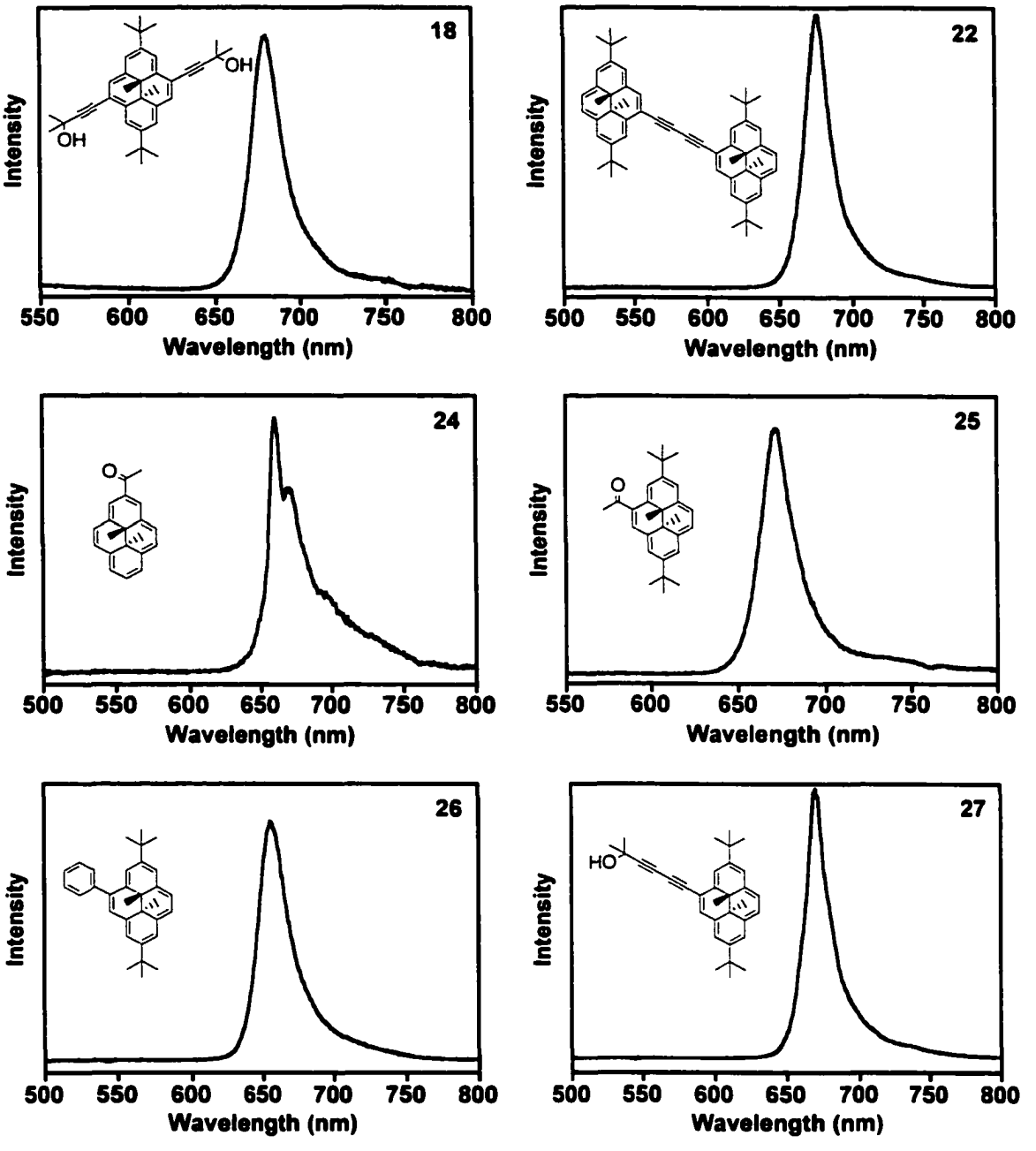

Figure B2. Room temperature fluorescence spectra of DMDHP derivatives. The structure of the compound is shown as an inset in the figure. The number for each derivative as it appears in the text is given in the top right corner.

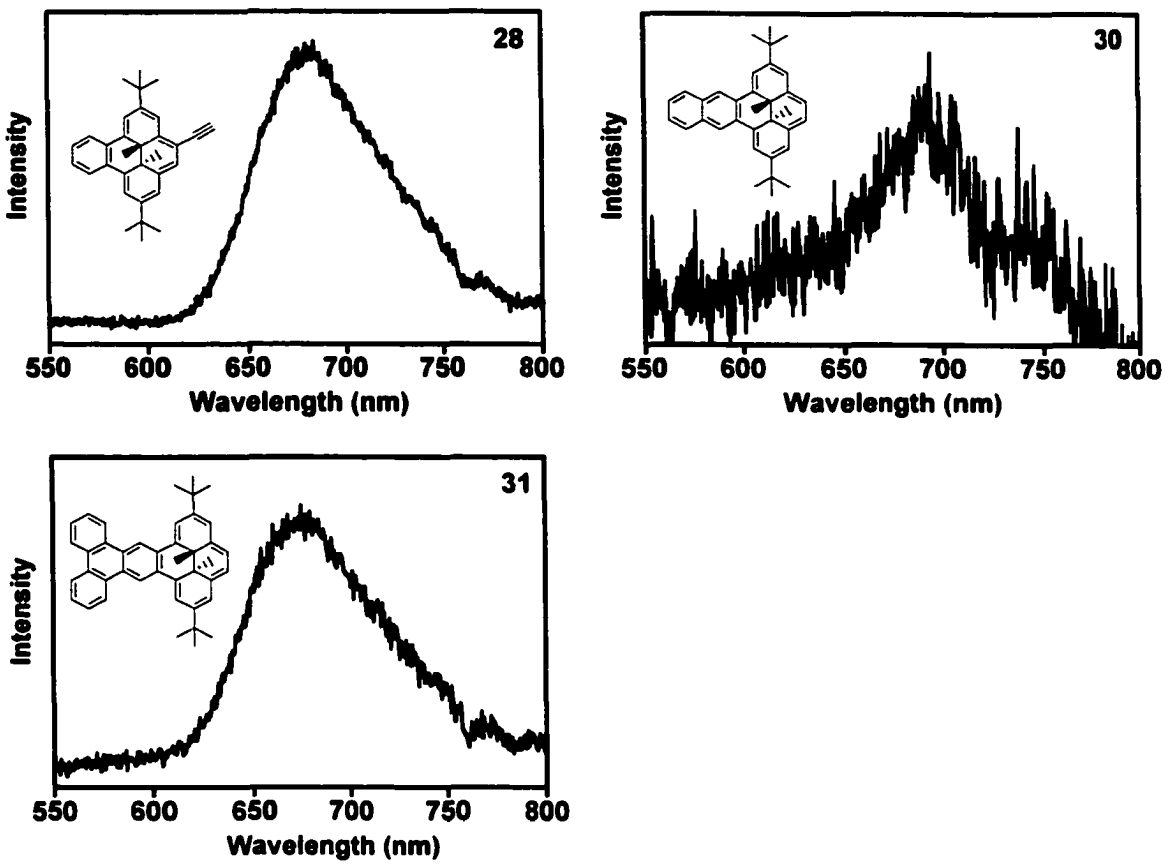

Figure B3. Room temperature fluorescence spectra of DMDHP derivatives. The structure of the compound is shown as an inset in the figure. The number for each derivative as it appears in the text is given in the top right corner.

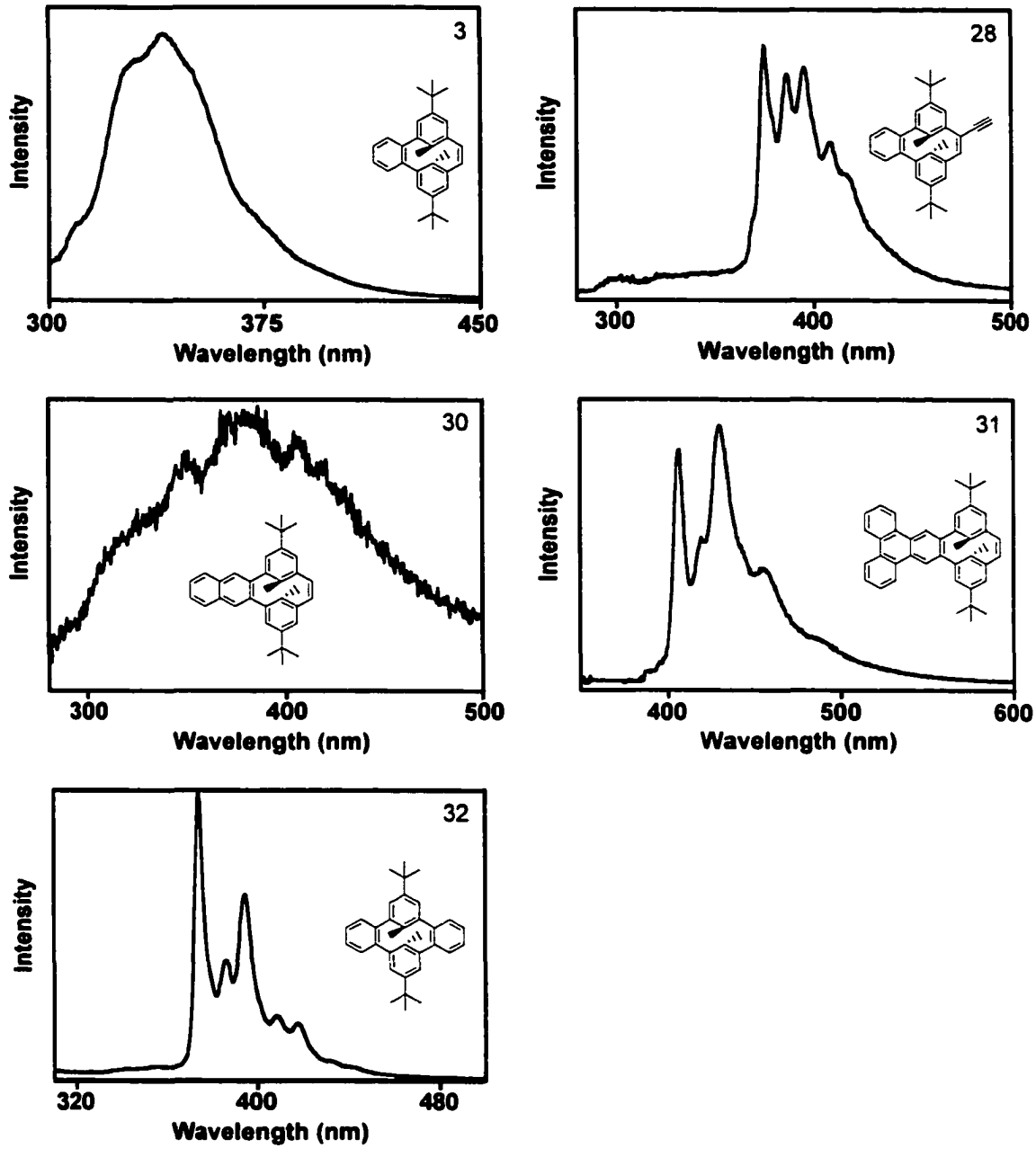

Figure B4. Room temperature fluorescence spectra of CPD derivatives. The structure of the compound is shown as an inset in the figure. The number for each derivative as it appears in the text is given in the top right corner.

APPENDIX C

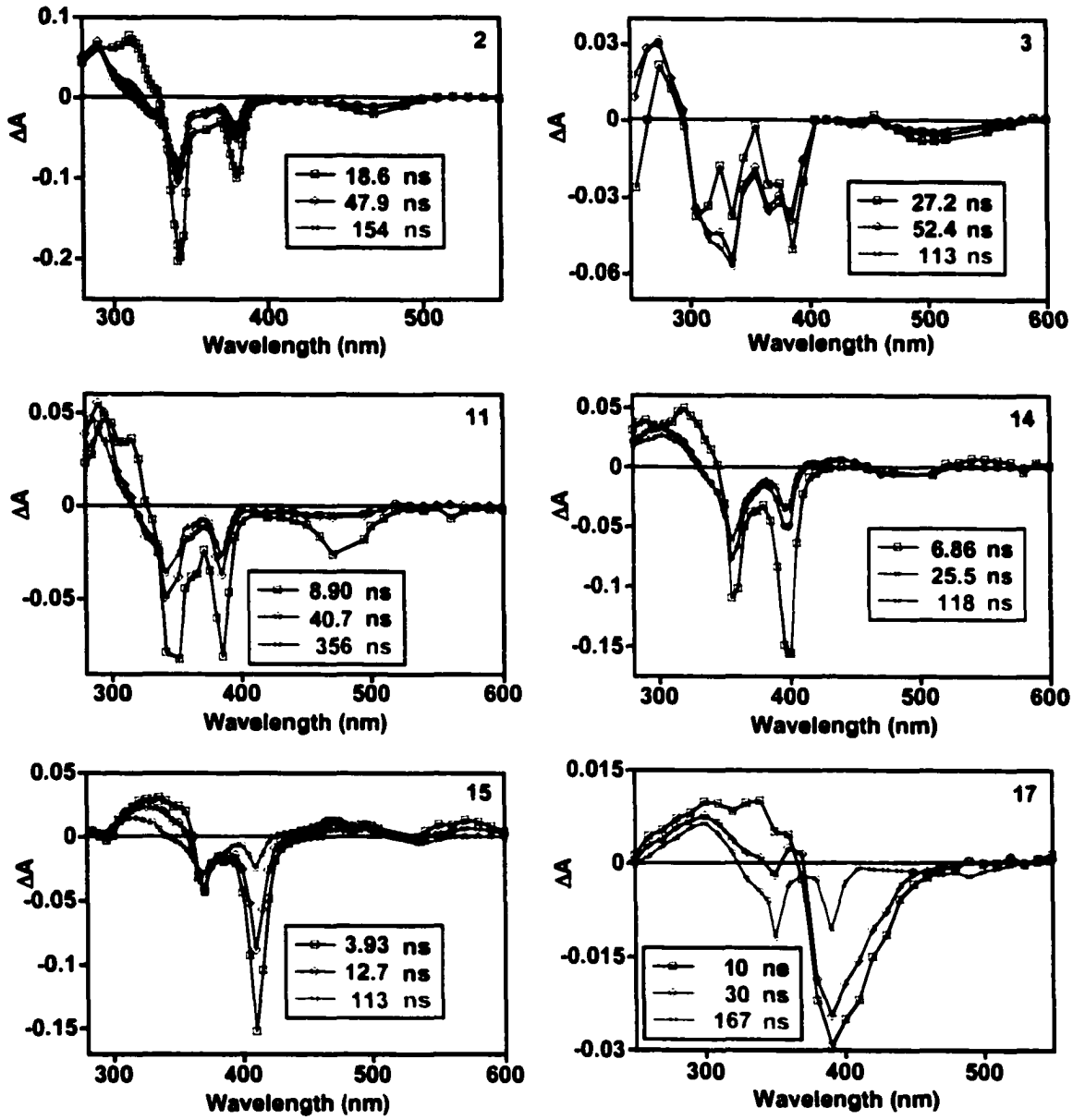

Figure C1. Transient absorption spectra of DMDHP derivatives. The delays for each spectrum are shown as an inset in the figure. The number for each derivative as it appears in the text is given in the top right corner.

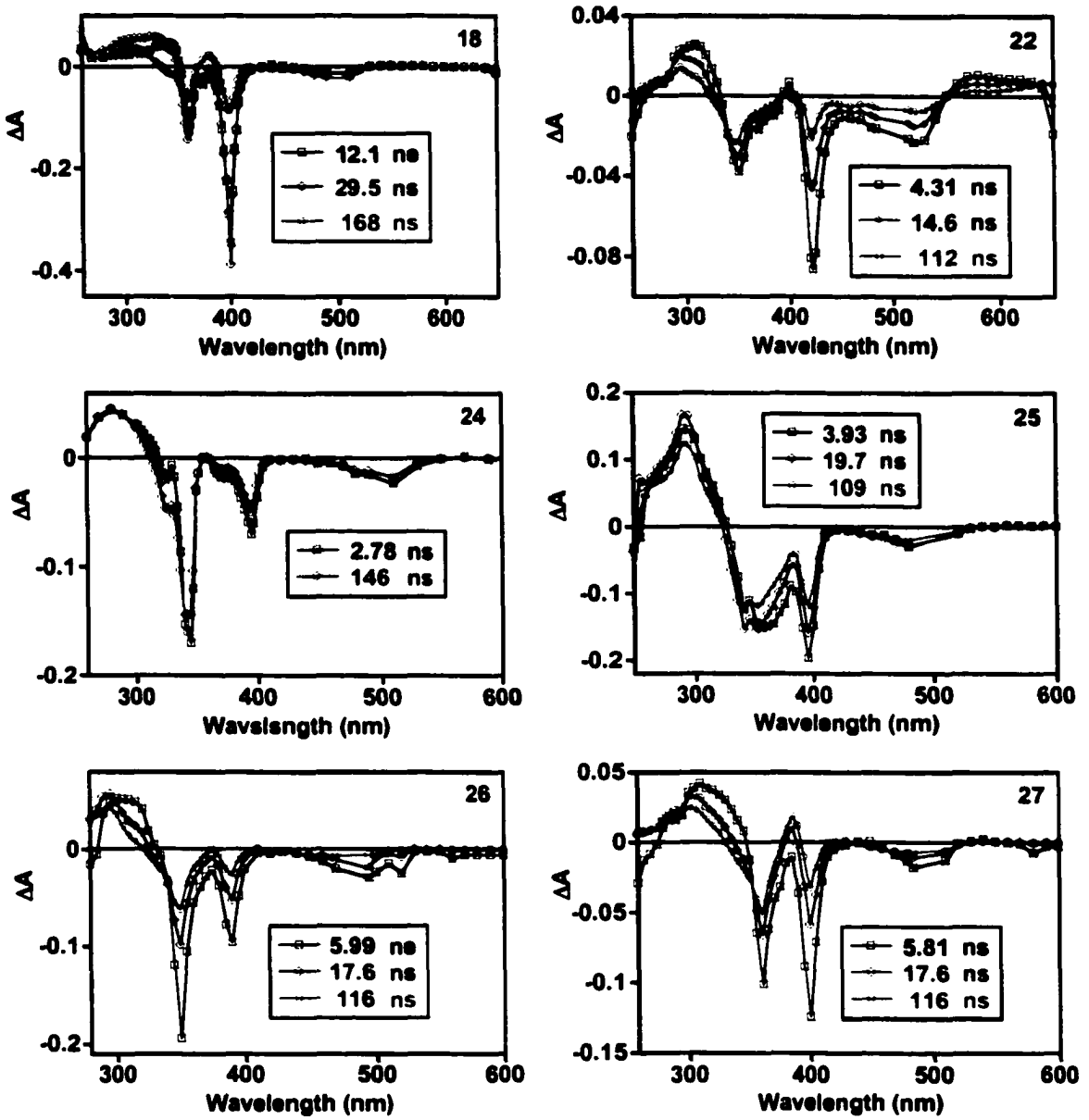

Figure C2. Transient absorption spectra of DMDHP derivatives. The delays for each spectrum are shown as an inset in the figure. The number for each derivative as it appears in the text is given in the top right corner.

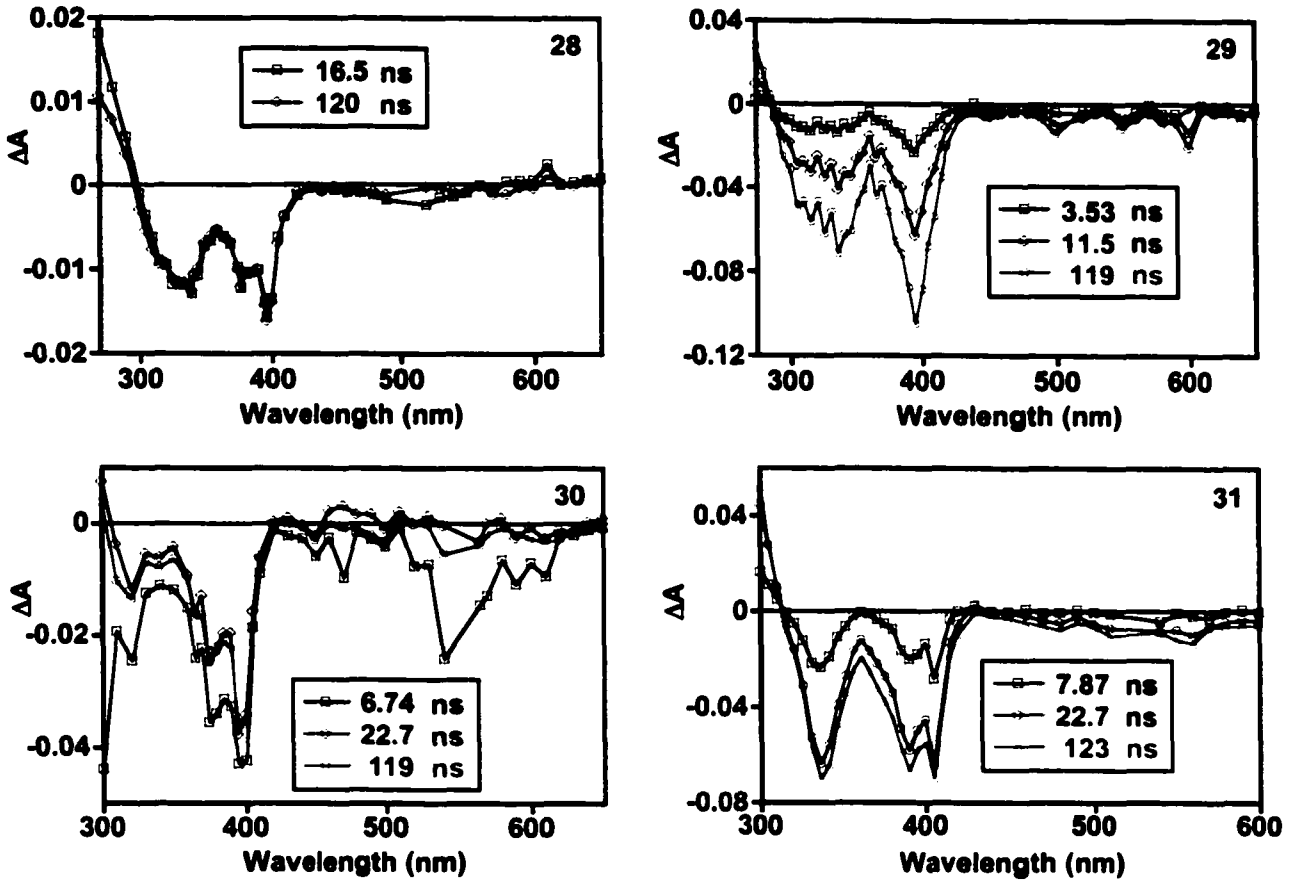

Figure C3. Transient absorption spectra of DMDHP derivatives. The delays for each spectrum are shown as an inset in the figure. The number for each derivative as it appears in the text is also given in the top right corner.

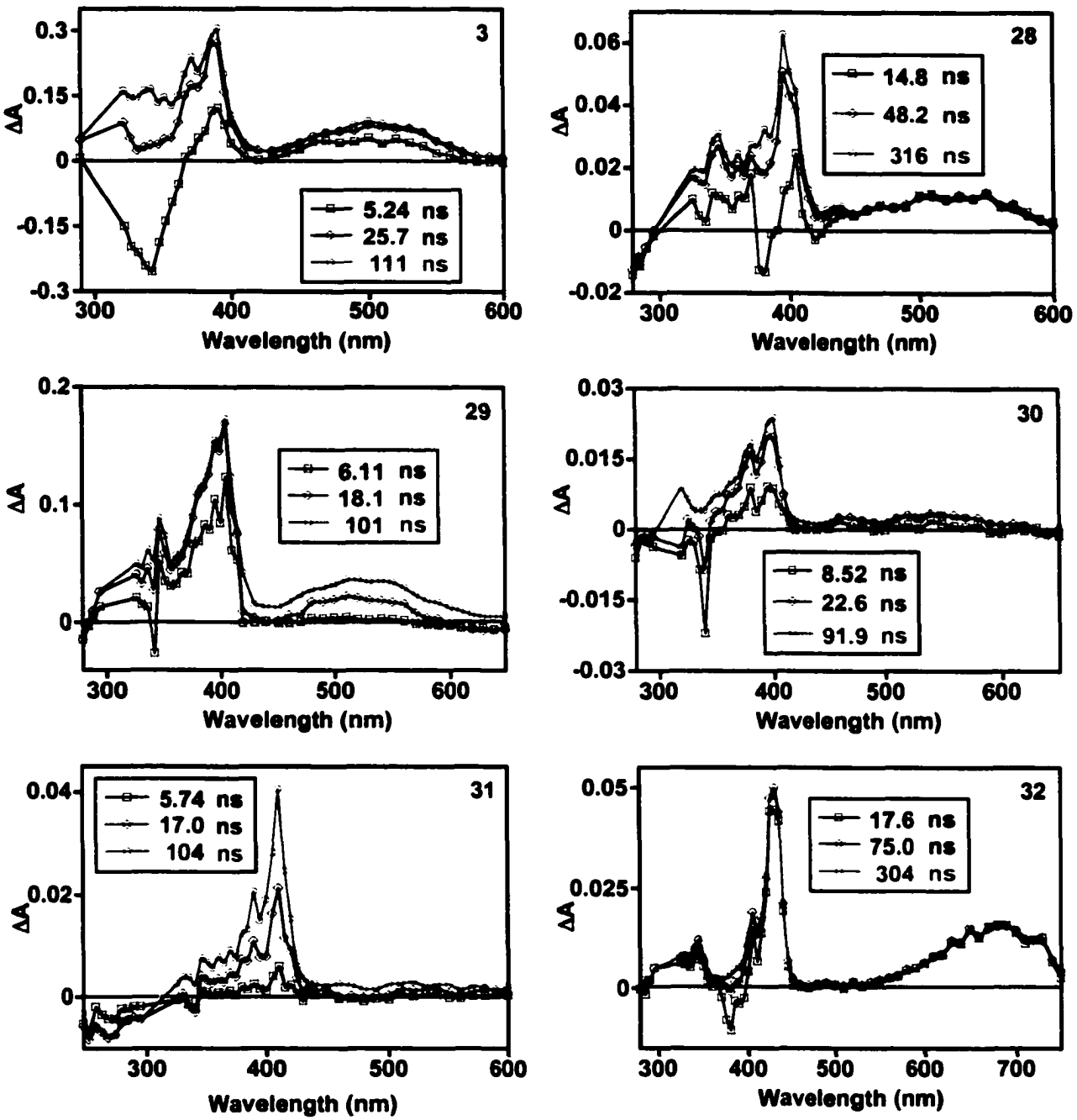

Figure C4. Transient absorption spectra of CPD derivatives. The delays for each spectrum are shown as an inset in the figure. The number for each derivative as it appears in the text is also given in the top right corner.